University of Cape Town
Faculty of Science
Department of Molecular and Cell Biology

RESEARCH REPORT

Submitted in fulfilment of the requirements for the degree of

Master of Science (Molecular Biology)

February 2006

Evolutionary analysis and functional characterization of the Forkhead transcription factor FoxG1

Nicholas Bredenkamp

Evolutionary analysis and functional characterization of the Forkhead transcription factor FoxG1

Nicholas Bredenkamp

BRDNIC011

Submitted in fulfilment of the requirements for the degree of

Master of Science (Molecular Biology)

February 2006

Table of Contents

Abstract

Forkhead box G1 (FoxG1) is a winged-helix transcription factor that plays a crucial role in the development of the telencephalon, the most rostral region of the brain. Here, FoxG1 acts as a transcriptional repressor and maintains the population of cortical progenitor cells by promoting their proliferation and inhibiting differentiation. Vertebrate FoxG1 orthologs have highly conserved DNA-binding and carboxy-terminal domains that have functional roles. Conversely, no functional role has yet been assigned to the N-terminal domain which shows a high degree of variability across vertebrates, with a remarkable stretch of consecutive histidine, proline and glutamine (HPQ) residues in the mammalian orthologs. In this study it was tested whether differences in FoxG1 sequence amongst vertebrates might account for the increased cortex size of mammals compared to non-mammals. Furthermore, changes in the sub-cellular localization of FoxG1 in response to fibroblast growth factor 2 (FGF-2) were investigated in a neural precursor cell line.

To examine the variability of FoxG1 orthologs more comprehensively, nine new FoxG1 orthologs were cloned during this study. FoxG1 sequence is presented for three reptiles, a vertebrate class that previously had no FoxG1 members, and six mammals, chosen to represent a spread across mammalian evolutionary relationships. Together with previously available orthologs, it is shown that the N-terminal domain of FoxG1 exhibits distinct differences between the mammal and non-mammal orthologs while there is relatively high conservation within the mammalian group. The HPQ region is shown to be present in all mammalian orthologs and drastically reduced in all non-mammal orthologs. The functional role of this N-terminal variability is investigated using transient transfection assays that tested the hypothesis that constitutive expression of a mammalian ortholog would differentially affect cell survival compared to constitutive expression of a non-mammalian ortholog. However, this study showed no difference in transfection

efficiency between the mouse and *Xenopus* FoxG1 orthologs. Furthermore, FoxG1 orthologs share an unusually highly conserved 3' untranslated region which is shown, by *in silico* analysis, to be the possible target of microRNA regulation.

Next, because FOXG1 is mutated in a human microcephaly (reduced brain size) phenotype, it was investigated if positive selection is acting on FoxG1, implicating it as a determinant of the enlarged cerebral cortex size in humans. Analysis in the primate lineage leading to humans showed no evidence for positive selection acting on FoxG1. Additionally, the reported FOXG1 duplication in humans – another possible determinant of brain size – is shown not to exist, with only one form of human FOXG1 being detected using PCR and genome analysis.

The post-translational regulators of FoxG1 activity have not been identified. The change in sub-cellular localization of FoxG1 in a neural precursor cell line, OP27, in response to FGF-2 induced signalling, is investigated in this study using immunocytochemistry. The state of OP27 differentiation was confirmed by monitoring changes in morphology and expression of the neural signalling pathway components, Delta1 and Notch1. FoxG1 showed reduced nuclear and increased cytoplasmic localization following FGF-2 induced differentiation, indicating that FGF-2 signalling may regulate the transcriptional activity of FoxG1.

Acknowledgments

I would to thank Nicola Illing for her supervision and guidance, Faezah Davids and Aubrey Shoko for their unlimited advice and technical support, Dirk Lang for help with the microscopy and, Helen Collett, Keke Tloti and the rest of the laboratory for their general assistance. Thanks also to Nancy Papalopulu and Tarik Regad for sharing their unpublished results relating to this project as well as the generous supply of antibodies. Thanks to the undergraduate project students Lourie Badenhorst, Lauren Beukes, Johann Eicher, Gavin Jones, Dean Peters and Jennifer Miller for help with the FoxG1 ortholog cloning. Finally, my sincere gratitude to my family and Sarah Lea for all their support and encouragement throughout this project.

Abbreviations

actNotch	Activated Notch
ASPM	Abnormal spindle-like microcephaly associated gene
BLAST	Basic local alignment search tool
BLASTn	Nucleotide-nucleotide BLAST
BMP	Bone morphogenetic protein
BSA	Bovine serum albumin
CMV	Cytomegalovirus
CP	Calcium phosphate
C-terminal	Carboxy-terminal
DAPI	4´,6´-Diamidino-2-phenyllindole
DMEM	Dulbecco's modified Eagle's medium
DMEM-10	Dulbecco's modified Eagle's medium with 10% fetal bovine serum
DTT	Dithiothreitol
ECFP	Enhanced cyan fluorescent protein
EDTA	Ethylene diamine tetraacetic acid
FBS	Fetal bovine serum
FGF(R)	Fibroblast growth factor (receptor)
Fox	Forkhead box
GFP	Green fluorescent protein
HPQ	Histidine, proline and glutamine rich region in the N-terminal domain of FoxG1
IPTG	Isopropyl-β-D-thiogalactopyranoside
K_a	Rate of non-synonymous mutations
K_s	Rate of synonymous mutations
LM	Liposome mediated
mFoxG1	Mouse FoxG1
M-MLV	Moloney Murine Leukaemia Virus
NCBI	National Centre for Biotechnology Information
nls	Nuclear localization sequence
NWM	New World monkey
OMP	Olfactory marker protein
OP	Olfactory placode
ORN	Olfactory receptor neuron
OWM	Old World monkey
PBS	Phosphate buffered saline
RACE	Rapid amplification of cDNA ends
RT-PCR	Reverse transcription polymerase chain reaction
TGF-β	Transforming growth factor-β
Gro/TLE	Groucho/Transducin-like enhancer of split
U	Enzyme activity
UTR	Untranslated region
XFoxG1	*Xenopus* FoxG1
X-gal	5-bromo-4-chloro-3-indolyl-β-D-galactosidase

List of Figures

List of Tables

CHAPTER 1

Introduction

1.1. Forebrain development

During nervous system development the rostral region of the neural tube gives rise to the brain (Kandel et al., 1991). Brain regionalization is initially defined by three vesicles called the forebrain, midbrain and hindbrain. The forebrain subsequently subdivides into two regions, the telencephalon (rostral) – which forms as two lateral vesicles – and the diencephalon (caudal). Within the telencephalic vesicles, the dorsal region gives rise to the pallium (or cerebral cortex) which is further subdivided into dorsal, ventral, medial and lateral regions, giving rise to the neocortex, claustrum and part of the amygdala, hippocampus and olfactory bulb, respectively, while the ventral region of the pallium gives rise to the basal ganglia (Sur and Rubenstein, 2005). The development of the telencephalon occurs during the approximate interval of embryonic day 10.5 and 17.5 (E10.5-17.5) in mice (Caviness et al., 1995). The molecular factors and pathways that control the initial brain patterning and subsequent morphogenesis are complex and involve a large number of molecular components.

1.2. FoxG1* in neural development

One of the transcription factors that plays a fundamental role in brain development is Forkhead box G1 (FoxG1) (formerly Brain Factor1 (BF-1), renamed in Kaestner et al., 2000). FoxG1 is a member of the fork head or winged-helix gene transcription factor family, that includes the *Drosophila* central nervous system gene, *fork head* (Weigel et al., 1989) and the mammalian liver-specific gene activators, hepatocyte nuclear factor (HNF) 3α, 3β and 3γ (Lai et al., 1990).

* Technical note: in the nomenclature revision for the winged helix transcription factor family (Kaestner et al., 2000) it was stipulated that abbreviations for human proteins should contain all uppercase letters (i.e. FOXG1), mouse should only contain the first letter capitalized (i.e. Foxg1) and all other chordates should have the first and subclass letters capitalized (i.e. FoxG1). During this study, human orthologs are written as such, however, due to the constant use of mouse and other orthologs in the same section/paragraph/sentence, all other orthologs are written as FoxG1.

In humans, there are at least 43 members of the Forkhead box (FOX) gene family with biological functions that include roles in organogenesis during development as well as the maintenance of physiological homeostasis (Katoh and Katoh, 2004). Mutations in the FOX genes can result in chronic human disorders. For example, a FOXN1 mutation causes thymic cell immunodeficiency and a skin disorder (Frank et al., 1999) and a FOXP2 mutation results in a speech and language disorder (Lai et al., 2001).

FoxG1 was first cloned by screening a rat brain cDNA library with an HNF-3α probe (Tao and Lai, 1992) and was subsequently cloned from mouse by using the rat FoxG1 probe to screen a mouse brain cDNA library (Li et al., 1996). Further analysis showed that FoxG1 was expressed in fetal and adult rat brain but showed several-fold more abundant expression in fetal brain. Additionally, in the rat embryo brain, FoxG1 expression was localized, by in situ hybridization, to the telencephalon derived structures – the cortex, hippocampus and olfactory bulb – but was absent in the midbrain and hindbrain. FoxG1 is also expressed in the optic chiasm and was shown to be an important regulator of retinal ganglion cell development and axon projection in mice (Pratt et al., 2004). Furthermore, FoxG1 showed expression in the anterior region of the developing neural tube in zebrafish and the primitive chordate, amphioxus (Toresson et al., 1998). This conserved region-specific expression suggested that FoxG1 may play an important role in the specification and development of the telencephalon.

The suggestion that FoxG1 plays a role in forebrain development was confirmed using FoxG1 null mutant mice (Xuan et al., 1995). At E9.5, during the early stages of telencephalon development, these FoxG1 null mutant mice embryos showed minimal differences in their telencephalon morphology compared to wildtype embryos. However, at E10.5 and E12.5 the mutants showed a severely reduced and malformed telencephalon compared to the wildtype

embryos. This was shown to be a result of a decrease in proliferating cells in the telencephalic neuroepithelium, as determined by a reduction in the number of bromodeoxyuridine (BrdU) labelled cells in the mutant, resulting in a reduced telencephalon size. Additionally, it was shown that the reduction in progenitor cell proliferation was coupled with an early onset of neuronal differentiation: while E12.5 wildtype embryos showed a characteristic uniform layer of differentiated neurons on the surface of the telencephalon ventricular zone, the mutant embryos showed up to a 75% increase in the number of differentiated neurons (Xuan et al., 1995). Indeed, it was later shown that FoxG1 suppresses the generation of the earliest born neurons, the Cajal-Retzius (CR) cells, in the progenitor cells in the telencephalon (Hanashima et al., 2004). This was shown by a substantial increase in the number of reelin (CR cell maker) positive cells in the telencephalon of FoxG1 null mutant mice embryos. Thus, it is postulated that FoxG1 plays an important role in the continual proliferation and timing of neuronal differentiation in the telencephalic progenitor cells and consequently may play a role in determining the size of the telencephalon in vertebrates.

1.2.1. FoxG1 has different roles in the ventral and dorsal telencephalon

Importantly, Xuan et al. (1995) noted that in FoxG1 null mutant mice the ventral telencephalon was more severely affected than the dorsal telencephalon. In E12.5 mice embryos, the ventral telencephalon was severely reduced in size with the ganglionic eminence (the primordia of the basal ganglia) almost completely absent, while the dorsal telencephalon formed, although it was reduced in size. It was inferred that in the absence of FoxG1, the proliferation rate in the ventral telencephalon was significantly reduced compared to that in the dorsal telencephalon, resulting in the severe reduction of the ventral telencephalic tissue. Recent cell cycle kinetics studies showed, however, that while the there was a reduction in the progenitor cell cycle rate in the mutant dorsal telencephalon compared to wildtype embryos at E10.5 (in agreement with Xuan et al., 1995), there was no reduction in the proliferation rate in the ventral region of the

telencephalon (Martynoga et al., 2005). Rather, it has been suggested that there is no specification of the ventral telencephalon in the absence of FoxG1. Indeed, Xuan et al. (1995) and Martynoga et al. (2005) showed that the supposed ventral telencephalon region in FoxG1 mutant mice exhibited no markers characteristic to this region. This suggests that FoxG1 is required for the correct patterning of the ventral telencephalon while in the dorsal telencephalon it promotes the proliferation and inhibits neuronal differentiation of the cortical progenitor cells.

1.2.2. Alterations in dorsal telencephalic patterning in the absence of FoxG1

Muzio and Mallamaci (2005) have presented an alternative hypothesis and have argued that FoxG1 also plays a role in the patterning of the dorsal telencephalon. They argue that in the absence of FoxG1, the neocortical plate is missing and is substituted by the more caudal hippocampal plate. Thus, rather than interpreting the excess of the reelin positive, Cajal-Retzius neurons in the FoxG1 null mutant mice embryos as being a consequence of premature neuronal differentiation (Hanashima et al., 2004) these authors argue that this is a consequence of the neocortex being patterned as the hippocampal plate.

1.2.3. FoxG1 may regulate apoptosis

It was initially postulated that the hypoplasia of the telencephalon in FoxG1 null mutant mice embryos might be caused by an increase in the rate of apoptosis, as well as the early onset of neuronal differentiation. This was supported by previous work that showed that retroviral over-expression of FoxG1 in the avian embryo brain resulted in a significant decrease in neuroepithelium apoptosis (Ahlgren et al., 2003). However, the opposite was observed in E10.5 FoxG1 null mutant mice embryos, where the rostral region of the telencephalon showed a clear reduction in the number of apoptotic labelled cells compared to the wildtype embryos (Martynoga et al., 2005). These contrasting differences remain unexplained but may result from

a different ortholog (i.e. chicken vs mouse) mode of action or the different experimental techniques.

1.2.4. *Xenopus* FoxG1 has a dosage dependent effect on neuronal differentiation

In *Xenopus*, high doses (500pg) of *in vitro* transcribed *Xenopus* FoxG1 (XFoxG1) mRNA injected into one blastomere of two-cell stage *Xenopus* embryos, resulted in an expansion of the neural progenitor cells and the suppression of neuronal differentiation in the injected region – a similar effect to mouse FoxG1 (Bourguignon et al., 1998). Additionally, neuronal differentiation occurred adjacent to the injection region where cells expressed the XFoxG1 mRNA. However, a dosage effect was observed when XFoxG1 mRNA was injected into the embryos at low doses (90pg). In this case, there was an increase in neuronal differentiation and no expansion of the progenitor cell population in the injected region. This dosage effect indicates that high doses of FoxG1 promote cell proliferation and inhibit neuronal differentiation, while low doses have the opposite effect. This suggests that FoxG1 could act in a gradient dependent manner during telencephalon development – indeed, it has been suggested that a rostral^{high}-to-caudal^{low} FoxG1 gradient plays a fundamental in determining the early patterning of the mouse telencephalon (Muzio and Mallamaci, 2005). Despite these complexities, it is evident that FoxG1 plays a role in regulating the balance between neuronal progenitor proliferation and differentiation.

1.3. How does FoxG1 mediate its effect on progenitor proliferation and differentiation?

1.3.1. FoxG1 has transcriptional repressor properties

Insight into the potential activity of FoxG1 was initially uncovered through work done on the oncogene *qin* (Li and Vogt, 1993; Li et al., 1995; Li et al., 1997). *Qin* was isolated from the genome of avian sarcoma virus, found in connective tissue tumours in adult chickens, and is closely related to rat FoxG1, binding to the same DNA consensus sequence. *Qin* was shown to be a transcriptional repressor, inferring a similar role for FoxG1. Indeed, in *Xenopus laevis*,

XFoxG1 fused to a strong repressor domain mimicked the effect of wildtype XFoxG1 (Bourguignon et al., 1998). Additionally, however, XFoxG1 fused to an activator domain also mimicked the effect of wildtype XFoxG1, indicating that XFoxG1 may also act as a transcriptional activator. Furthermore in *Xenopus laevis*, XFoxG1 was shown to regulate $p27^{XIC1}$ – a cyclin-dependent kinase (cdk) inhibitor which causes cell cycle arrest by inhibiting cdk activity – in a dose-dependent manner, with a high or low dose suppressing or inducing its expression, respectively (Hardcastle and Papalopulu, 2000). Thus, XFoxG1 was implicated in controlling the cell cycle of *Xenopus* neural precursor cells through the regulation of a cdk inhibitor.

1.3.2. FoxG1 interacts with Groucho/TLE proteins to repress transcription

The transcriptional repressor activity of FoxG1 was also shown to act through a number of mechanisms in mammals. Firstly, FoxG1 was shown to interact with Groucho/transducin-like Enhancer of split (Gro/TLE) (Yao et al., 2001). Gro/TLE proteins have been shown to form repressor complexes that negatively regulate the differentiation of the telencephalon progenitor cells by inhibiting the expression of the proneural genes (normally expressed in cells that have been specified for a neuronal fate) (Yao et al., 2000). Gro/TLE proteins have no intrinsic DNA-binding activity, so FoxG1 acts as a corepressor by forming a complex with Gro/TLE and binding to the repressor domains of proneural genes. In a second complex, FoxG1 acts as an adaptor of repression by forming a complex with Hairy/Enhancer of split (Hes) and Gro/TLE, where Hes fulfils the DNA-binding function of the complex (Yao et al., 2001). The formation of these complexes was shown to be disrupted by Gro/TLE-related gene product 6 (Grg6) – promoting the differentiation of the telencephalic progenitor cells (Marçal et al., 2005). Additionally, FoxG1 was shown to associate with histone deacetylase 1, in an interaction probably mediated by TLE proteins, to repress proneural gene expression (Yao et al., 2001).

Thus, FoxG1 may act to inhibit neuronal differentiation in the developing telencephalon by interacting with Hes and Gro/TLE proteins to repress proneural genes.

1.3.3. FoxG1 disrupts the TGF-β signalling pathway to promote cell proliferation

Secondly, FoxG1 has also been shown to interact with the transforming growth factor-β (TGF-β) signalling pathway. The TGF-β pathway, which inhibits the proliferation of many types of epithelial cells, is expressed in the developing brain, indicating its role as an inhibitor of progenitor proliferation in this region (Pelting et al., 1991). TGF-β ligands bind to their cell surface receptor kinases, which then phosphorylate the cytoplasmic Smad protein specific to that receptor (Smad2/3), triggering an association with Smad4 and subsequent translocation into the nucleus. In the nucleus, the Smad complex interacts with a binding partner (e.g. FoxH, FoxO) and activates the transcription of cell proliferation inhibiting genes (Derynck et al., 1998). FoxG1 has been shown to disrupt the interaction between the binding partner, FoxH1 and the nuclear Smad complex (Dou et al., 2000), and associate with Smad2/3/4 to disrupt the formation of the Smad complex (Rodriguez et al., 2001). Additionally, FoxG1 was shown to disrupt the FoxO-associated TGF-β pathway by associating with Smad3/4 or FoxO3, specifically inhibiting the expression of another cell cycle arresting cdk inhibitor, p21Cip1 (Seoane et al., 2004). The FoxO-associated TGF-β signalling pathway specifically activates the expression of p21Cip1, which was shown to be up-regulated in mouse E10.5 telencephalon progenitor cells in the absence of FoxG1. Furthermore, the Carboxy (C)-terminal of FoxG1 was shown to mediate this disruption of the TGF- β signalling pathway. Thus, FoxG1 maintains the proliferative state of the progenitor cells in the developing telencephalon by disrupting the TGF-β signalling pathway and specifically, inhibits the expression of the cell cycle inhibitor, p21Cip1, in this region.

1.3.4. FoxG1 may be a regulator of BMP and FGF-8 growth factors

The patterns of expression of two growth factors in FoxG1 null mutant mice embryos indicated that FoxG1 may be involved in their regulation. Bone morphogenetic protein 4 (BMP4) has been shown to inhibit the proliferation of cortical progenitor cells (Li et al., 1998). BMP-induced signalling uses a similar mechanism to TGF-β signalling, but using Smad1/5/8 as the receptor-activated Smads (Derynck et al, 1998). In wildtype E11.5 mice embryos, the medial most region of the dorsal telencephalic neuroepithelium shows an absence of FoxG1 expression and high levels of BMP4 expression, while in the more lateral regions FoxG1 is highly expressed and BMP4 is absent. In the absence of FoxG1 the medial expression of BMP4 expands extensively into the lateral regions where FoxG1 is normally expressed, indicating that BMP4's inhibition of progenitor cell proliferation in the dorsal telencephalon may be directly or indirectly suppressed by FoxG1. Additionally, BMPs 2, 6, 7 exhibit similar ectopic expression patterns in FoxG1 null mutant mice (Hanashima et al., 2002). Due to the similarity of the signalling pathways, it may be that FoxG1 disrupts the BMP pathway in the same way as it does the TGF-β pathway, i.e. through a C-terminal mediated interaction (DNA-binding domain independent). Surprisingly, however, Hanashima et al. (2002) showed that ectopic BMP expression patterns in FoxG1 null mutant embryos were similar to the patterns in the FoxG1 DNA-binding domain defective mutant embryos, indicating that the DNA-binding capacity is required for BMP regulation.

Secondly, in the absence of FoxG1, mice E10.5 embryos showed a striking reduction in fibroblast growth factor 8 (FGF-8) expression in the rostral telencephalon compared to wildtype embryos (Martynoga et al., 2005). FGF-8 has been shown to be important for rostrocaudal patterning of the telencephalon (Fukuchi-Shimogori and Grove, 2001) and when ectopically expressed in the midbrain caused continual proliferation of the progenitor cells and prevented neurogenesis (Lee et al., 1997). Thus, it appears that FoxG1 may up-regulate the expression of FGF-8, stimulating the proliferation of the telencephalic precursor cells. Incidentally, Martynoga

et al. (2005) showed that BMP did not repress the expression of FGF-8 in FoxG1 null mutant embryos because the reduction in FGF-8 expression (E10.5) occurred before there was a change in the expansion of the BMP signalling components (E11.5).

1.4. FoxG1 proteins have three distinct domains

FoxG1 has been cloned from mammals (human, mouse, rat), chicken, *Xenopus laevis* and zebrafish. Additionally, the FoxG1 sequence is also available for chimpanzee from the completed genome project (*Pan troglodytes* NCBI map viewer release November 2004). However, the completed genome sequences for other available vertebrates, dog, (*Canis familaris,* NCBI map viewer release September 2005) and cow (*Bos taurus*, NCBI map viewer release October 2005) are incomplete at their respective FoxG1 loci. These FoxG1 orthologs share a highly conserved 110 amino acid DNA-binding domain – the defining characteristic of the winged-helix family of transcription factors. This DNA-binding domain is made up of three α-helices, three β-sheets and three loops (two long and one short); the α-helices form a central core and together with the wing-like extensions of the two long loops give this family its "winged-helix" name (Lai et al., 1993).

The FoxG1 orthologs also share a highly conserved 211 amino acid C-terminal domain; the two most distantly related orthologs, humans and zebrafish, share an amino acid conservation of 91% in this domain. In humans FOXG1 is grouped into class 1 (there are 43 FOX members grouped into 2 classes), as it contains a basic region in the C-terminal, the defining feature of this class (Katoh and Katoh, 2004). Lastly, the FoxG1 orthologs have an N-terminal domain that exhibits a large degree of variability. The initial 30 amino acid residues are highly conserved and contain a predicted Casein kinase 1 phosphorylation site that is conserved across all orthologs (T Regad and N Papalopulu, personal communication) (Fig. 1.1, arrowheads) Following this region, there is a divergent region that varies in length from 135 residues in humans to 67 residues in

zebrafish. The defining characteristic in the N-terminal is a low complexity region of histidine, proline and glutamine residues that is greatly extended in the mammalian orthologs (Fig. 1.1, solid line). Furthermore, there are glycine/alanine-rich regions that occur to a greater extent in the mammalian and chicken orthologs (Fig. 1.1, *).

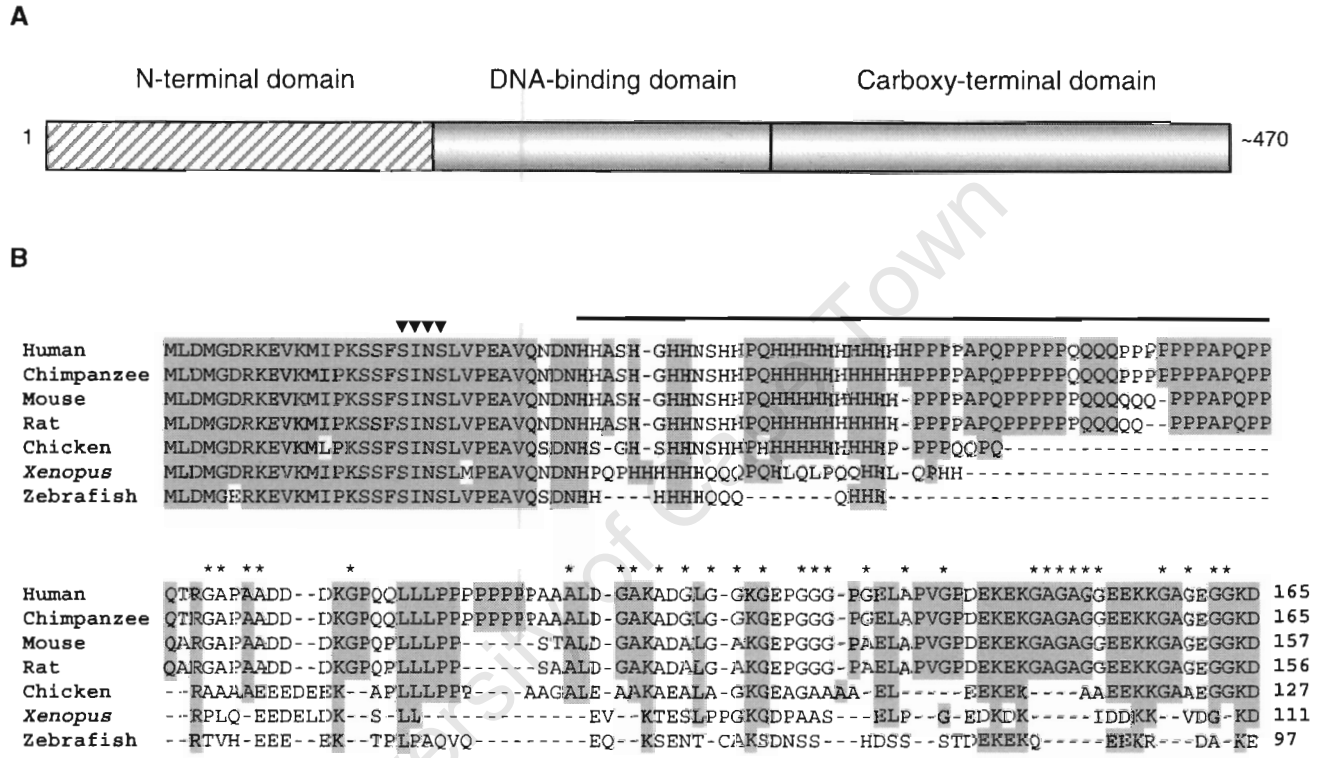

Figure 1.1. Protein domains and alignment of the N-terminal of sequenced FoxG1 orthologs. (A) General structure of the FoxG1 protein with the three domains indicated, the variable N-terminal domain is hatched and shown in **(B).** Notice the extended histidine, proline and glutamine region (solid line). Glycine/alanine-rich regions are shown (*). A predicted Casein kinase 1 phosphorylation site is shown (▼▼▼▼) (T Regad and N Papalopulu, personal communication). Shading homology is 80%, excluding gaps.

1.4.1. The DNA-binding and C-terminal domains mediate region-specific functions of FoxG1

The high homology across orthologs in the DNA-binding and C-terminal domains suggests that these domains may be under strong functional constraints. Indeed, it has been shown that the C-terminal domain is the region of the FoxG1 protein that associates with the Smads and Smad binding partners (FoxH1 and FoxO3) to disrupt the TGF-β signalling pathway (Dou et al., 1999;

Rodriguez et al., 2001; Seoane et al., 2004). The DNA-binding domain of FoxG1 is required to bind to the repressor domain of proneural genes allowing the FoxG1/TLE complex to inhibit their expression (Yao et al., 2001). Additionally, the DNA-binding domain may be important for FoxG1's down-regulation of the anti-proliferative BMPs in the telencephalon (Hanashima et al., 2002).

FoxG1 DNA-binding dependent and independent modes of action were shown to have region-specific activity in the developing mouse telencephalon. Hanashima et al. (2002) showed that an inducible DNA-binding defective FoxG1 protein could restore the growth of the dorsal telencephalon in E13.5 mice embryos, by improving the proliferation of progenitor cells. The "rescued" dorsal telencephalon was nearly equivalent to the size of the wildtype telencephalon. Conversely, the ventral telencephalon could not be rescued and showed the same phenotype as the FoxG1 null mutant embryo in this region. It was thus concluded that FoxG1 acts in a DNA-binding independent and dependent manner in the dorsal and ventral telencephalon, respectively.

The DNA-binding independent mode of action in the dorsal telencephalon was postulated to be as a result of FoxG1's disruption of the TGF-β signalling pathway, which is mediated by the C-terminal domain of FoxG1. The inability of the ventral telencephalon to be restored by the DNA-binding defective FoxG1 protein indicates that FoxG1 functions in a DNA-binding dependent manner in this region. It was inferred that the DNA-binding ability of FoxG1 is required to mediate its effect on cortical progenitor cell proliferation in the ventral telencephalon. However, in FoxG1 null mutant mice it was shown that the ventral telencephalon region did not exhibit any characteristic region specific markers and hence was deemed not to be specified in the absence of FoxG1 (Martynoga et al., 2005; Muzio and Mallamaci, 2005). Thus it appears that the DNA-binding dependent activity of FoxG1 may be required for the specification of the ventral telencephalon.

1.4.2. The N-terminal domain is not well characterized

The divergence of the N-terminal domain may account for the morphological variation in the size of the cerebral cortex in vertebrates. To date, there have been no published functional studies relating to the N-terminal domain. However, a phosphorylation site within the conserved first 30 amino acids in the N-terminal domain has recently been identified as important for the localization of FoxG1 to the nucleus – presumably regulating its transcriptional activity (T Regad and N Papalopulu, personal communication).

Previous work showed that when a high dose of mouse FoxG1 mRNA was injected into *Xenopus* embryos it resulted in a more severe effect compared to the equivalent *Xenopus* FoxG1 mRNA injection (N Illing and N Papalopulu, unpublished data). The embryos injected with a high dose of mouse FoxG1 mRNA showed a greater number of ruptured cells on the injected side, resulting in ruptured embryos, compared to embryos injected with an equivalent high dose of *Xenopus* FoxG1 mRNA Thus, it appears that constitutive expression of FoxG1 may affect cell survival, and that the effect may be more severe for mouse FoxG1 compared to *Xenopus* FoxG1. Due to the highly conserved DNA-binding and C-terminal it was postulated that the variable region in the N-terminal domain may be responsible for these different effects on cell survival. Thus, an initial test into the possible effect of the N-terminal domain was carried out in this study, by comparing the transfection efficiencies of mammalian, *Xenopus* and an HPQ deletion FoxG1 constructs in a neural precursor cell line.

1.5. Could FoxG1 be playing a role in the evolution of cortical size and complexity?

In addition to the above transfection studies, the N-terminal sequence from a spectrum of vertebrates was also investigated in this study. Vertebrates show a remarkable evolutionary increase in cortical size and complexity. Indeed, mammals have a six-layered neocortex structure that is a recent evolutionary acquisition not found in birds and reptiles (Fig. 1.2). Furthermore,

the distinguishing feature of mammalian brain morphology is the dramatic expansion of the cerebral cortex in primates compared to other mammals: while the relative thickness of the cortex differs by a factor of only 2 between mice and humans, there is a 1000-fold expansion in the surface area in humans compared to mice (Sultan, 2002). Even within the primate lineage the human brain is roughly three times the size of the chimpanzee brain, its closest relative, and 6-9 times the size of the macaque brain, a member of the most closely related non-ape primate lineage (Williams, 2002). Because the cortex is the site of higher cognitive functions, there is a general correlation across taxa between the level of cortex complexity and cognitive ability (Williams, 2002).

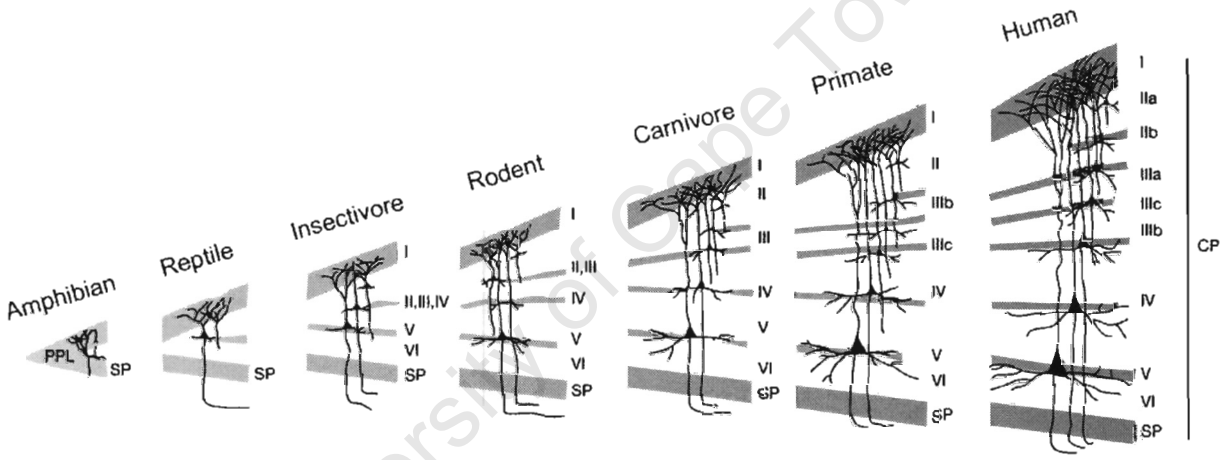

Figure 1.2. Differences in cerebral cortical size are associated with differences in the cerebral cortex circuit diagram. The cerebral cortex derives from two developmental cell populations: the primordial plexiform layer (PPL) and the cortical plate (CP). The primordial layer seems to be the same as simple cortical structures in amphibians and reptiles, and appears first temporally during mammalian brain development. The cortical plate develops as a second population that splits the primordial plexiform layer into two layers – layer I at the top and the subplate (SP) at the bottom. Cortical-plate-derived cortical layers are added developmentally from deeper first (VI, V) to more superficial last (III, II). Notice that cortical layers are progressively elaborated in mammals, for example, insectivores have a single layer II/III/IV that is progressively divided into II, III, IV, then IIa, IIb, and so on, in mammals with larger brains. (From Hill and Walsh, 2005).

It is probable that rates of proliferation and cell death during brain development are important determinants of mammalian brain size. Indeed, it has been shown that cortical neuronal progenitors in mice undergo 11 rounds of cell division (Kornack and Rakic, 1998) compared to 28 in the macaque (an Old World monkey) (Takahashi et al., 1995) and probably far more in

humans. This extended period of progenitor division in primates not only generates a larger cortex, but also adds novel neurons and layers to the cortex (Fig. 1.2; Hill and Walsh, 2005). The upper cortical layers, generated later in neurogenesis, are more developed in the primate cerebral cortex (Marin-Padilla, 1992) and specialized deep layer neurons are unique to primates (Allman et al., 2002) (Fig. 1.2).

Because FoxG1 regulates the proliferation of the dorsal telencephalic neural progenitors, it is possible that changes in FoxG1 function may account for these changes in cortical size and complexity. These postulated changes in FoxG1 function, if determined at a sequence level, may be derived from changes in the variable N-terminal domain, which shows distinct differences between the limited number of mammalian, *Xenopus* and zebrafish orthologs (Fig. 1.1). Thus, one of the aims of this study was to clone a range of vertebrate FoxG1 orthologs in order to correlate the changes in the sequence of FoxG1 with the expansion of the cerebral cortex across vertebrate evolution.

1.5.1. Adaptive evolution and FoxG1

The genetic basis for the increase in cortex size and neurogenesis complexity (Fig. 1.2) lies in three possible mechanisms of evolutionary change: (1) addition or subtraction of entire genes from the genome, (2) alterations in levels or patterns of gene expression, and (3) alterations in the coding sequence of genes (Hill and Walsh, 2005). While evidence exists for all of these possibilities, it is the last mechanism that has recently been of particular interest to researchers, as they attempt to identify specific genes whose evolution at the DNA sequence level may have contributed to the evolutionary expansion of the cortex in primates.

Genes that show changes in their coding sequence over the course of brain evolution – implicating them as a possible determinant of brain size – can be identified by comparing the

DNA changes that occur in closely related species, for example in primates. DNA substitutions that do not alter the amino acid sequence, because they occur at degenerate sites in the codon, are called synonymous mutations (for example, a CCA to CCG change is synonymous because both codons encode proline). Synonymous mutations are normally neutral because they do not alter the sequence and properties of the encoded protein and are often equated to the rate of neutral nucleotide substitution (Miyata et al., 1980). DNA substitutions that do alter the amino acid sequence are called non-synonymous mutations and are normally detrimental to protein function, and as such occur at a much lower rate than that of synonymous substitutions. In this case DNA changes are said to be subject to purifying (or negative) selection, the extent of which varies from gene to gene (Kimura, 1983). For some genes, however, the non-synonymous mutations that occur may be beneficial to protein function and, hence are maintained in future generations. In this case the DNA changes are said to be subject to positive selection or adaptive evolution. A ratio of non-synonymous (K_a) to synonymous (K_s) defines the selection characteristics of a certain protein and measures the pace of the evolution scaled to the mutation rate. For most proteins $K_a/K_s << 1$, where the K_a substitution rate is very small compared to K_s, indicating that non-synonymous changes are detrimental. Conversely, $K_a/K_s > 1$ indicates that the K_a substitution rate is greater than the K_s substitution rate, signifying that the non-synonymous substitutions are beneficial and thus subject to positive selection or adaptive evolution.

In order to examine if genes involved in brain development and function were indeed targets of positive selection – and therefore potential determinants of brain size – a broad-level study compared the K_a/K_s ratios of 214 nervous system genes and 95 housekeeping genes (Dorus et al., 2004). These ratios were compared in primates, between macaques and humans, and in rodents, between mice and rats. It was shown that brain/nervous system related genes showed more evidence of positive selection between macaques and humans than between mice and rats – indicating a possible reason for the increase in neural complexity in humans. More specifically,

certain genes that are fundamental in cerebral cortex development have been shown to be under positive selection in the lineage leading to humans. Abnormal spindle-like microcephaly associated (ASPM) and microcephalin genes are mutated in the human disease primary microcephaly, characterized by a severely reduced cerebral cortex (Mochida and Walsh, 2001; Dobyns, 2002; Jackson et al., 2002; Bond et al., 2002 and 2003). Studies in the primate lineage showed that both these genes were under positive selection and thus were major determinants of the expanded brain size in humans. ASPM shows a K_a/K_s ratio of 1.44 from the chimpanzee-human ancestor lineage to the human lineage and microcephalin shows a ratio of 1.05 from the entire simian lineage to the human lineage (Kumar et al., 2002; Evans et al., 2004a and 2004b; Ponting and Jackson, 2005). Furthermore, ASPM and microcephalin both have genetic variants that arose ~5800 and ~37000 years ago respectively, which have been shown to be under strong positive selection and are thus represented at a high frequency across the world's population (Evans et al., 2005; Mekel-Bobrov et al., 2005).

Due to the role of FoxG1 in regulating the development of the dorsal telencephalon, from which the cerebral cortex develops, it was initially postulated that it may exhibit characteristics of positive selection in the lineage leading to humans. Furthermore, a recent study showed that a human patient with mental retardation, brain malformations and microcephaly carried a FOXG1 gene that was affected by a 720 bp inversion near its locus on chromosome 14q12 (Schoichet et al., 2005). The similar FoxG1 and APSM/microcephalin mutant phenotypes added further weight to the suggestion that positive selection may be acting on FoxG1. Thus, one of this study's aims was to determine whether FoxG1 exhibits the characteristic signatures of positive selection – rendering it as a determinant of the expanded cortex size in humans.

Another mechanism for the evolutionary change in brain size is the addition or duplication of genes in the human genome. Two forms of human FOXG1, A and B, were reported to be

clustered on chromosome 14q11-13 (Wiese et al., 1995). Thus, another one of the aims of this study was to investigate if this FOXG1 duplication in humans had a role in determining the increased cortex size in humans.

1.6. Sub-cellular localization of FoxG1

Work on FoxG1 has primarily focussed on its effect on progenitor proliferation and neuronal differentiation as well as the mechanisms mediating these effects. To date however, no work has been published on how FoxG1 may be regulated spatially. This has been the focus of current work that shows that the sub-cellular localization of FoxG1 is influenced by various factors such as Casein kinase 1 and fibroblast growth factor (FGF) signalling (T Regad, M Roth, N Bredenkamp, N Illing and N Papalopulu, manuscript in preparation). While phosphorylation of FoxG1 by Casein kinase 1 targets it to the nucleus, phosphorylation by FGF signalling promotes its nuclear export – indicating mechanisms that control the transcriptional activity of FoxG1. Furthermore, it appears that when FGF is ectopically expressed in the developing *Xenopus* brain, the nuclear export of FoxG1 in the neural progenitor cells, correlates with an increase in neurogenesis (T Regad and N Papalopulu, personal communication). This may suggest that in order for neural progenitors to differentiate, the nuclear activity of FoxG1 is down-regulated by exclusion from the nucleus – in agreement with the cell proliferation promoting activity of FoxG1.

Studies in a mouse olfactory precursor cell line, OP27, showed that exposure to FGF-2 promoted neuronal differentiation (Shoko et al., manuscript under review). In this study it was investigated whether the FGF-2 induced change in the differentiation state of the OP27 cells could be correlated with any changes in FoxG1 sub-cellular localization, confirming the above observations of the effect of ectopic FGF expression *Xenopus* brain (T Regad and N Papalopulu, personal communication).

1.7. Study aims

In summary, the aims of this study were to:

1. Characterize the variation in the N-terminal sequence of FoxG1 orthologs across vertebrates.
2. Determine whether FoxG1 is under positive selection, implicating it as a candidate gene playing a role in the increase in cerebral cortex size across vertebrates.
3. Investigate whether differences in the N-terminal region translate into differences in transient transfection efficiencies between mouse and *Xenopus* orthologs.
4. Investigate whether there are changes in sub-cellular localization of FoxG1 in the neural precursor cell line, OP27, in response to FGF-2 induced differentiation.

CHAPTER 2

FoxG1 sequence and selection analysis

2.1. Introduction

2.1.1. Characterizing FoxG1 sequence across vertebrates

FoxG1 orthologs from a spectrum of vertebrates were cloned and sequenced to test the hypothesis that changes in the coding sequence of FoxG1 might play a role in the evolution of the forebrain in vertebrates. FoxG1 sequence information was available in public databases for the model organisms human, mouse, rat, chicken, *Xenopus* and zebrafish, and for chimpanzee, from the completed genome sequence (*Pan troglodytes,* NCBI map viewer release November 2004) (Fig. 2.1). Conversely, the completed genome sequences for other available vertebrates, dog, (*Canis familaris,* NCBI map viewer release September 2005) and cow (*Bos taurus*, NCBI map viewer release October 2005) were incomplete at their respective FoxG1 loci. The available FoxG1 orthologs share a highly conserved 110 amino acid DNA-binding domain; across all orthologs there are only 4 amino acids that exhibit any divergence in this domain. Additionally, these FoxG1 orthologs have a C-terminal domain that is also highly conserved. For example, at the amino acid level, the identity between *Xenopus* and human (the two most distantly related available orthologs) is 91% and between mouse and human (two closely related available mammalian orthologs) is 99.5%. The only variable region of FoxG1 is the N-terminal domain, which shows a remarkable expansion of histidine, proline and glutamine residues that is especially evident in mammals. FoxG1 was therefore cloned from nine new vertebrates to characterize the variability in the sequence of the N-terminal domain across a number of vertebrates.

Mammalian organisms were selected to represent a spread across evolutionary relationships according to a mitochondrial gene derived-tree in Arnason et al., 2002 (Fig. 2.1). Because FoxG1

mammalian orthologs were only available for primates and rodents, orthologs were cloned during this study from mammalian taxa that are more distantly related to primates than rodents to primates (namely zebra, rhinoceros and two species of bat) generating an evolutionary spread of FoxG1 sequence information (Fig. 2.1). Additionally, three reptiles – tortoise, crocodile and lizard – were selected to represent a vertebrate class that previously had no FoxG1 members. During telencephalon development there are molecularly defined regions in amphibians, reptiles and birds that are analogous to the developing telencephalon of mammals (Smith Fernandez et al., 1998). It is in these regions that FoxG1 plays a role in regulating progenitor cell proliferation and differentiation. However, adult reptiles lack the six-layered neocortex structure of mammals that develops from the dorsal pallium (Fig. 1.2). Furthermore, the argument over reptilian phylogeny has historically been based on two characteristics, skull morphology versus physiology/external surface (Ridley, 2004). Thus, it was examined if coding differences in FoxG1 might account for the difference in structure of the reptilian forebrain within reptiles and, compared to mammals. FoxG1 was therefore cloned from three phylogenetically important reptile groups (crocodiles, turtles/tortoises and squamates (lizard)) to provide insight into the evolution of FoxG1 within this vertebrate class.

2.1.2. FoxG1 as a determinant of forebrain size in humans

Recent evidence has suggested that the increased cortex size in humans may be as a result of the accelerated adaptive evolution of certain genes, such as ASPM and microcephalin, which determine the size of the human brain (Kumar et al., 2002; Dorus et al., 2004; Evans et al., 2004a and 2004b). Mutations in these two genes in humans result in primary microcephaly, characterized by the severe reductions in brain size, particularly the cerebral cortex (Mochida and Walsh, 2001; Dobyns, 2002; Jackson et al., 2002; Bond et al., 2002 and 2003). Because FoxG1 is an important regulator of cerebral cortex development and mutant expression in a human patient resulted in a phenotype of brain malformations and microcephaly (Shoichet et al.,

2005), it was hypothesized that FoxG1 may show evidence of adaptive evolution in the lineage leading to humans. Selection analysis was performed by comparing primate and human FoxG1 selection rates in order to determine if FoxG1 exhibited characteristics of adaptive evolution.

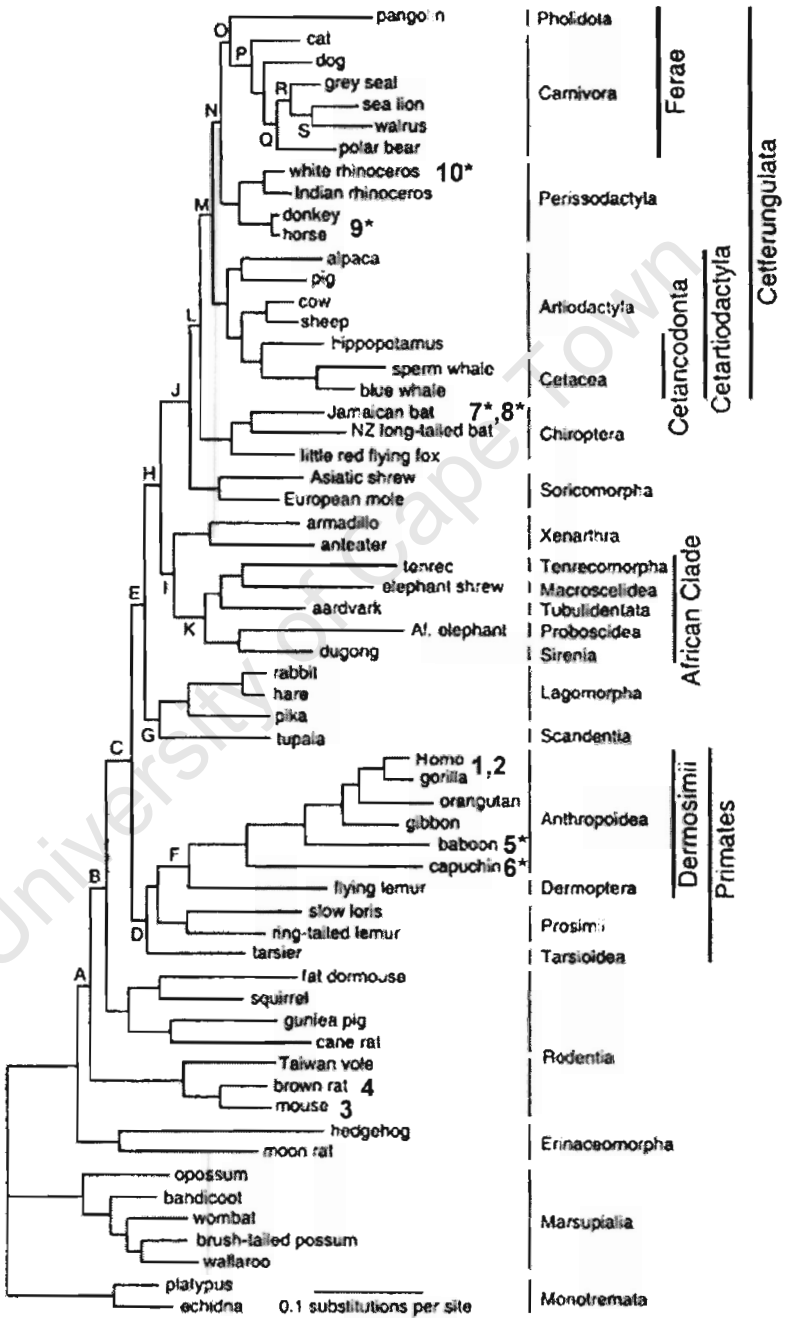

Figure 2.1. Maximum likelihood tree showing mammalian evolutionary relationships based on protein-coding mitochondrial genes (from Arnason et al., 2002). Numbers without * indicate organisms or closely related organisms for which FoxG1 sequences were available: (1) human, (2) chimpanzee, (3) mouse and (4) rat. Numbers with * indicate organisms or closely related organisms for which FoxG1 sequences were obtained during this study: (5*) Vervet monkey (Old World monkey), (6*) White-throated capuchin (New World monkey), (7*) Rusty bat (microbat), (8*) Fruit bat (megabat), (9*) Burchell's zebra and (10*) White rhinoceros.

Gene duplication has been well documented as a driving force behind morphological variation (Carroll, 2005). Since Wiese et al. (1995) reported that FOXG1 had been duplicated in humans with FOXG1A and FOXG1B clustering on chromosome 14, the hypothesis that the increased cortex size in humans may be as result of this duplication, was investigated. It was sought to determine at which point during vertebrate evolution this duplication occurred, in order to establish if it played a role in determining cortex size in humans. For example, if the duplication event occurred subsequent to the split of humans from the primate lineage, then FoxG1 may be a factor responsible for the enlarged human cortex.

2.2. Materials and Methods

2.2.1. Extraction of total RNA and first strand cDNA synthesis

Total RNA was extracted from 100mg of Old World Monkey (Vervet Monkey, *Chlorocebus pygerythrus*) and Nile Crocodile (*Crocodylus niloticus*) forebrain tissue using Tri Reagent according to the manufacturer's protocol (Molecular Research Centre). Vervet monkey brain tissue was obtained from the Diabetes/Primate Research Unit, Medical Research Council, Cape Town, South Africa; Nile crocodile brain tissue was obtained from Le Bonheur Crocodile Farm, Paarl, South Africa. RNA integrity was verified on a 1% formaldehyde agarose gel and quantified by measuring the absorbance at 260nm. Reverse transcription (RT) was performed with an additional heat denaturation step to obtain full-length 5' cDNAs (method adapted from Hüttemann, 2002). A mixture of 5µg of total RNA, 20U Ribonuclease inhibitor (Roche), 2mM dNTPs, 250ng random hexamer primer, 250ng oligo (dT) primer and nuclease-free H_2O (to 17.25µl) was denatured at 80°C for 3 minutes and snap-cooled on ice for 2 minutes. Next, 1× First-strand buffer (50mM Tris-HCl pH 8.3, 75mM KCl, 3mM $MgCl_2$, 10mM DTT), 2.5µg BSA and 300U M-MLV Reverse Transcriptase (Promega) were added and the mixture was incubated at 42°C for 90 minutes, denatured at 85°C for 3 minutes and snap-cooled on ice for 2 minutes.

An additional 200U of M-MLV Reverse Transcriptase was then added and the mixture was incubated at 42°C for 60 minutes and heat inactivated at 75°C for 10 minutes.

2.2.2. Extraction of genomic DNA

2.2.2.1. Genomic DNA extraction from tissue

Genomic DNA was extracted from various tissue samples: Rusty Bat (microbat, *Pipistrellus rusticus*) and Gambian Epauletted Fruit Bat (megabat, *Epomophorus gambianus*) wing punctures, Cape Lizard (*Agama attra*) liver and Burchell's Zebra (*Equus burchelli*) skin fibroblast cell line. These tissues were obtained from: David Jacobs (Department of Zoology, University of Cape Town) – bat punctures; Ingrid Baumgarten (Division of Chemical Pathology, University of Cape Town) – zebra cell line; Nicola Illing (Department of Molecular and Cell Biology, University of Cape Town) – lizard liver. Tissue samples were suspended in 300-500µl hexadecyl-trimethylammonium bromide (CTAB) buffer (100mM Tris pH 8, 1.4M NaCl, 20mM EDTA, 0.2% β-Mercaptoethanol (v/v), 2% CTAB (w/v) and digested with 100µg/ml Proteinase K for 1 hour at 60°C. The aqueous phase was sequentially extracted by centrifugation (13000 rpm for 5 minutes in a bench-top centrifuge) using an equal volume of chloroform, then phenol (pH 8):chloroform:isoamyl alcohol (25:24:1) and finally, chloroform:isoamyl alcohol (49:1). The DNA was precipitated by centrifugation (13000 rpm for 30 minutes in a bench-top centrifuge) using 0.3M sodium acetate (pH 5.2) and desalted with 2 volumes of 100% ice-cold ethanol, air-dried and then resuspended in nuclease-free H_2O containing RNase A (100µg/ml). DNA integrity was verified on a 1% agarose gel and quantified by measuring the absorbance at 260nm. Geometric Tortoise (*Psammobates geometricus*) and White Rhinoceros (*Ceratotherium simun*) genomic DNA was obtained from Dr. Colleen O'Ryan (Department of Molecular and Cell Biology, University of Cape Town).

2.2.2.2. Human and primate buccal cell genomic DNA extraction

Human (Caucasian male) and New World Monkey (White-throated Capuchin, *Cebus capucinus*) buccal cells were collected on cotton swabs by vigorously rubbing the inside of the cheeks. Capuchin swabs were taken at Monkey Town, Somerset West, South Africa. The swabs were incubated in a lysis solution (30mM NaCl, 10mM EDTA, 1% SDS (w/v)) for 5 hours and then squeezed out and removed. Proteinase K was then added (100µg/ml) and the solution was incubated at 56°C overnight. Salt-saturated 6M NaCl (0.5× lysis solution volume) was added and the remaining cotton sediment was pelleted by centrifugation (13000 rpm for 15 minutes in a bench-top centrifuge). The supernatant was mixed with ice-cold isopropanol (2× lysis solution volume) and the DNA was precipitated by incubation at -20°C for 1 hour and then centrifugation (13000 rpm for 10 minutes). The DNA pellet was then washed twice with 70% ethanol, air-dried and re-suspended in nuclease-free H_2O containing RNase A (100µg/ml). DNA integrity was verified on a 1% agarose gel and quantified by measuring the absorbance at 260nm.

2.2.3. PCR amplification of FoxG1 orthologs

Approximately 500ng of first strand cDNA or 50-100ng of genomic DNA was used as a template in the following standard 20µl reaction mix: 1× Expand High Fidelity Buffer, 1.5mM $MgCl_2$, 0.8mM dNTPs, 1µM of each primer, 1.2M betaine and 2.1U Expand High Fidelity Enzyme Mix (Roche). Because the N-terminal domain has a high GC content (around 70% in some orthologs) betaine (N,N,N-trimethylglycine) was added to the PCR reactions to destabilize the secondary structures that formed in this region (Henke et al., 1997). The full-length coding region for each ortholog was amplified using BF15'start and BF13'FL primers (Table 2.1, Fig. 2.2). The PCR cycling conditions were as follows: 95°C for 3 minutes (1 cycle), 95°C for 30 seconds, 52°C for 30 seconds, 72°C for 2 minutes (35 cycles) and 72°C for 5 minutes (1 cycle). To amplify the 5' end of human FOXG1 the same reaction mix and cycling conditions were used with BF15'start and BF15'R (Table 2.1) primers with an elongation time of 1:30 minutes. To

amplify the A and B form of human FOXG1 the same reaction mix was used with 0.5μM of FOXG1hAf or FOXG1hBf and FOXG1hA/Br primers (Table 2.1, Fig. 2.7). The PCR cycling conditions were as follows: 95°C for 3.5 minutes (1 cycle), 95°C for 30 seconds, 60°C or 65°C for 1 minute, 72°C for 1:30 minutes (30 cycles) and 72°C for 5 minutes (1 cycle). All PCR was performed using a PE Biosystems GeneAmp PCR System 9700 machine.

Table 2.1. Details of FoxG1 specific primers used in this study.

Primer name	Target gene	Primer sequence (5' - 3')	T_m (°C)
1. FoxG1 ortholog cloning			
BF15'start	FoxG1	GTGATG(CT)TGGA(CT)ATGGG(AG)GA(TA)AG (with BF15'R, forms primer pair (iii) in Fig. 2.7)	57 – 70
BF13'FL	FoxG1	GGTGTAAAA(CT)GTTCACTTACAGTCTG	58 or 60
BF1700F	FoxG1	TACCG(CG)GAGAACAAGCAGG	61 or 62
BF15'R	FoxG1	GGGTCIA(AG)CATCCAGTAGTT	56 or 59
FOXG1hAf	Human FOXG1A	GTTGTTCCGCCGCGCACGCA (with FOXG1hA/B, forms primer pair (i) in Fig. 2.7)	77
FOXG1hBf	Human FOXG1B	ACGGGGCTAAAGCGGACGGGCTG (with FOXG1hA/B, forms primer pair (ii) in Fig. 2.7)	76
FOXG1hA/Br	Human FOXG1A/B	GCGCTCATGGACGTGCTGCTCTGC	76
2. Monkey and crocodile RACE primers			
MBF1gsp1	Monkey FoxG1	GAGTGGTTGTTGCCCAGCGAGTTTG	72
MBF1gsp2	Monkey FoxG1	CCTCCACCGGCCTCACCTTCATG	73
MBF1ngsp1	Monkey FoxG1	TCAACACGGAGCTGTAGGGCATGG	71
CBF1gsp1	Crocodile FoxG1	GAGTTACAATGGCACCACGTCCGCCTACC	75
CBF1gsp2	Crocodile FoxG1	GCGCTGCTGCTGTGAGGTGATGAGTG	75
CBF1ngsp1	Crocodile FoxG1	GCGTAAGGTATCTCTCCATTGACTAGTC	63

Table notes:
1. All primers designed during this study.
2. Degenerate bases are shown in brackets.
3. I – Inosine.
4. T_m (melting temperature) calculated using nearest-neighbour thermodynamic values methods (Breslauer et al., 1986).

2.2.4. Rapid Amplification of cDNA ends (RACE)

Approximately 1µg of total forebrain RNA (Vervet monkey and Nile crocodile) was used to prepare 5' and 3' RACE-Ready first strand cDNA according to the manufacturer's protocol (SMART RACE cDNA Amplification Kit, BD Biosciences). For 5' cDNA synthesis a number of protocol modifications were performed in separate reactions: pre-synthesis incubation temperature was increased from 70°C to 80°C, the synthesis reaction temperature was increased from 42°C to 52°, and 1M betaine (Sigma) was added to the synthesis reactions (at 42°C and 52°C). Sequence that was generated from the monkey and crocodile FoxG1 cDNA clones (Section 2.2.3) were used to design gene specific primers for RACE PCR. Monkey primers MBFgsp1, MBFgsp2 and MBF1ngsp1 (nested) and crocodile primers CBF1gsp1, CBF1gsp2 and CBF1ngsp1 (nested) were designed (Table 2.1) and used in RACE PCR. For 5' RACE, the primary PCR product was diluted 1:50 and used in nested RACE PCR. All RACE PCR reactions were performed using the BD Advantage 2 PCR Enzyme System (BD Biosciences) according to the manufacturer's protocol. While the 3' RACE was successful, the 5' RACE was unsuccessful for both the monkey and crocodile.

2.2.5. Ligation of FoxG1 PCR-amplified fragments into pGEM-T Easy and transformation into *E. coli*

PCR products were resolved on a 1% low melting point agarose gel, excised and purified using the GenClean Kit according to the manufacturer's protocol (BIO101). Purified DNA was ligated into the pGEM-T Easy vector according to the manufacturer's protocol (Promega). For each ligation experiment a positive control (kit-supplied insert DNA) and a background control (no insert) were performed. The ligation mix was transformed into *E. coli* XL1-Blue competent cells (Chung et al., 1989). Initial positive transformants (white colonies) were screened by β-galactosidase insertional inactivation and ampicillin resistance on Luria agar plates supplemented with 0.5mM IPTG, 80µg/ml X-Gal and 100µg/ml ampicillin.

2.2.6. Screening transformants for correct inserts

Random white colonies were screened by PCR using either the overnight culture or mini-preparation purified plasmid as template. Plasmid insert sizes were screened using SP6 and T7 primers in the following 20µl PCR reaction: 10ng plasmid or 1µl overnight culture as template, 1× Supertherm buffer, 1.5mM $MgCl_2$, 0.8mM dNTPs, 0.5µM of each primer and 0.5U Supertherm Taq DNA polymerase (Southern Cross Biotechnology). The PCR cycling conditions were as follows: 94°C for 3 minutes (1 cycle), 94°C for 30 seconds, 52°C for 30 seconds and 72°C for 1-2 minutes (30 cycles) and 72°C for 5 minutes (1 cycle). Selected positive clones were then purified, using the High Pure Plasmid Isolation Kit according to the manufacturer's protocol (Roche), quantified by measuring absorbance at 260nm and sequenced.

2.2.7. Sequencing FoxG1 orthologs or fragments cloned into the pGEM-T easy vector

Sequencing was performed in both directions using vector-specific primers (M13F and M13R) and gene specific primers to complete or verify sequence information. The sequencing strategy for full-length FoxG1 orthologs is described in Fig. 2.2. Sequencing was performed on a MegaBACE 1000 DNA Sequencing System in the Department of Molecular and Cell Biology, University of Cape Town.

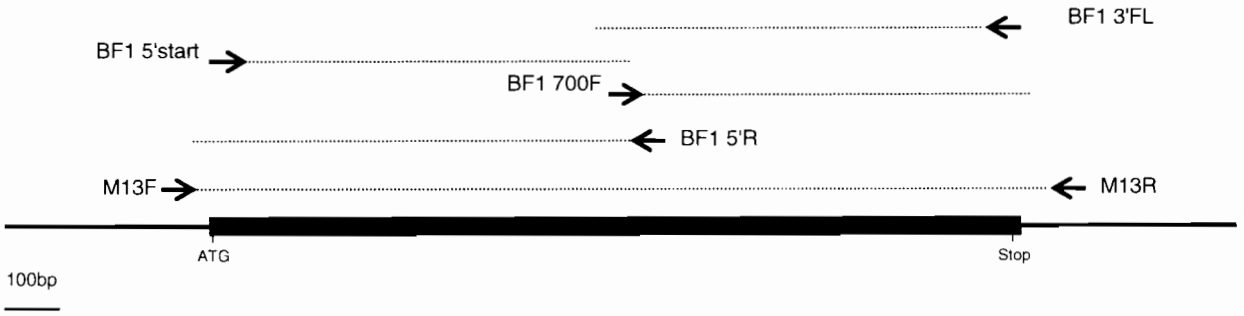

Figure 2.2. Sequencing summary for full-length FoxG1 orthologs. Six primers (arrows) as described in Table 2.1 were used to complete and confirm the sequencing of full-length FoxG1 orthologs that were cloned into the pGEM-T easy vector. The primers generated sequence fragments (dashed lines) which were then assembled into the full-length sequence (thick black line). M13F and M13R are the vector (thin black line) specific primers that were used. The position of the start (ATG) and stop codons are shown. Sequencing reactions contained 1.2M betaine.

2.2.8. Bioinformatic analysis of FoxG1 orthologs

2.2.8.1. FoxG1 sequences

FoxG1 orthologs were obtained from GenBank: Human (*Homo sapiens*) FOXG1A X74143, FOXG1B NM_005249 and X74142, FOXG1C X74144; Chimpanzee (*Pan troglodytes*) XM_522813; Mouse (*Mus musculus*) NM_008241; Rat (*Rattus rattus*) NM_012560; Chicken (*Gallus gallus*) NM_205193; *Xenopus laevis* AF101387; zebrafish (*Danio rerio*) NM_131067. FoxG1 orthologs sequenced in this study have been submitted to Genbank with the following accession numbers (release date 1 June 2006): White-throated capuchin DQ387961, Vervet monkey DQ387962, Rusty bat DQ387963, Gambian Epauletted Fruit Bat DQ387964, Burchell's zebra DQ387965, White rhinoceros DQ387966, Nile crocodile DQ387967, Geometric tortoise DQ387968 and Cape lizard DQ387969.

2.2.8.2. Phylogenetic analysis

Sequence alignments were performed with ClustalX 1.83 (Thompson et al., 1997) by first aligning mammal and non-mammal orthologs separately and then using the profile alignment function to align the two groups. Sequence alignment manipulation and analysis was performed using BioEdit 7.0.2 (Hall, 1999). The FoxG1 maximum likelihood phylogenetic tree was constructed from the in-frame nucleotide alignment using the DNAML program, the bootstrap test (1000 replicates) was performed using the SEQBOOT program and lastly, the consensus tree was derived using the CONSENSE program. These three programs were obtained from the Phylogeny Inference Package (Phylip) 3.63 (Felsenstein, 2004). The consensus tree was viewed using TreeView 1.6.6.

2.2.8.3. Selection analysis

Selection (K_a/K_s) analysis was performed using the Pamilo-Bianchi-Li method (Pamilo and Bianchi, 1993; Li, 1993) in the MEGA3 program (Kumar et al., 2004). Amino acid orthologs

were aligned and then converted into the corresponding nucleotide alignment (generating an in-frame alignment), any codon gaps were then deleted and the selection analysis was performed. This selection analysis technique was first verified by independently repeating the analysis performed in Dorus et al., 2004 (Table 2.2). The percent difference column, representing the difference between K_a/K_s values from the reference and those obtained in this study, ranged from 0.0 to a maximum difference of 2.9% – indicating that the selection analysis technique used in this study was sound.

Table 2.2. Verification of K_a/K_s selection analysis technique.

	Gene	Primate			Rodent		
		Ref. K_a/K_s[a]	Own K_a/K_s[b]	Percent difference[c]	Ref. K_a/K_s[a]	Own K_a/K_s[b]	Percent difference[c]
	Neutral Evolution						
1	Calmodulin 1	0.000	0.000	0.0	0.010	0.010	0.0
3	Inhibitor of DNA Binding 2	0.132	0.134	1.5	0.089	0.089	0.0
4	Neuropeptide Y	0.093	0.095	2.2	0.125	0.125	0.0
2	Ribosomal Protein L27a	0.286	0.286	0.0	0.017	0.017	0.0
5	Sialyltransferase 8B	0.069	0.068	1.4	0.041	0.040	2.4
	Faster Evolution in primates						
6	Adenylylcyclase-activating Peptide 1	0.655	0.673	2.7	0.178	0.178	0.0
7	GDP Dissociation Inhibitor 1	0.035	0.034	2.9	0.000	0.000	0.0
8	Glutamate Receptor, Ionotropic, N-Methyl-D-Aspartate, Subunit 2A	0.127	0.127	0.0	0.043	0.043	0.0
9	LIM Homeo Box Gene 1	0.080	0.080	0.0	0.014	0.014	0.0
10	Sonic Hedgehog	0.319	0.319	0.0	0.129	0.129	0.0

[a] Reference (Ref.) values derived in Dorus et al., 2004.
[b] Values derived in this study, using the same sequences as the reference study, as a means of verifying the K_a/K_s analysis technique, using the MEGA3 software.
[c] Difference between the values obtained in this study and the Dorus et al., 2004 reference values.

2.2.8.4. Analysis of FoxG1 3' untranslated region (UTR)

The 3' UTR sequences were obtained from: reference mRNA sequences (human, mouse, rat, Xenopus and zebrafish), genome sequences (chimpanzee and dog) and, 3' RACE cloning during

this study (Vervet monkey and crocodile). While the dog FoxG1 sequence is incomplete within the coding region, there is sequence available for the 3' UTR, allowing it to be included in the analysis. Secondary structures in the 3' UTR of FoxG1 orthologs were predicted using RNAstructure 4.2 (at 37°C) (Mathews et al., 2004). In order to test the robustness of the secondary structure prediction, random sequences were generated in DNAMAN according to the base composition and length of the 3' UTR of FoxG1 orthologs. MicroRNA (miRNA) site prediction was performed using the PicTar algorithm (Krek et al., 2005). This program aligns the 3' UTRs of human, chimpanzee, rat, mouse, dog and chicken and then checks for conserved potential microRNA binding sites.

2.3. Results

2.3.1. FoxG1 ortholog cloning

2.3.1.1. New FoxG1 orthologs

The FoxG1 DNA-binding and C-terminal domains are highly conserved; in the most distantly related available orthologs, zebrafish and human, there are only 21 differences out of 323 amino acid residues. In comparison, the N-terminal domain is more variable across vertebrates. In order to analyze this variability more comprehensively, 9 new FoxG1 orthologs, 6 mammals (New and Old world monkey, 2 species of bat, rhinoceros, and zebra) and 3 reptiles (tortoise, crocodile and lizard) were cloned. This was achieved by PCR using a universal FoxG1 primer pair targeted to the conserved regions spanning the start codon and in the 3' UTR. Old World monkey and crocodile orthologs were cloned by RT-PCR (due to the availability of fresh brain tissue) while all other orthologs were cloned from genomic DNA (Fig. 2.3).

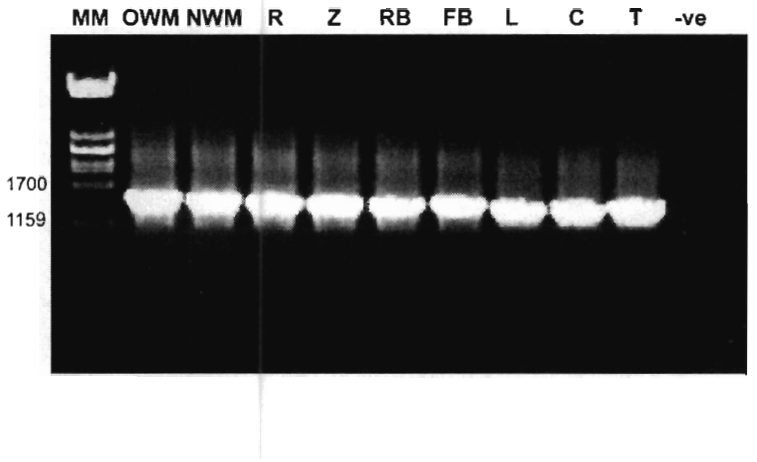

Figure 2.3. New full length FoxG1 orthologs amplified by PCR. Universal BF13'FL and BF15'start primers (Table 2.1, Fig. 2.2) were used to amplify nine new FoxG1 orthologs that showed an average size of ~1450 bp. MM: λDNA/*PstI* molecular marker (applicable fragment sizes (bp) are shown), OWM: Old World monkey (Vervet monkey), NWM: New World monkey (White throated Capuchin), R: Rhinoceros, Z: Zebra, RB: Rusty bat (microbat), FB: Fruit bat (megabat), L: Lizard, C: Crocodile, T: Tortoise, -ve: negative PCR control (water used as template).

Nucleotide sequence generated for each new ortholog was translated and aligned with existing FoxG1 orthologs (Fig 2.4). As expected, the DNA-binding and C-terminal domains were highly conserved across all orthologs while the N-terminal domain was variable. The source of the divergence between FoxG1 orthologs is primarily the N-terminal domain. This domain is conserved within mammals and chicken/reptiles, but shows variability between these two groups and between *Xenopus* and zebrafish orthologs. For example, in the primate lineage, the N-terminal domain of the human ortholog shows no difference, 1 difference (position 73) and 2 differences (position 87 and 113) in amino acid residues compared to chimpanzee, Old World monkey and New World monkey, respectively. The most distantly related mammalian orthologs, human and mouse, show 10 differences and 10 human insertions in the N-terminal domain, but still exhibits a relatively high amino acid identity of 88%. In the non-mammalian N-terminal domain, chicken and reptiles (crocodile, lizard and tortoise) share amino acid identities of 65-77% and 39-46%, among themselves and between *Xenopus* and zebrafish, respectively. Between mammals and non-mammals, amino acid identities in the N-terminal range from 31% to 57%.

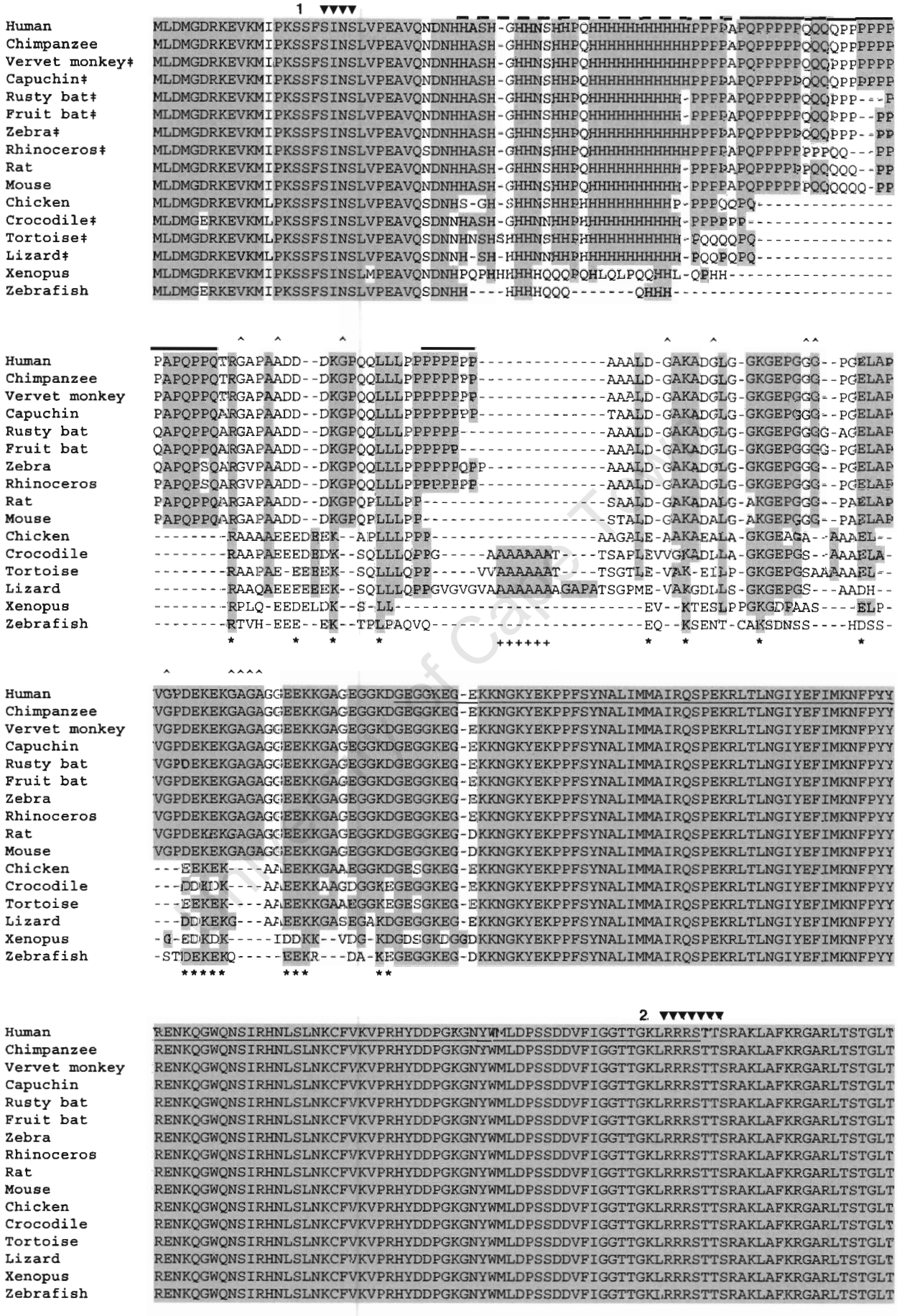
1
2
Human
Chimpanzee
Vervet monkey‡
Capuchin‡
Rusty bat‡
Fruit bat‡
Zebra‡
Rhinoceros‡
Rat
Mouse
Chicken
Crocodile‡
Tortoise‡
Lizard‡
Xenopus
Zebrafish
Human
Chimpanzee
Vervet monkey
Capuchin
Rusty bat
Fruit bat
Zebra
Rhinoceros
Rat
Mouse
Chicken
Crocodile
Tortoise
Lizard
Xenopus
Zebrafish
Human
Chimpanzee
Vervet monkey
Capuchin
Rusty bat
Fruit bat
Zebra
Rhinoceros
Rat
Mouse
Chicken
Crocodile
Tortoise
Lizard
Xenopus
Zebrafish
Human
Chimpanzee
Vervet monkey
Capuchin
Rusty bat
Fruit bat
Zebra
Rhinoceros
Rat
Mouse
Chicken
Crocodile
Tortoise
Lizard
Xenopus
Zebrafish

Figure 2.4

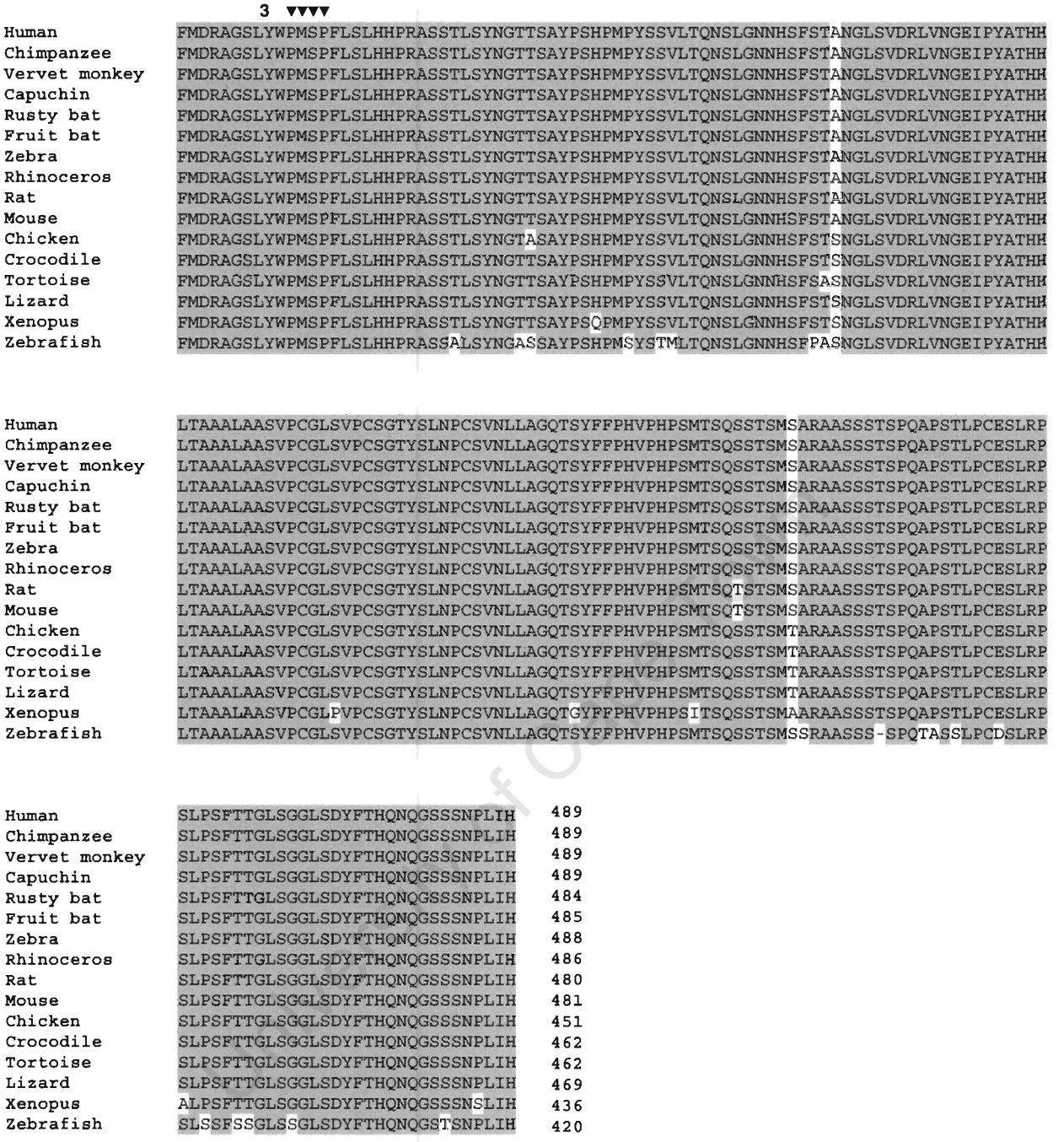

Figure 2.4 continued. Amino acid alignment of FoxG1 orthologs. (‡) indicates the orthologs cloned in this study. The underlined residues for the human ortholog show the DNA-binding domain, which is applicable to all other orthologs – upstream is the N-terminal domain and downstream is the C-terminal domain. The histidine/proline-rich region common to all orthologs (to a lesser extent in *Xenopus* and zebrafish) (**---**), the mammalian specific proline/glutamine inserts ( ), the stretch of alanines in reptiles (+) and the glycine/alanine-rich region in mammals (^) are shown. Identical or similar conserved residues in the variable region of the N-terminal are shown (*). The three predicted phosphorylation consensus sites are shown: (1) Casein kinase 1, (2) Protein kinase B, (3) MAP kinase (▼) (T Regad and N Papalopulu, personal communication). Shading identity is 80%, calculated excluding gaps.

Following a conserved region of approximately 32 residues, is the most striking characteristic of the N-terminal domain: an expanded region of histidine, proline and glutamine (HPQ) residues. The consecutive histidine stretch is conserved among all vertebrates, although in *Xenopus* and zebrafish it is severely reduced (Fig. 2.4, dashed line). The significant difference between the mammals and non-mammals is the insertion of 17-21 proline and glutamine residues in mammals (Fig. 2.4, solid line). Primates show the largest insertion while the remainder of the mammalian orthologs have 1-4 fewer residues compared to primates. Another smaller insert exists further on with 3-6 proline residues inserted in some of the mammalian orthologs; interestingly, this small insertion is absent in rodents (Fig. 2.4, solid line). Following the HPQ region, there are 18 conserved residues in the remainder of the N-terminal (Fig. 2.4, shown by *), 17 of them are glutamate/aspartate or lysine residues. Interestingly, there are glycine/alanine rich regions in the variable region of the N-terminal domain in mammals and non-mammals; some of these residues are conserved in mammals and absent in non-mammals (Fig. 2.4, shown by ^) Furthermore, in reptiles there is a conserved stretch of 6 alanine residues (Fig 2.4, shown by +), which is not present in any other organism.

There are three predicted phosphorylation sites in the FoxG1 protein (1) Casein kinase 1, (2) Protein kinase B and, (3) MAP kinase (Fig. 2.4, shown by ▼). These sites were predicted from human, mouse, rat, chicken, *Xenopus* and zebrafish orthologs (T Regad and N Papalopulu, personal communication). This study shows that these sites are 100% conserved across all available orthologs, substantiating the evidence that they may be sites for phosphorylation.

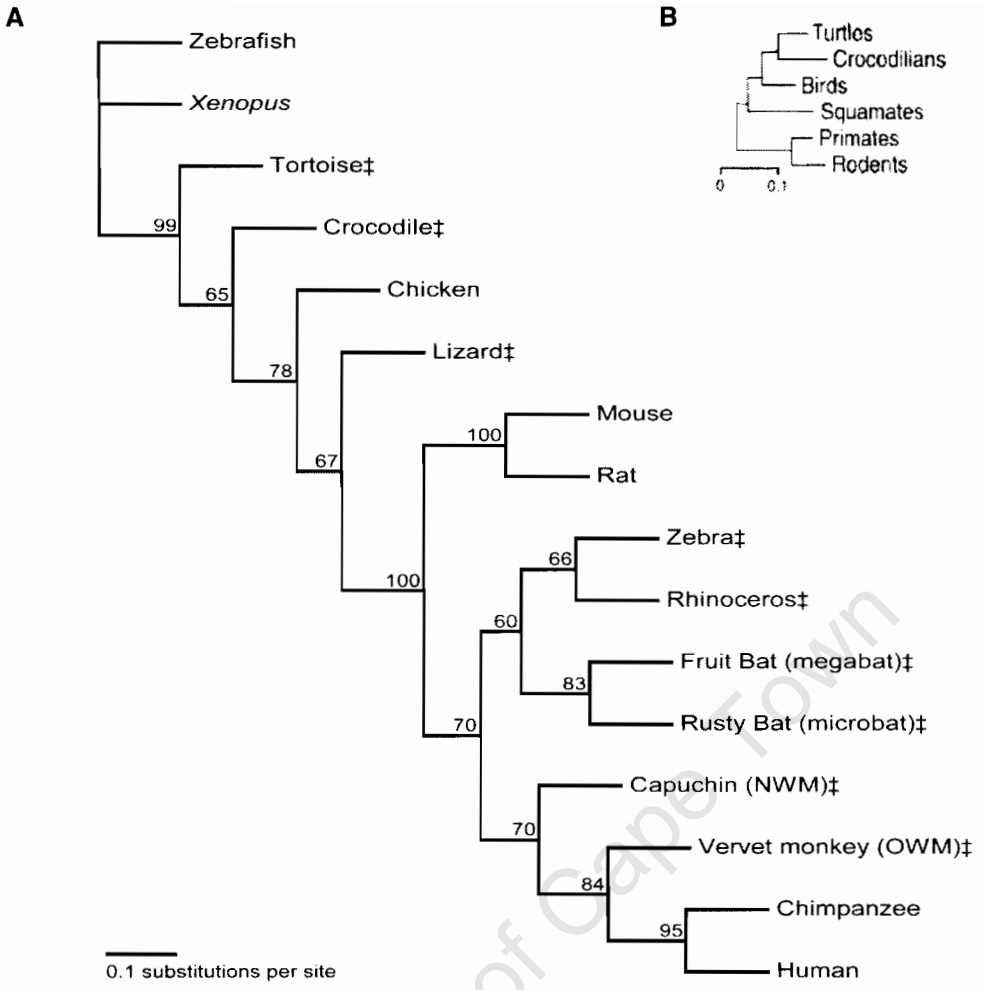

Figure 2.5. Maximum likelihood tree for FoxG1 orthologs. **(A)** The tree was constructed using a nucleotide in-frame alignment. (‡) indicates the orthologs cloned in this study. Numbers at nodes represent the bootstrap test values (1000 replicate test). OWM: Old World monkey, NWM: New World money. Scale bar represents 0.1 nucleotide substitutions per site. **(B)** Maximum likelihood phylogeny of combined sequences from 11 nuclear proteins from Hedges and Poling (1999). Scale bar indicates amino acid substitutions per site. Squamates include lizards and snakes.

The corresponding maximum likelihood phylogenetic tree was constructed from the in-frame nucleotide alignment (Fig 2.5A). The general evolutionary relationships are as expected with the mammals grouping together. The primate lineage shows that the human FoxG1 ortholog is most closely related to chimpanzee and then the Old World Monkey followed by the New World monkey ortholog. The next branch shows that bats, zebra and rhinoceros FoxG1 orthologs are more closely related to primates than to rodents. This is different from the initial hypothesis that the bats, zebra and rhinoceros FoxG1 orthologs should be more distantly related to the primates

that the rodents to the primates. The closest related non-mammalian FoxG1 ortholog is the lizard, followed by chicken, crocodile, tortoise, *Xenopus* and zebrafish. While the relationship between reptiles, birds and mammals remains debated, the FoxG1 evolutionary relationships agree, in general, with the work published by Hedges and Poling (1999) (Fig. 2.5B).

2.3.1.2. FoxG1 3' UTR is conserved in mammals

The 3' RACE cloning using Vervet monkey and crocodile cDNA generated sequence information for the 3' UTR of these FoxG1 orthologs. When these sequences were aligned with other available mammalian FoxG1 orthologs (human, chimpanzee, mouse, rat and dog), obtained from the respective completed genome sequences, the 3' UTR showed a remarkable degree of conservation (Fig. 2.6). The average nucleotide identity for the mammalian FoxG1 3' UTR (94% over approximately 1000 bp) was comparable to the average identity for the coding region (96%). This high 3' UTR conservation is surprising as most genes show a more limited degree of cross-species identity in non-coding sequence. Furthermore, the mammalian orthologs shared a relatively high identity of 75% and 71% with the crocodile and chicken orthologs, respectively, while the identity between mammals and zebrafish was lower at 50% (Fig. 2.6). The majority of the differences in sequence identity in the 3' UTRs of FoxG1 orthologs stem from large insertions (Fig. 2.6, arrowheads) as opposed to nucleotide changes within regions of similar aligned sequences. These insertions are particularly evident in the dog, chicken and crocodile orthologs. If the insertions indicated by the arrowheads in Fig. 2.6 are removed, the identity among mammals increases to 96%, and the identity between mammals and the crocodile, chicken and zebrafish orthologs increases to 81%, 80% and 56%, respectively.

Compared to the 3' UTR of FoxG1, other neural genes showed lower conservation levels in this region. For example, the ASPM gene, involved in brain development, has an identity of 43% across mammals (over ~1800 bp). The transcription factor paired box gene 6 (Pax6), expressed

in the developing forebrain, hindbrain and olfactory placodes and shown to play a crucial role in eye development (Grindley et al., 1995), also exhibits a low nucleotide 3' UTR identity of only 52% (~1000 bp). Conversely, the hairy and enhancer of split (Hes1) basic-helix-loop-helix transcription factor, involved in the Delta/Notch signalling pathway, has a relatively high shared identity of 83% in mammals, although the 3' UTR region is only ~400 bp. The high degree of conservation in the mammalian FoxG1 3' UTR indicates that this region may fulfil a functional role, for example in the regulation of FoxG1 expression. Two possible regulatory mechanisms, secondary structure and microRNA regulation, were investigated further using software prediction tools.

2.3.1.2.1. There is no conserved secondary structure in the 3' UTR of FoxG1 orthologs

The 3' UTRs of eukaryote mRNA transcripts perform a variety of functions such as controlling stability, localization and regulating translation (Decker and Parker, 1995). The formation of secondary structures in the 3' UTRs of some mRNAs have been shown to affect post-transcriptional regulation and mRNA stability (Hew et al., 1999; Wedemeyera et al., 2000). The 3' UTRs of FoxG1 orthologs were examined for secondary structure formation and similarity, as a conserved mechanism of transcriptional regulation, across orthologs. Human, mouse and crocodile 3' UTR secondary structures exhibited free energies of -937, -934 and -959kJ/mol, respectively. While these negative free energies indicate that these secondary structures form spontaneously, 3' UTRs that have been implicated in post-transcriptional regulation showed much lower free energies of between -1643 and -1693kJ/mol (Wedemeyera et al., 2000). Additionally, 3' UTR predicted structures of FoxG1 orthologs showed no conservation across the orthologs, indicating that a conserved mechanism of secondary structure transcriptional regulation is not at work. Furthermore, three randomly generated sequences, with similar base

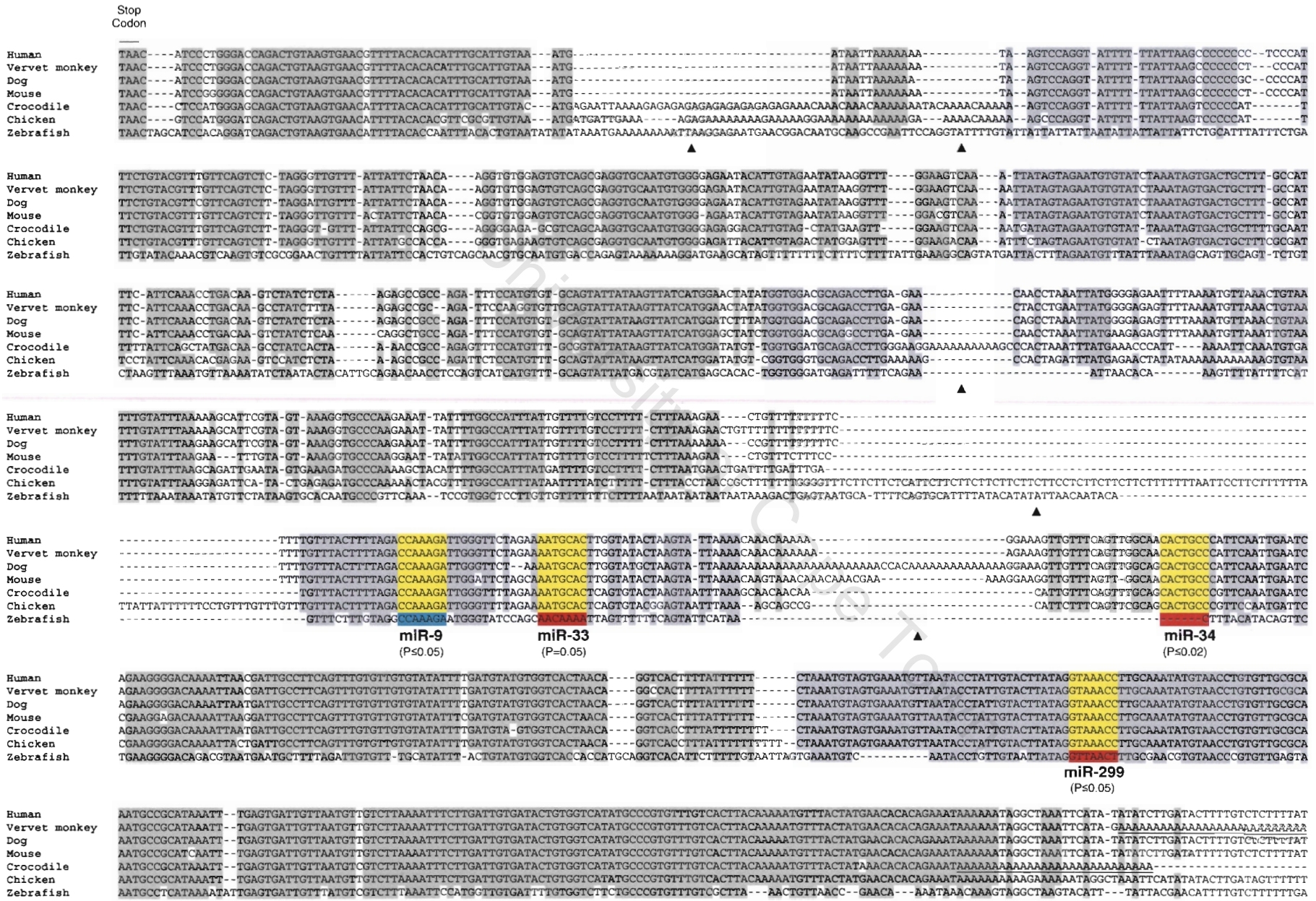
Stop Codon
Human
Vervet monkey
Dog
Mouse
Crocodile
Chicken
Zebrafish
miR-9
(P≤0.05)
miR-33
(P=0.05)
miR-34
(P≤0.02)
miR-299
(P≤0.05)

Figure 2.6

Figure 2.6. Nucleotide alignment of the FoxG1 3' untranslated region. The stop codon is indicated at the start of the 3' UTR. The poly (A) tails that were cloned from Vervet monkey and crocodile using 3' RACE are underlined, indicating the end of the 3' UTR. mRNA sequence is shown for human, Vervet monkey, mouse, crocodile, chicken and zebrafish while the dog sequence was obtained from its genome sequence. Yellow shadings are the miRNA sites that were identified using the PicTar program, with the corresponding miRNA shown as well as the P-value after testing the validity of the site (the P-value was calculated using an alignment of the human, chimpanzee, mouse, rat, dog and chicken orthologs). The red and blue shading shows the potential miRNA that are not conserved and conserved in zebrafish, respectively. Regions of large insertions are shown (▲). Grey shading identity is 80%, including gaps.

composition and length as the 3' UTR of the FoxG1 orthologs, showed very similar free energies that ranged from -900kJ/mol to -973kJ/mol, suggesting that the 3' UTRs of FoxG1 orthologs do not have secondary structure specific sequences.

2.3.1.2.1. FoxG1 may be a target for post-transcriptional regulation by microRNAs

MicroRNAs (miRNA) are small non-coding RNAs (~22 nucleotides) that have been shown to post-transcriptionally regulate gene expression in animals and plants by binding to complementary regions in the 3' UTR of mRNA transcripts (reviewed in Ambros, 2004). The high conservation of the 3' UTR across FoxG1 orthologs from mammals to chicken and crocodile, suggests that this region may possibly be under selection to maintain certain sequences, for example miRNA binding sites. Thus, potential target sites for miRNAs in the 3' UTRs of FoxG1 orthologs were investigated.

MiRNA prediction analysis was performed using the PicTar algorithm (Krek et al., 2005). This program aligned FoxG1 Genbank reference sequences for human, chimpanzee, mouse, rat, dog and chicken and, subsequently searched for potential miRNA sites. The inclusion of the chicken genome substantially increases the signal-to-noise ratio from 2.3 for human, chimpanzee, mouse and dog to 3.6 (Krek et al., 2005). PicTar identified 4 significant miRNA target sites conserved across all tested FoxG1 orthologs, and the corresponding miRNA recognizing the site (Fig. 2.6, yellow shading). The highest ranked miRNA hit was miR-34 ($P < 0.02$), followed by miR-9 ($P \leq 0.05$), miR-33 ($P = 0.05$) and miR-299 ($P = 0.05$). It has been estimated that a single miRNA

may target around 200 mRNA transcripts (Krek et al., 2005; Lewis et al., 2005) – allowing possible FoxG1 specific miRNAs to be identified from previously known miRNA databases. Most interesting of the possible miRNAs that target FoxG1 is miR-9. This miRNA was cloned from mouse brain tissue and has been shown to be expressed in proliferating cells of the brain, and in the cortex and the olfactory bulb (the regions of FoxG1 activity), as well as in the midbrain and hindbrain (Lagos-Quintana et al., 2002; Farh et al., 2005). Of the other positive hits, miR-34 and miR-299 were expressed in a mouse embryonic cell line with miR-299 showing additional expression in a neuroblastoma cell line (Houbaviy et al., 2003; Altuvia et al., 2005), while miR-33 was cloned from humans, although no tissue specificity has been determined (Lagos-Quintana et al., 2001). Thus, the prediction of miRNA sites, in particular miR-9, in the 3' UTR of FoxG1 orthologs can be further substantiated by the brain/neural specific expression of the miRNAs.

Furthermore, because PicTar does not allow for user sequence input, the sequences for Vervet monkey, crocodile and zebrafish were aligned with the PicTar generated alignment of human, chimpanzee, dog, mouse, rat, dog and chicken orthologs (the chimpanzee and rat orthologs are not shown Fig. 2.6) in order to check if the identified sites were conserved in these orthologs. The Vervet monkey and crocodile orthologs showed complete conservation across the four PicTar predicted sites (Fig. 2.6). Conversely, the zebrafish ortholog was not conserved at the miR-34, miR-33 and miR-299 sites (Fig. 2.6, red shading) but was conserved at the miR-9 site (Fig. 2.6, blue shading). The conservation of the miR-9 site from zebrafish to human together with the brain specific expression of this miRNA, suggests that it may be a regulator of FoxG1 expression.

2.3.2. Investigation into FoxG1 as a determinant of forebrain size in humans

2.3.2.1. FOXG1 is not duplicated in humans

Because FOXG1 was reported to be duplicated in humans (Wiese et al., 1995) (Fig. 2.7A), it was investigated at which point during vertebrate evolution this duplication occurred. These duplicate forms are referenced as FOXG1A and FOXG1B. Additionally there is a third human FOXG1 sequence in Genbank, called FOXG1C, which was also investigated in this study. Initially, the FOXG1 duplication was investigated in the closely related primate lineage using the following methods: PCR analysis of Vervet Monkey (Old World Monkey) genomic DNA (data not shown) and analysis of the latest draft of the chimpanzee genome sequence (NCBI map viewer release November 2004). This genome search was conducted by blasting FOXG1A and FOXG1B specific sequence against the chimpanzee genome (using BLASTn). In both cases there was no evidence of FoxG1 duplication, but rather only one form of FoxG1 could be detected. The absence of this duplication in the primate lineage, especially in chimpanzee, the closest relative of humans, offers two possible explanations: (1) the duplication event arose after humans diverged from chimpanzee or (2) there is no FOXG1 duplication in humans.

Next, the latest draft of the human genome sequence (NCBI map viewer release August 2004) was used to investigate FOXG1 duplication in humans. The reference mRNA sequences for human FOXG1A, B and C (Table 2.3) were blasted against the human genome. All the sequences mapped to chromosome 14 (E value = 0, Score > 1174) and showed no other significant alignments to the genome, except for small regions (< 200 nucleotides, E value > 9e-30, Score < 139) corresponding to the conserved fork head family DNA-binding domains.

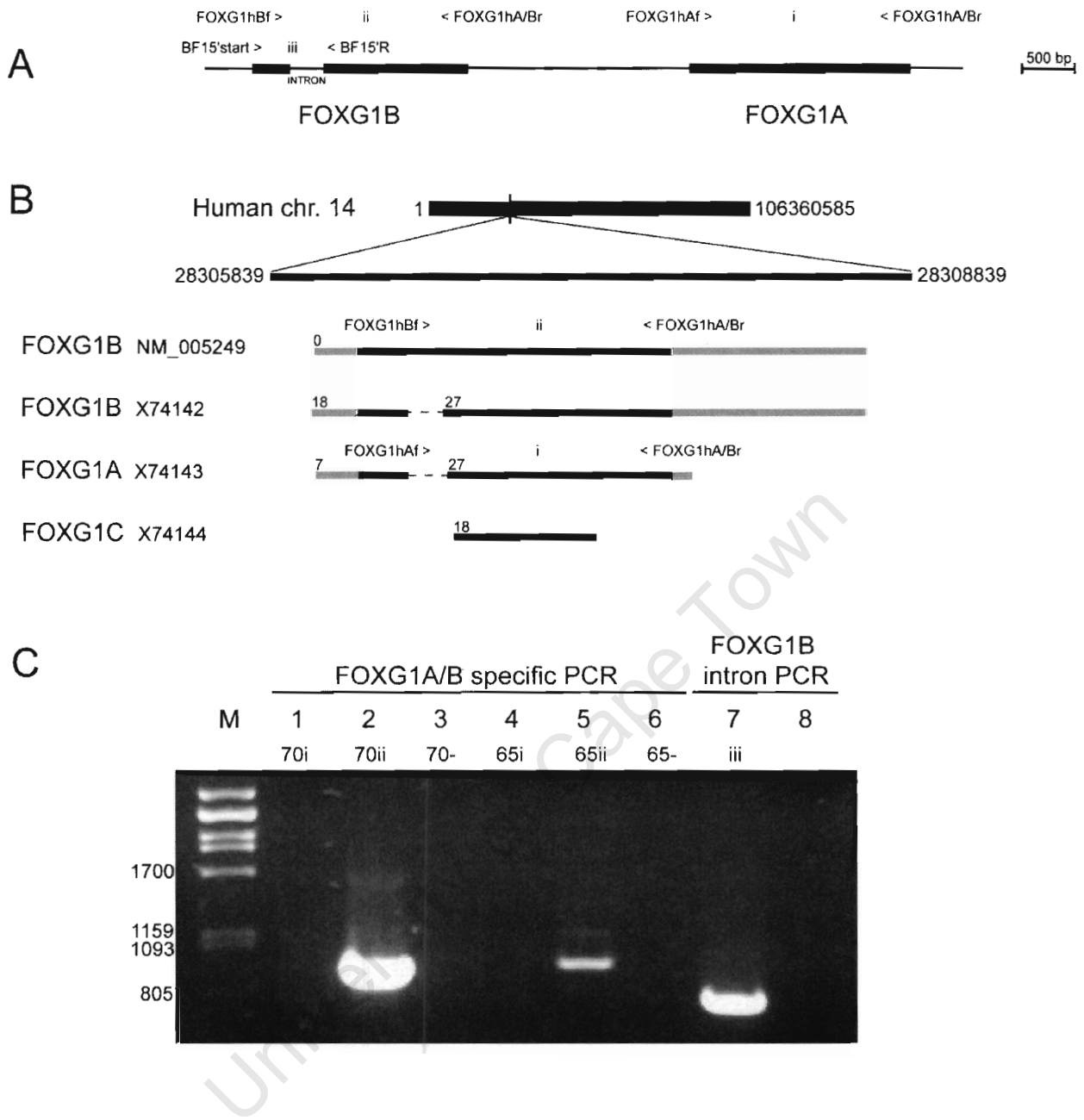

Figure 2.7. Genomic structure of human FOXG1. **(A)** Wiese et al., 1995 reported that FOXG1B and FOXG1A clustered on chromosome 14q11-13 and that FOXG1B contained a 500 bp intron. **(B)** Subsequent genome analysis shows that all the forms of FOXG1 align at the same locus on chromosome 14. FOXG1B (NM_005249) matches the genome sequence exactly, while all other reference mRNAs show some identity differences (the number of mismatches for each fragment and extended regions that show no homology to genome (---) are shown). The coding (▬) and non-coding (▬) regions are shown for each reference sequence. The location of the primers used for PCR analysis in (C) are shown in (A) and (B): > or < indicates the position and direction of the primer with the primer name indicated. **(C)** FOXG1A specific primers (primer pair i, melting temperatures 76°C) produced no product at annealing temperatures of 70°C (lane 1, 70i) and 65°C (lane 4, 65i), compared to the analogous FOXG1B primers (primer pair ii) that produced a 953 bp product at the same annealing temperatures (lane 2, 70ii and 5, 65ii); negative water template controls (-) for each annealing temperature PCR produced no product (lane 3, 70- and 6, 65-). PCR using primers (pair iii) that transversed the supposed FOXG1B intron produced a 775 bp product, indicating that FOXG1B does not contain an intron (lane 7); negative water template control showed no product (lane 8). Primers are indicated by the arrowheads and names in A and B.

Table 2.3. mRNA sequence references for human FOXG1.

Gene Name	Gene Symbol	Location	mRNA sequence accession number	Previous Names
Forkhead Box G1A	FOXG1A	14q11-13	X74143*	HFK2, HBF-2
Forkhead Box G1B	FOXG1B	14q13	X74142* NM_005249	HFK1, HBF-1
Forkhead Box G1C	FOXG1C	14q11.2	X74144*	HFK3, HBF3

* Sequences referenced from Murphy et al., 1994 and Wiese et al., 1995

More specifically, all the FOXG1 forms mapped to the same locus (Fig. 2.7B) on chromosome 14 (between nucleotides 28306021 and 28308662). FOXG1B (NM_005249) showed a 100% identity to the genome sequence, while the other FOXG1B reference sequence, X74142, showed some identity discrepancies with a 163 nucleotide gap within the N-terminal domain and 45 nucleotide mismatches compared to genome sequence. Additionally, the intron that FOXG1B was reported to contain (Wiese et al., 1995) does not occur in the genomic sequence, as the mRNA sequence matches the genomic reference without any gaps. This was confirmed by PCR on human genomic DNA using primers that transversed the FOXG1B intron (Fig. 2.7A, primer pair iii). These primers should produce a 1275 bp fragment if an intron is present and 775 bp fragment if it is not. The resultant PCR produced a 775 bp fragment (Fig. 2.7C, lane 7) that was sequenced and confirmed to be FOXG1B. Thus, the mRNA reference sequence that represents FOXG1B is NM_005249 and FOXG1B does not contain any introns.

Strikingly, FOXG1A did not cluster 3 kb from FOXG1B on chromosome 14, as reported (Wiese et al., 1995), but rather mapped to the same locus, exhibiting a 181 nucleotide gap within the N-terminal domain and 34 nucleotide mismatches compared to genome sequence, suggesting that this form of FOXG1 does not exist. This was confirmed by PCR on human genomic DNA using primers specific to FOXG1A (Fig. 2.7A, B, primer pair i). FOXG1A specific primers (76°C melting temperature) produced no product at an annealing temperature of 70°C or 65°C (Fig.

2.7C, lane 1 and 4) compared to the analogous FOXG1B primers (Fig. 2.7A, B, primer pair ii) that produced a 953 bp fragment, at the same annealing temperatures (Fig. 2.7C, lanes 2 and 5).

Furthermore, computational analysis of the genomic sequence up- and downstream of the FOXG1B locus, using homology searches with FOXG1A specific sequence, showed no evidence of the FOXG1A gene. Finally, FOXG1C also mapped to the same locus and appears to be a fragment of the FOXG1B gene, although the reference sequence contains 18 nucleotide mismatches. Therefore, FOXG1A and FOXG1C genes appear to be erroneous versions of FOXG1B which cannot be located on the human genome in Genbank or in the independently isolated human DNA. This conclusion is partially presented in a human FOX gene family review where it is indicated that FOXG1A, B and C are derived from the same locus (Katoh and Katoh, 2004), although the molecular mechanics are not explained.

2.3.2.2. Selection characteristics of FoxG1

Because FoxG1 is an important regulator of brain development and exhibits similar mutant phenotypes in humans to genes such as ASPM and microcephalin, it was sought to determine whether positive selection was acting on FoxG1 in the lineage leading to humans (as is the case for ASPM and microcephalin). An excellent means of initially identifying a gene that shows positive selection is to compare the evolutionary rates of the gene in primates (human and Old world monkey) and rodents (rat and mouse) (Dorus et al., 2004). The basis for this comparison is that the evolutionary time separating human and Old World monkey (OWM) is generally comparable to that separating mouse and rat, while the ratio of brain size to body size is significantly different (mouse:rat 1:1, OWM:human 1:6-9) (Williams, 2002). Thus, the comparison of the K_a/K_s ratios of brain-related genes between these four taxa allows the preliminary identification of genes that show different molecular evolutionary rates in the context of the different brain phenotypes that have evolved in these two mammalian orders.

The K_a/K_s values for an Old World monkey, Vervet monkey, and human FoxG1 orthologs were compared to those from mouse and rat (Table 2.4). The K_a/K_s ratios were determined for full-length FoxG1 as well as for each of the three domains. As expected, the DNA-binding and C-terminal domains showed K_a/K_s ratios of 0 as there are no non-synonymous mutations in these domains. In contrast, the N-terminal domain, showed a K_a/K_s value of 0.07 for primates compared to 0.028 for rodents, which represents a 2.5 fold increase in primates. Across the full-length gene the K_a/K_s value was comparable at 0.020 for primates and 0.017 for rodents (these values represent the non-synonymous mutations that are found exclusively in the N-terminal domain 'diluted' across the entire gene). Thus, with a fold difference of 2.5 compared to rodents, the N-terminal domain of FoxG1 exhibits some evidence for an increased rate of evolution in primates. This difference, however, is not entirely convincing at this point – for genes/regions of similar lengths (411-555 bp), Dorus et al. (2004) showed evidence of positive selection when there were fold differences of 3.4-4.4 between primates and rodents. Thus, subsequent tests specific to the primate lineage were conducted.

Table 2.4. FoxG1 K_a/K_s values for primates (human and Old World monkey) and rodents (mouse and rat).

	K_a/K_s		Length compared (bp)	Fold difference
	Primate	**Rodents**		
Full length FoxG1	0.020	0.017	1443	1.2
N-terminal domain	0.070	0.028	468	2.5
DNA-binding domain	0.000	0.000	336	0.0
C-terminal domain	0.000	0.000	639	0.0

The increase in cortex size is particularly dramatic in the lineage leading to humans (Williams, 2002). If the higher comparative primate K_a/K_s for the N-terminal domain of FoxG1 is the product of adaptive evolution, then it is expected that this accelerated evolution should be more dramatic in the lineage leading from human-Vervet monkey (H-VM) ancestors to humans than

the lineage leading to Vervet monkey. A New World monkey (White-throated capuchin) sequence was used as an outgroup to derive the H-VM ancestral sequence (node 'a' in Fig. 2.8) (Evans et al., 2004b; Dorus et al., 2004). This ancestral sequence was then compared to Vervet monkey (a2 in Fig. 2.8) and human-chimpanzee (H-C) ancestral (a1 in Fig. 2.8) FoxG1 sequences in order to determine the K_a/K_s values for the full length gene and for each domain for the two respective branches. The K_a/K_s values for the H-VM ancestor-Vervet monkey comparison were 0.08, 0.17, 0 and 0 for the full length gene, the N-terminal domain, the DNA-binding domain and the C-terminal, respectively. In contrast, the H-VM ancestor-H-C ancestor comparisons yielded values K_a/K_s values of 0 for the full length gene and the all the domains. Thus, FoxG1 shows a comparatively faster rate of evolution in the lineage leading to Vervet monkey compared to the lineage leading to humans.

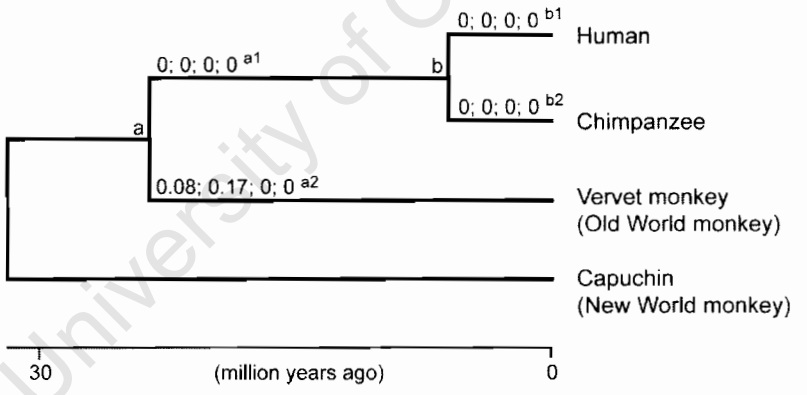

Figure 2.8. Primate phylogenetic tree depicting K_a/K_s values for FoxG1 in lineages leading to humans and non-human primates. FoxG1 K_a/K_s values are shown for full-length, N-terminal domain, DNA-binding domain and C-terminal domain, respectively. (a) shows the human-Vervet monkey ancestor that was used to calculate the corresponding K_a/K_s comparisons for human-chimpanzee ancestor (a1) and Vervet monkey (a2). (b) shows the human-chimpanzee ancestor that was used to calculate the corresponding K_a/K_s comparisons for human (b1) and chimpanzee (b2), indicated.

To confirm this absence of accelerated evolution in lineage leading to humans, another phylogeny based test was conducted. Similar to the previous test, if the higher comparative primate K_a/K_s for the N-terminal domain of FoxG1 is the product of adaptive evolution, then it is

expected that this accelerated evolution should be more dramatic in the lineage leading from H-C ancestors to humans than the lineage leading to chimpanzee. The Vervet monkey sequence was used as an outgroup to determine the H-C ancestral sequence (node 'b' in Fig. 2.8) (Evans et al., 2004b; Dorus et al., 2004). This ancestral sequence was the compared to chimpanzee (b2 in Fig. 2.8) and human (b1 in Fig. 2.8) FoxG1 sequences. For both lineages, there was no evidence for any accelerated evolution with K_a/K_s values of 0 for all comparisons. Thus, taken together with the H-VM lineage comparison, it can be concluded that full length FoxG1 or any of its domains do not show any accelerated evolution in the lineage leading to humans.

2.4. Discussion

Because FoxG1 plays a role in regulating the proliferation of the cortical progenitor cells and thus may play a role in determining the size of the brain in vertebrates, nine new orthologs were cloned to characterize the change in FoxG1 sequence across vertebrate evolution. At a phylogenetic level the evolutionary relationships of primate FoxG1 orthologs were generally as expected. FoxG1 was cloned from bat, zebra and rhinoceros because they were deemed to be more distantly related to primates than rodents to primates (Arnason et al., 2002) However, the FoxG1 orthologs of bat, zebra and rhinoceros were shown to be more closely related to primates than rodents to primates. Thus, the evolutionary position of the new orthologs near the primate lineage is surprising. However, it should be noted that the evolutionary relationships of the FoxG1 orthologs and indeed nuclear genes do not always match the evolutionary relationships of the respective organisms, which are derived from many nuclear and mitochondrial genes. Furthermore, the phylogenetic relationship of reptiles remains indistinct: the traditional phylogeny has crocodiles and birds grouped together, with squamates (lizards and snakes) on a separate branch and turtles/tortoises at the base of the tree (Romer, 1966), while recently it has been shown that crocodiles and turtles/tortoises group together, with birds on a separate branch and squamates at the base of the tree (Hedges and Poling, 1999). The FoxG1 orthologs show

similar relationships to those derived in Hedges and Poling (1999) with the squamates most closely related to mammals, followed by birds and then turtles and crocodiles.

As expected the FoxG1 orthologs that were cloned in this study exhibited highly conserved DNA-binding and C-terminal domains. In contrast, the N-terminal domain exhibited some divergence across vertebrates, but was relatively conserved within mammals. There is a repetitive region of histidine and proline residues that is conserved in reptiles, birds and mammals and is reduced in amphibians and fish (Fig. 2.4, dashed line). All the mammal orthologs exhibited an additional proline and glutamine extension of this region, that was completely absent in non-mammals (Fig. 2.4 solid line). Another characteristic of the N-terminal domain is a predicted Casein kinase 1 (CK1) phosphorylation site (Fig 2.4A) that has been show to be important for sub-cellular FoxG1 localization (T Regad and N Papalopulu, personal communication). The 100% conservation of this site across all orthologs substantiates it as a target for phosphorylation-mediated regulation of the localization of FoxG1. Furthermore, the histidine- and glutamine-rich regions and conserved glutamate/aspartate and lysine residues confer a hydrophilic profile to this region. It is possible that the hydrophilic nature of this region is required to make the phosphorylation site available to CK1 on the surface/exterior of the FoxG1 protein. A protein-protein BLAST, using the HPQ-rich region of the N-terminal domain of the human FOXG1, shows that it shares some homology with a small number of transcription factors, such as bromodomain protein 4, which is associated with an increase in cell division (Dey et al., 2000). This indicates that this region may play a role in the activity of these transcription factors, however, no functional role for this HPQ-rich region has been identified. Additionally, it is difficult to assign any importance, functional or otherwise, to the extended histidine and glutamine region in mammals; it is possible that this region may have arisen due to an insertion that occurred at the start of the evolution of mammals. Functional differences

between a mammal (mouse), non-mammal (*Xenopus*) and a mouse HPQ deletion mutant are investigated in Chapter 4, in an attempt to assign some functional importance to the HPQ region.

The role of FoxG1 as a determinant of cortex size in humans was also investigated. The similarity of FoxG1, in terms of function and mutant phenotypes, to genes that show strong signatures of adaptive evolution, led to the hypothesis that FoxG1 may play a role in the development of the enlarged cortex in humans. This role was postulated to be achieved via changes in the FoxG1 coding region (i.e. adaptive evolution) and/or via gene duplication. It was initially investigated at what point in the primate lineage that reported FoxG1 duplication occurred. However, PCR and human genome analysis showed that the duplicated form of FOXG1, FOXG1A could not be located in the human genome or in independently isolated human DNA. Thus, the earlier report of gene duplication cannot be substantiated. Lastly, the adaptive evolution of FoxG1 was investigated in the primate lineage. The N-terminal domain of FoxG1 showed some evidence of accelerated evolution in primates compared to rodents, with a 2.5 fold faster rate of evolution in primates. To confirm this, the rate of FoxG1 adaptive evolution was investigated in the lineage leading to humans. If changes in the coding region of FoxG1 do play a role in the increased cortex size, one would predict an increased K_a/K_s value in the lineage leading to humans compared to other primate lineages. However comparison of the K_a/K_s for the N-terminal domains of human, chimpanzee and Old World monkey orthologs showed that there was no adaptive evolution of FoxG1 in the lineage leading to humans.

While FoxG1 shows no evidence for positive selection in the primate lineage, other mechanisms of its influence on brain evolution can be postulated. All mammalian FoxG1 orthologs show a high level of conservation compared to non-mammal orthologs; the main difference between these two groups is the extended HPQ region in the N-terminal of mammalian orthologs. Thus, it is tempting to speculate, at a sequence level, that if FoxG1 is playing a role in the evolution of

the telencephalon, then it is doing so at the mammal/non-mammal split. In other words, FoxG1 may have played a role in the formation of the six-layered neocortex in mammals (a structure which is absent in reptiles and birds) but not in the evolutionary increase in the size and complexity of this structure within mammals. It would therefore be pertinent to compare the K_a/K_s values for FoxG1 orthologs at the mammal/non-mammal split. However, because the selection comparison is required to be performed across aligned codons, with any codon gaps that occur in any orthologs, along with the corresponding codon of other orthologs, being deleted, K_a/K_s comparisons between mammal and non-mammal orthologs would be inaccurate. This means that the main source of variation between mammal and non-mammal orthologs (the HPQ region in mammals and any other insertions that occur between the two groups) would be deleted before the K_a/K_s values are calculated, rendering the comparison inaccurate. To this end, functional studies are performed in Chapter 4 to address the sequence differences observed between mammalian and non-mammalian orthologs. Furthermore, if FoxG1 is playing a role in the evolution of the telencephalon, then it may be fulfil this role through mechanisms that are independent of changes in its coding region. These include mechanisms such as expansion of the number of cis-regulatory elements in the promoter region (Carroll et al., 2005) or changes in 3' UTR-mediated regulatory elements that may be influenced by the change in sequence in this region.

A striking characteristic of FoxG1 orthologs is the highly conserved 3' UTR. In this study, Vervet monkey and crocodile 3' UTRs were cloned via RT-PCR and showed remarkable homology with other orthologs (Fig. 2.6). This high conservation suggests a regulatory role for the 3' UTR of FoxG1. Two mechanisms of 3' UTR were investigated: secondary structure formation and miRNA regulation. While no conserved secondary structure was predicted, four miRNA target sites were identified in the 3' UTR of FoxG1. Of these sites, miR-9 showed brain specific expression, while miR-299 was identified from a neuroblast (proliferating neuronal

precursor) cell line – which suggests that these two miRNAs may regulate the expression of FoxG1. Conversely, miR-34, identified from mouse embryonic stem cells (a developmental stage that temporally precedes the activity of FoxG1) and miR-33, which, as yet, shows no tissue specificity, are less likely to be regulators FoxG1. A major consideration when predicting miRNA sites is the relatively high signal-to-noise ratio, which was estimated at approximately 3.6 for the orthologs used to predict the FoxG1 miRNA sites. However, because four miRNA target sites were identified in the 3' UTR of FoxG1, it is more likely that a least one of them is a functional miRNA site, compared to if, for example, only one or two sites were predicted. Furthermore, the miR-9 site was conserved in zebrafish indicating that there is selective evolutionary pressure to maintain this site in vertebrates, substantiating a functional role for this miRNA. Thus, this study suggests that FoxG1 may be regulated by microRNAs, and in particular miR-9.

In summary, this study has provided a comprehensive examination of the sequence characteristics of various vertebrate FoxG1 orthologs by providing the FoxG1 sequence from nine new organisms. The 3' UTR of FoxG1 orthologs are highly conserved which indicates that FoxG1 may be the target of miRNA regulation with several conserved miRNA target sites identified in its 3' UTR. One of the sites, miR-9, showed conservation in zebrafish as well as brain specific expression, substantiating the evidence that this miRNA may play a role in the regulation of FoxG1. Additionally, although FoxG1 is an excellent candidate for a major determinant of the cortex size in humans, it in fact shows no signatures of accelerated evolution in the lineage leading to humans.

CHAPTER 3

Changes in FoxG1 localization in response to FGF-2 induced differentiation in the OP27 cell line

---

3.1. Introduction

Three conserved putative phosphorylation sites have been identified in FoxG1 orthologs (T Regad and N Papalopulu, personal communication; Fig. 2.4). Protein kinase B was shown to phosphorylate one of these sites (at a site on the carboxy side of the DNA-binding domain) in response to fibroblast growth factor (FGF) signalling. This phosphorylation caused FoxG1 to be excluded from the nucleus of HeLa cells – indicating potential mechanisms for regulating the transcriptional activity of FoxG1 (T Regad and N Papalopulu, personal communication). Furthermore, when FGF-2 was ectopically expressed in the developing *Xenopus* telencephalon, FoxG1 expression in the cells in this region changed from nuclear to cytoplasmic which correlated with an increase in neurogenesis (T Regad and N Papalopulu, personal communication). This suggests that neural progenitor differentiation requires the down-regulation of FoxG1 activity, which is achieved by exporting it from the nucleus. These observations are verified in this chapter by tracking the changes in the spatial localization of endogenous FoxG1, in the OP27 neural precursor cell line, in response to FGF-2 signalling.

The olfactory neuroepithelium has the ability to support continual neurogenesis – rendering it as an important model for investigating the molecular pathways that control neuronal differentiation. Accordingly, conditionally-immortalized clonal cell lines were derived from the E10 mouse olfactory placode (OP) as a tool for examining neuronal development (Illing et al., 2002). These cell lines were isolated by infection of primary cultures of dispersed cells from the embryonic olfactory placode, with a retrovirus carrying the temperature-sensitive allele of the SV40 large T antigen. At the permissive temperature (33°C) the SV40 large T antigen drives

proliferation of the cells, while a shift to the non-permissive temperature (39^{0}C) inactivates the antigen which stops mitosis, allowing normal lineage development to proceed. One of these cell lines, OP27, has a molecular profile that represents the intermediate transition stage in the olfactory receptor neuron (ORN) lineage. These cells can be induced with retinoic acid to differentiate, at the non-permissive temperature, into mature bipolar ORNs that express the characteristic olfactory marker protein and specific olfactory odorant receptor transcripts (Illing et al., 2002).

OP27 cells have been shown to express the FGF receptor (FGFR) isoforms, FGFR-1 IIIc and FGFR-2 IIIc (Shoko et al., manuscript under review), which can be activated by the FGF-2 ligand (Ornitz et al., 1996). Furthermore, when grown at the non-permissive temperature in differentiation media containing FGF-2, a sub-population of the OP27 cells undergo morphological changes from flat, irregular shaped cells to bipolar cells with phase bright cell bodies and neurite-like extensions (Shoko et al., manuscript under review; this study). After FGF-2 treatment, the OP27 cells express markers that are characteristic of neuronal development and the ORN differentiation lineage, as determined by semi-quantitative RT-PCR (Shoko, 2004; Shoko et al., manuscript under review). These include regulators of the lateral inhibition neuronal patterning pathway, Delta1 and Notch1, which are expressed in dividing OP27 cells and in FGF-2 induced differentiated cells. Neuorogenic factor D (NeuroD), normally expressed at the start of post-mitotic neuronal differentiation, is transiently expressed in OP27 cells between 2 and 4 days following FGF-2 treatment. Similarly, the expression of growth associated protein-43 (GAP-43), normally expressed in immature ORNs that are not terminally differentiated, is transiently up-regulated after FGF-2 treatment. Furthermore, the OP27 cells are induced to express mRNA transcripts for olfactory receptors following FGF-2 treatment. In contrast, the olfactory marker protein (OMP), expressed in mature ORNs, is not reproducibly detectable following FGF-2 treatment; after 10 days minimal OMP expression was detected in

some experiments. These expression patterns suggest that the OP27 cells differentiate along the ORN lineage, following FGF-2 treatment, into immature olfactory neurons expressing olfactory receptors.

Initial in situ hybridization studies showed that FoxG1 is expressed in various regions in the rat embryonic forebrain, including the olfactory placode (Tao and Lai, 1992). FoxG1 expression in the OP27 cell line was confirmed using RT-PCR (Illing et al., 2002 and Shoko, 2004). It is detected in the undifferentiated state (33°C) at day 0 and in the FGF-2 induced differentiated state (39°C) after 1, 2, 4, 6, 8 and 10 days. The level of expression, determined by semi-quantitative RT-PCR, was similar at all the time points (Shoko, 2004). It was investigated here whether FoxG1 is exported from the nuclei of OP27 cells in response to FGF-2 induced differentiation, by immunocytochemistry. The differentiation state of the cells was assessed by measuring neurite outgrowth and Delta1 and Notch1 immunocytochemistry.

3.2. Materials and Methods

3.2.1. OP27 cell culture conditions

OP27 cells were routinely maintained at 33°C and 10% CO_2 concentration in Dulbecco's Modified Eagle's medium (DMEM, Gibco) supplemented with 10% heat-inactivated fetal bovine serum (FBS, Highveld Biological) (medium called DM-10) (Illing et al., 2002). Cells were sub-cultured by washing with 1× phosphate buffered saline (PBS) (140mM NaCl, 2.7mM KCl, 8mM Na_2HPO_4, pH 7.2) and then harvested using 0.25% trypsin (w/v) and 0.04% EDTA (w/v). Trypsin/EDTA was inactivated by addition of DM-10, and removed by centrifugation (1000×g for 5 minutes), followed by cell resuspension and plating at the required density. Viable cells were counted in a haemocytometer after incubation in an equal volume of trypan blue, which stains dead cells blue.

3.2.2. FGF-2 induced differentiation in the OP27 cells

OP27 cells were plated onto coverslips in 24-well plates at a density of 10000 cells/cm^2 and incubated for 1-2 days at 33°C until they reached approximately 70% confluency. DM-10 was then exchanged for differentiation media (1:1 mixture of DMEM:Ham's F12 (Gibco) containing 5µg/ml insulin, 100µg/ml transferrin, 100µM putrescein, 20nM progesterone and 30nM sodium selenite) containing 50µg/ml gentamycin sulphate (Highveld Biological), 5U/ml heparin (Sigma) and 5ng/ml basic human FGF-2 (Promega). Cells were then shifted to 39°C for the desired length of time (1, 2, 4, 8 or 12 days). Control cells corresponding to each time point were maintained in DM-10 at 33°C (including an additional 0 day time point) and at 39°C.

3.2.3. OP27 immunocytochemistry

The immunocytochemistry protocol used to characterize the expression of FoxG1, Delta1 and Notch1 is described in Fig. 3.1. Two immunocytochemistry control experiments were also conducted: (1) no primary and no secondary antibodies were included, to determine the natural fluorescence of the OP27 cells, and (2) only secondary antibody was included, to determine the background fluorescence of any non-specific bound secondary antibody. In both cases, no fluorescence could be detected at the exposure used to capture images after primary and secondary antibody detection. Furthermore, the immunocytochemistry experiments where repeated twice using independently FGF-2 differentiated OP27 cells.

1. Fixation	Rinse cells with serum-free DMEM. Incubate at -20°C for 5 minutes in methanol. Fix with 4% paraformaldehyde (10 minutes at room temperature).
	↓ Wash 3× 5 minutes with PBS
2. Block	Incubate with PBS containing 1% BSA (blocking solution) (30 minutes at room temperature).
	↓
3. Primary incubation	• Single FoxG1 incubation: 1µg/ml (1:500) goat anti-FoxG1 (Abcam, AB3394) diluted in blocking solution (overnight at 4°C). • Double incubation: 1µg/ml (1:500) goat anti-FoxG1 and 1µg/ml (1:250) rabbit anti-activated Notch1 (Abcam, AB8925) or 0.8µg/ml (1:250) rabbit anti-Delta1 (Santa Cruz, SC8303) diluted in blocking solution (overnight at 4°C).
	↓ Wash 2× with PBS
4. Secondary incubation	Incubate with 1.5µg/ml (1:1000) Cy3-conjugated donkey anti-goat IgG (Jackson ImmunoResearch) without (for FoxG1 detection) or with (for double detection) 2µg/ml (1:1000) Alexa Fluor 488-conjugated chicken anti-rabbit IgG (Molecular Probes), diluted in blocking solution (2 hours at room temperature in the dark).
	↓ Wash 2× with PBS
5. Nuclear stain	Incubate with 130ng/ml 4´,6´-Diamidino-2-phenyllindole (DAPI) (3 minutes at room temperature in the dark).
	↓ Wash 2× 10 minutes with PBS
6. Mounting	Coverslips were mounted onto glass slides with mounting medium containing N-propyl gallate (anti-fade) and allowed to fix overnight. Slides were stored at 4°C in the dark.
	↓
7. Microscopy	Cells were viewed using a Zeiss Axiovert 200M microscope and images were captured using a Zeiss AxioCam HRm camera. The following filters were used for detection: • DAPI – excitation 365 (band pass), emission 470 (long pass). • Alexa Fluor 488 – excitation 450-490 (band pass), emission 515-565 (band pass). • Cy3 – excitation 575-625 (band pass), emission 660-710 (band pass).

Figure 3.1. Summary of the protocol used for FoxG1/Delta1/Notch1 immunocytochemistry in the OP27 cell line. From step 2 onwards, the steps were carried out on coverslips in a humidified chamber.

3.3. Results

3.3.1. FoxG1 is excluded from the nucleus in morphologically differentiated OP27 cells

Fluorescent immunocytochemistry was used to track the localization of FoxG1 in dividing, undifferentiated OP27 cells (cultured in maintenance medium DM-10, at either the permissive and non-permissive temperature) and in differentiating OP27 cells (cultured in differentiation medium in the presence of FGF-2 at the non-permissive temperature). FoxG1 localization in undifferentiated cells (in DM-10 medium) at the permissive and non-permissive temperature establishes that any changes are due to the effect of the FGF-2 containing differentiation media and not as a result of the growth conditions. This is especially important at the non-permissive temperature as the SV40 large T antigen becomes inactivated; in this instance there are only a small number of cells that differentiate into bipolar cells in maintenance medium, while the addition of FGF-2 differentiation medium substantially increases the number of bipolar cells.

At the time the cells are shifted to the non-permissive temperature (day 0), cells at the permissive temperature are flat and irregular, characteristic of the undifferentiated state (Fig. 3.2A, A1). Here, FoxG1 is expressed in a strong punctuate pattern in the nucleus with some residual punctuate expression in the cytoplasm (Fig. 3.2A, A1). Nuclear expression is confirmed by DAPI staining in a corresponding figure for each condition and time point (Fig. 3.2A1-P1). This punctuate nuclear expression pattern is similar for all time points for morphologically undifferentiated cells at 33°C and at 39°C in maintenance medium (Fig. 3.2B-K, B1-K1).

When shifted to the non-permissive temperature, in differentiation medium containing FGF-2, OP27 cells start to differentiate as determined by a change from flat, irregular shaped cells to bipolar cells. At day 1, although the cell population has been shown to be mitotic (Shoko et al.,

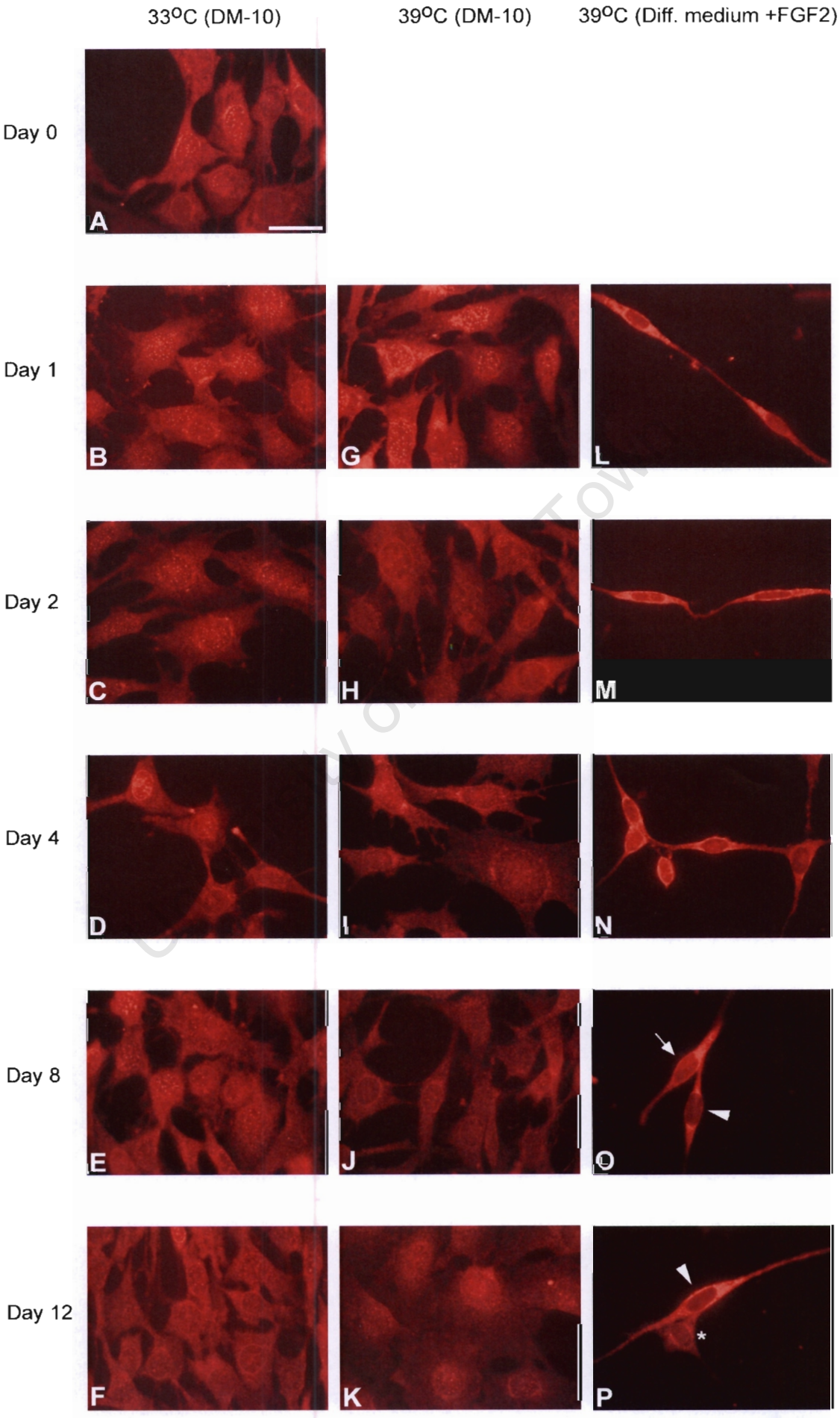
33°C (DM-10)
39°C (DM-10)
39°C (Diff. medium +FGF2)
Day 0
Day 1
Day 2
Day 4
Day 8
Day 12
A
B
C
D
E
F
G
H
I
J
K
L
M
N
O
P

Figure 3.2

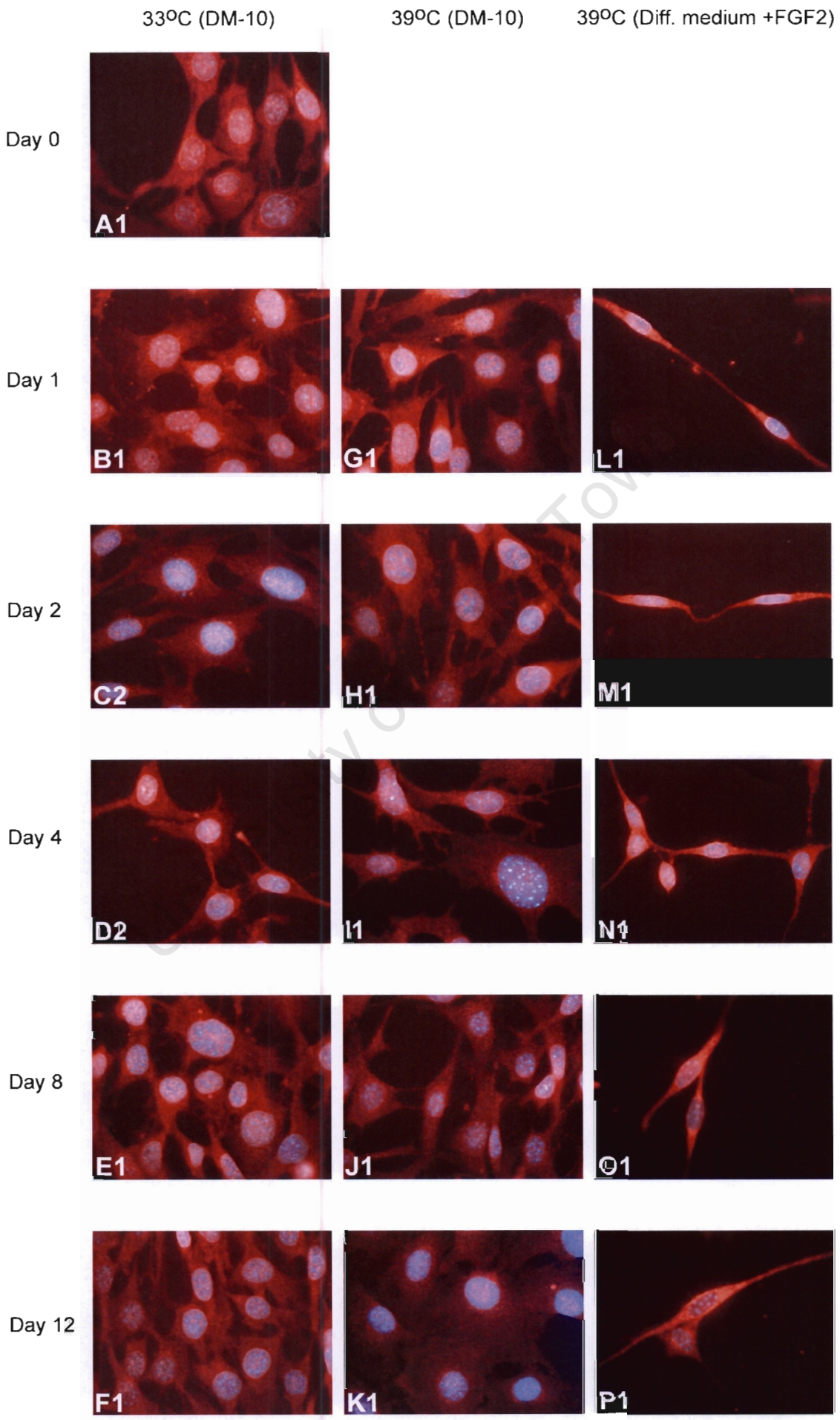

Figure 3.2 continued

Figure 3.2. Changes in FoxG1 localization in response to FGF-2 induced differentiation in the OP27 cell line. Fluorescent immunocytochemistry was used to detect the expression of FoxG1 (red). A1-P1 corresponds to A-P, but with DAPI staining (blue) to show the nuclei. In the undifferentiated state (33°C and 39°C in maintenance medium (DM-10), A-K and A1-K1) FoxG1 is present throughout the cells, with a distinct punctuate expression pattern in the nucleus. Upon differentiation with FGF-2 (Diff. medium +FGF2), FoxG1 localization becomes reduced in the nuclei and increased in the cytoplasm (L-P, L1-P1), compared to the undifferentiated state. Residual punctuate FoxG1 expression remains in the nuclei of bipolar cells (L, M, N and arrow in O), but at later times points FoxG1 is completely excluded from the nucleus (arrowheads in O and P). Cells that do not differentiate in the FGF-2 differentiation media maintain nuclear FoxG1 expression (*). Note the bipolar and irregular morphology that characterize the differentiated and undifferentiated cells, respectively. All images were taken at the same exposure at 100× magnification. Scale bar represents 100μm for all images.

manuscript under review), approximately 16% of the cells differentiate into bipolar ORNs (Fig. 3.3). This percentage increases to 31 and 42% following 2 and 4 days of FGF-2 treatment, respectively. The maximum percent is obtained after 8 days of FGF-2 treatment with approximately 56% of the cells exhibiting the bipolar morphology which falls to approximately 49% after 12 days.

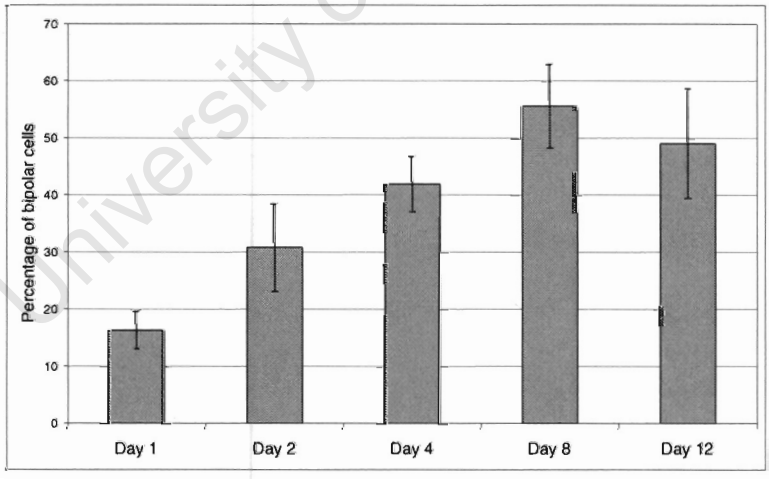

Figure 3.3. Change in morphology of the OP27 cells in response to FGF-2 induced differentiation. After various FGF-2 treatment times, as indicated, the percentage of OP27 cells that exhibit the differentiated, bipolar morphology was determined. Bipolar cells were defined as having phase-bright cell bodies with two opposite neurite-like extensions that were both at least the length of the cell body diameter (Harada et al., 2005). Twenty fields of view (10 each for 2 separate experiments) were taken for each time point. Error bars show standard deviation.

After 1 day of FGF-2 treatment, FoxG1 expression is reduced in the nuclei and shows a increase in cytoplasmic expression in the bipolar cells (Fig. 3.2L, L1), compared to the control cells at the same time point (Fig. 3.2B, G, B1, G1). There is, however, some punctuate nuclear FoxG1 expression still evident in the nucleus of the bipolar cells (Fig. 3.2L). A similar pattern of expression occurs in bipolar cells at day 2 and 4 (Fig. 3.2M, N, M1, N1). However, as the cells are exposed to the FGF-2 differentiation medium for increased time periods, FoxG1 becomes completely excluded from the nucleus. At day 8, while some bipolar cells still exhibit low levels of punctuate nuclear staining (Fig. 3.2O, arrow), FoxG1 is entirely excluded from the nucleus in others (Fig. 3.2O, arrowhead). Similarly at day 12, FoxG1 is completely excluded from the nucleus (Fig. 3.2P, arrowhead) and shows a marked increase in cytoplasmic expression. Cells that remain morphologically undifferentiated, even in FGF-2 medium, maintain the punctuate FoxG1 nuclear expression (Fig. 3.2P, asterisk). Thus, as the OP27 cells differentiate into bipolar ORNs, there is change in FoxG1 expression: it is excluded from the nucleus and shows an increase in cytoplasmic localization. These changes become more evident if the cells are grown in the differentiation medium for increased time periods.

3.3.2. Molecular characterization of the bipolar OP27 cells

The expression of Delta and activated Notch (actNotch) was used to validate the hypothesis that bipolar cells which have exported FoxG1 from the nucleus are differentiating into immature ORNs. Delta1 is the membrane bound ligand for the Notch1 receptor. The Notch receptor is cleaved in response to the Delta signalling, and the activated intracellular domain is imported into the nucleus where it suppresses neuronal differentiation by inhibiting the expression of the proneural genes such as mammalian achaete-scute homologue gene 1 (MASH1) (Gilbert, 2000). In the model of lateral inhibition, neural progenitor cells express both Delta and Notch, with a low level of signalling between these cells. Cells that are selected to become neurons express increasing levels of Delta, which leads to increased Notch signalling in neighbouring cells. This

results in an increase in activated Notch in the nucleus, down-regulation of Delta expression, and a suppression of neuronal differentiation in these neighbouring cells. Thus, it was predicted that differentiating OP27 cells would have increased Delta staining and a decrease in expression of actNotch in the nucleus.

3.3.2.1. Delta1 is up-regulated in bipolar OP27 cells

Double fluorescent immunocytochemistry was used to monitor the expression patterns of FoxG1 and Delta1 at various time points (0, 1, 2, 4, 8 and 12 days) in undifferentiated and differentiated OP27 cells. Controls were performed with expression monitored at 33°C (day 0) and at 39°C in maintenance medium (DM-10) for all remaining time points. At day 0, FoxG1 expression is similar to the previous experiments with punctuate nuclear and moderate cytoplasmic expression (Fig. 3.4A1). At the same time point, Delta1 displays in a diffuse granular expression pattern that is concentrated around the cytoplasm (Fig. 3.4A2). Delta1 is a membrane bound ligand so any immunofluorescence detected is expected to be on the surface of the cell. While there appears to be less expression of Delta1 around/above the nuclei, surface specific expression was confirmed by examining the cells at different depths on the slide. At the highest depth, Delta1 surface expression above the nuclei was clear but caused the remainder of the cell and therefore the majority of the image to be out of focus. The merge of FoxG1 and Delta1 at day 0 shows that the expression overlaps to some extent; there is a yellow-green colour associated with the cytoplasm and a red colour, primarily FoxG1 expression, associated with the nucleus (Fig. 3.4A3).

After 1 day at 39°C in the maintenance medium, the cells showed a similar Delta1 and FoxG1 expression pattern (Fig. 3.4B1-3) to day 0. Upon FGF-2 induced differentiation, the cells adopt the characteristic bipolar morphology, with a slight reduction in nuclear FoxG1 (Fig. 3.4C1).

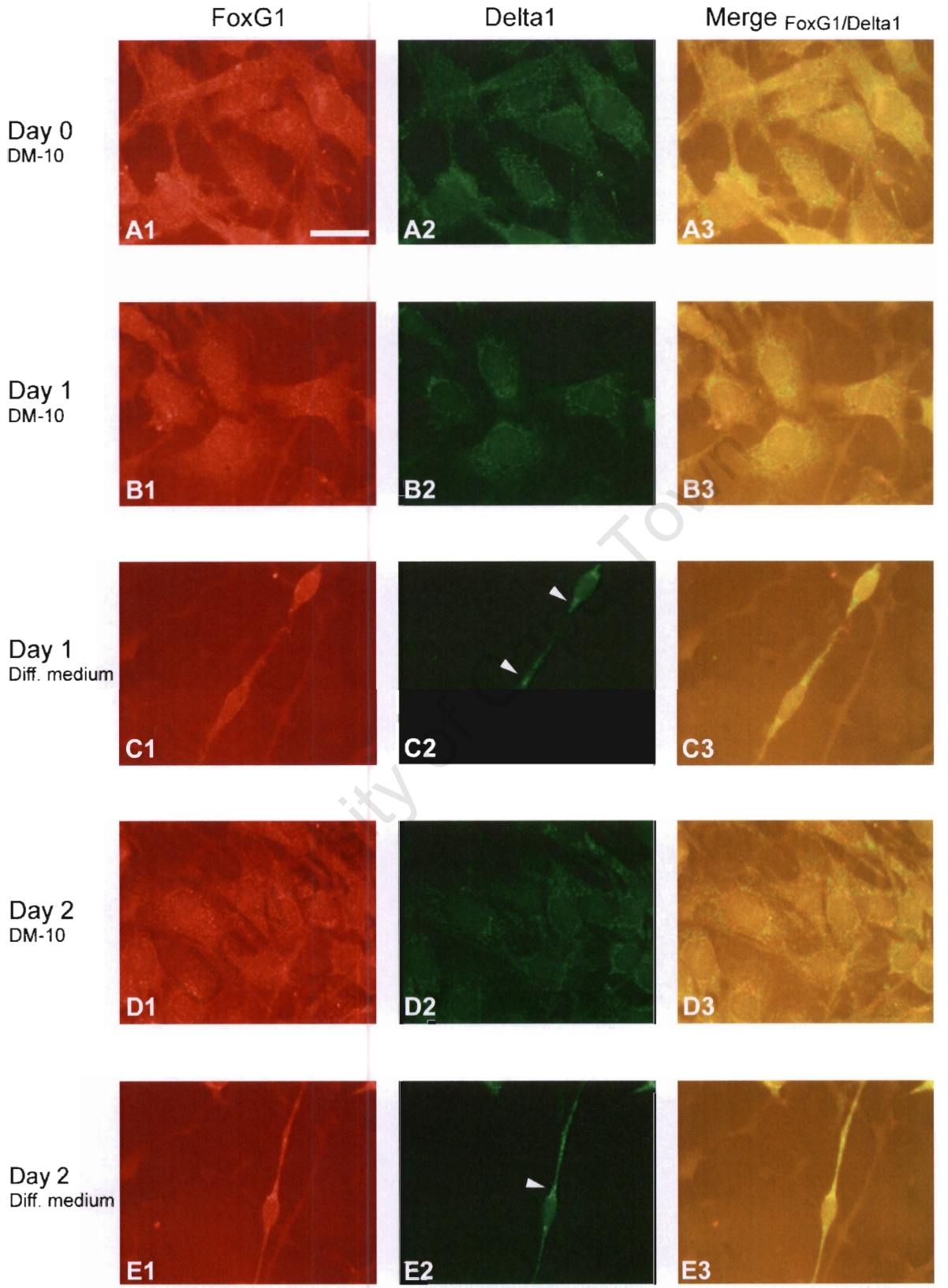
FoxG1
Delta1
Merge FoxG1/Delta1
Day 0
DM-10
A1
A2
A3
Day 1
DM-10
B1
B2
B3
Day 1
Diff. medium
C1
C2
C3
Day 2
DM-10
D1
D2
D3
Day 2
Diff. medium
E1
E2
E3

Figure 3.4

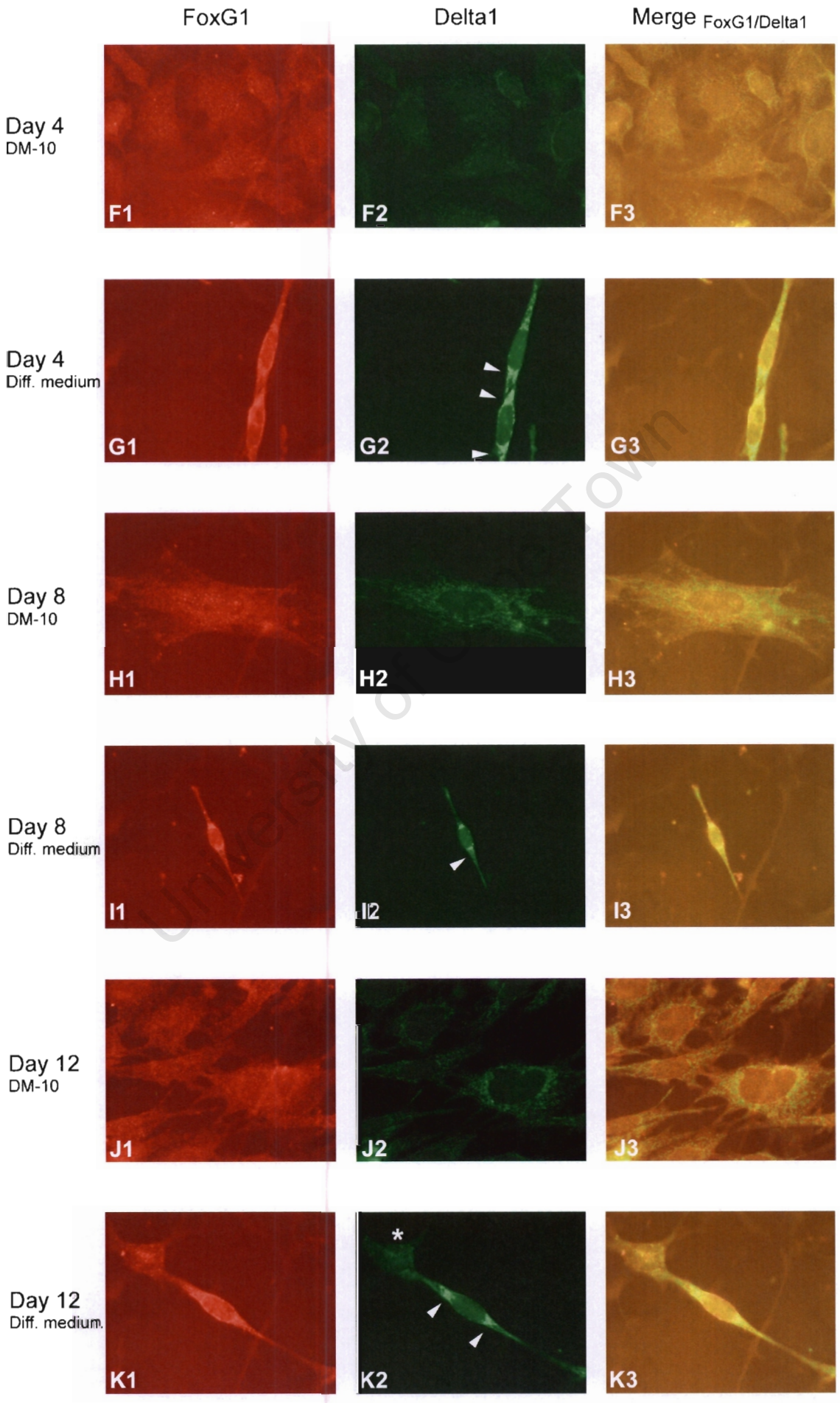

Figure 3.4 continued

Figure 3.4. Delta1 is up-regulated in bipolar OP27 cells following FGF-2 induced differentiation. Fluorescent immunocytochemistry was used to detect the expression of FoxG1 (red) and Delta1 (green). All growth conditions were at 39°C, except for day 0 (33°C), in maintenance medium (DM-10) or differentiation medium containing FGF-2 (Diff. medium), as indicated. Arrowheads indicate the increase in Delta1 expression associated with differentiation into bipolar ORNs. Cells that do not differentiate in the FGF-2 differentiation media maintain a lower level of Delta expression (*) compared to the bipolar cells. Note the bipolar and irregular morphology that characterize the differentiated and undifferentiated cells, respectively. All images were taken at the same exposure at 100× magnification. Scale bar represents 100μm for all images.

Delta1 expression also changes, compared to the day 0 and 1 control cells in DM-10, as there is an increase in intensity at the base of the neurite-like processes (Fig. 3.4C2, arrowheads). The resultant merge at day 1 shows a yellow colour in the processes (Fig. 3.4C3). FoxG1 expression at day 1 is comparable at the undifferentiated and differentiated state (Fig. 3.4B1, C1) and thus, the yellow expression colour in the FoxG1/Delta1 merge must be due to an increase in Delta1 expression.

The expression of Delta1 appears to be up-regulated in the bipolar cells for 2, 4, 8 and 12 days of FGF-2 treatment (Fig. 3.4E2, G2, I2, K2, arrowheads). Taken together with the increase in FoxG1 cytoplasmic expression, the resultant merged images of FoxG1/Delta1 show bright yellow regions of overlapping expression in the processes (Fig. 3.4E3, G3, I3, K3). Undifferentiated cells in the maintenance medium after 8 and 12 days (Fig 3.4H2, J2) show some increase in Delta1 expression, as a result of longer growth at 39°C, compared to similar cells at 1, 2 and 4 days. However, the FoxG1/Delta1 merged images of these cells at day 8 and 12 show a red FoxG1 nuclear staining, and a yellow-green cytoplasmic staining of Delta1 (Fig. 3.4H3, J3). In contrast, after treatment with FGF-2, the FoxG1/Delta1 merge shows a bright yellow colour in the bipolar cell processes and a reduction in red nuclear FoxG1 staining (Fig 3.4I3, K3). Cells that do not differentiate into bipolar ORNs, even in FGF-2 differentiation media, show a marked lower level of Delta1 expression compared to bipolar cells in the same conditions (Fig. 3.4K2, compare asterisk and arrowheads). Thus, Delta1 is up-regulated in OP27 cells that

differentiate into bipolar ORNs after FGF-2 treatment, compared to undifferentiated cells in maintenance medium.

3.3.2.2. Changes in Notch1 expression after FGF-2 induced differentiation

An actNotch1 antibody, which specifically recognizes the cleaved Notch1 intracellular domain (Conboy et al., 2005) was used to monitor the changes in activated Notch1 in the OP27 cells in response to FGF-2 signalling. Conboy et al. (2005) have shown that active Notch1 is localized to the cytoplasm in aged muscle cells which are unable to regenerate muscle, while it is strongly expressed in the nucleus of dividing progenitor cells which are able to regenerate. Expression of activated form of Notch1 is localized to the nuclei of the cells in the ventricular zone – the region of proliferating progenitor cells – in the developing mouse brain and is down-regulated in differentiating neurons (Tokunaga et al., 2004). Thus, it was predicted on the basis of these results that expression of the actNotch1 would be down-regulated and excluded from the nucleus in differentiating ORNs.

At day 0, actNotch1 is expressed in the nucleus in a strong punctuate pattern (Fig. 3.5A2). The number of spots of actNotch1 expression varies from approximately 3 to 10 per nucleus, with some background expression in the cytoplasm. This nuclear expression pattern is expected as the antibody used is targeted against the activated domain of Notch1; the background expression may be actNotch1 in the process of being transported to the nucleus. FoxG1 expression again shows punctuate nuclear and lower levels of cytoplasmic expression at day 0 (Fig. 3.5A1). The merge of actNotch1 and FoxG1 produces a general yellow-red colour in the cytoplasm, indicating the FoxG1/actNotch1 background expression overlap, green spots in the nucleus, corresponding to the concentrated actNotch1 expression and a red punctuate FoxG1 expression

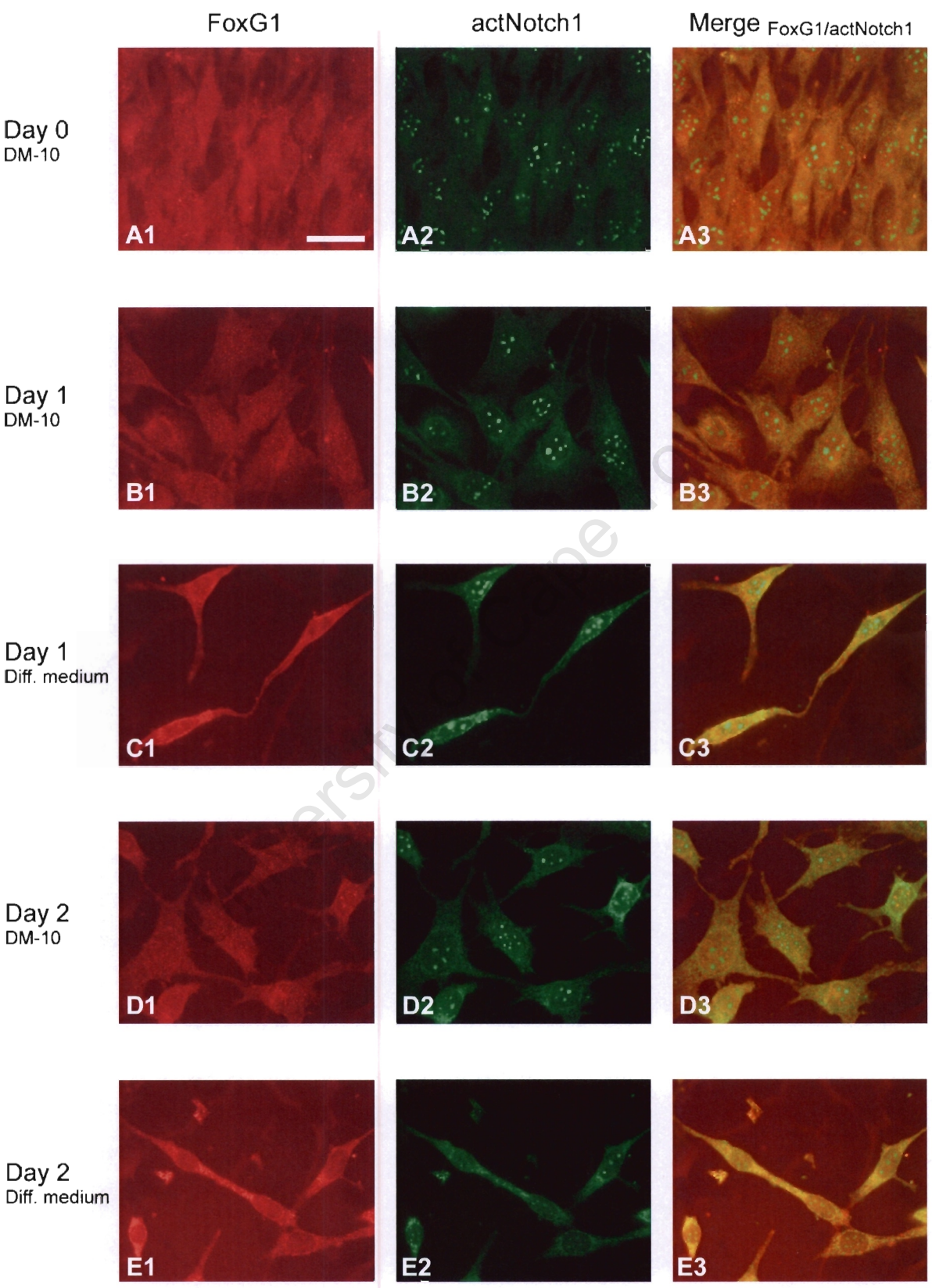
FoxG1
actNotch1
Merge FoxG1/actNotch1
Day 0
DM-10
A1
A2
A3
Day 1
DM-10
B1
B2
B3
Day 1
Diff. medium
C1
C2
C3
Day 2
DM-10
D1
D2
D3
Day 2
Diff. medium
E1
E2
E3

Figure 3.5

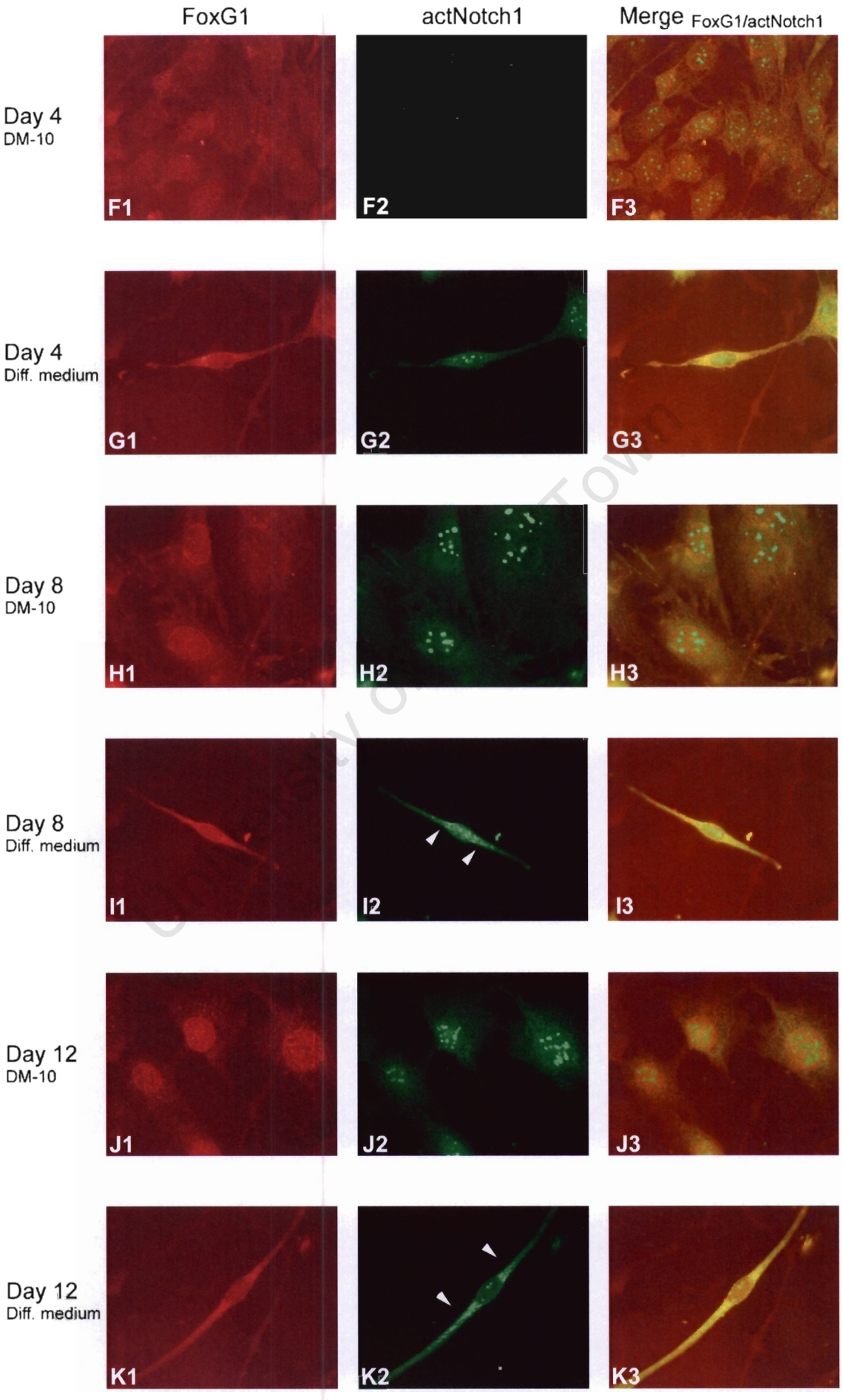

Figure 3.5 continued

Figure 3.5. Activated Notch1 (actNotch1) expression changes in the OP27 cells following FGF-2 induced differentiation. Fluorescent immunocytochemistry was used to detect the expression of FoxG1 (red) and actNotch1 (green). All growth conditions were at 39°C, except for day 0 (33°C), in maintenance medium (DM-10) or differentiation medium containing FGF-2 (Diff. medium), as indicated. Arrowheads indicate the increase in actNotch1 expression in the processes of the bipolar cells. Note the bipolar and radial morphology that characterize the differentiated and undifferentiated cells, respectively. All images were taken at the same exposure at 100× magnification. Scale bar represents 100μm for all images.

pattern in the nucleus (Fig. 3.5A3). Similar FoxG1 and actNotch1 expression patterns are observed at day 1, 2, 4, 8 and 12 in the maintenance medium (Fig. 3.5B1-3, D1-3, F1-3, H1-3, J1-3), with the continual expression of the actNotch1 in the nucleus.

After FGF-2 treatment, the OP27 cells adopt the characteristic bipolar morphology. The punctuate actNotch1 expression is still evident at day 1, 2, 4, 8 and 12 (Fig. 3.5C1-3, E1-3, G1-3, I1-3, K1-3). However, at day 2, 4, 8 and 12, the intensity of nuclear actNotch1 expression is reduced compared to the corresponding control cells in maintenance medium and bipolar cells at day 1. This reduction in nuclear actNotch1 expression is accompanied by an increase in cytoplasmic expression at day 8 and 12 (Fig. 3.5I2, K2, arrowheads). Taken together with the increase in cytoplasmic FoxG1 expression, the processes of the bipolar cells at day 8 and 12 exhibit a bright yellow colour where FoxG1 and actNotch1 expression is merged (Fig. 3.5I3, K3). Thus, when OP27 cells are exposed to FGF-2 treatment, it appears as if actNotch is excluded from the nucleus after 1 day and shows a marked increase in cytoplasmic expression after 8 and 12 days of treatment.

3.4. Discussion

The upstream regulators of FoxG1 localization and activity are presently under investigation (T Regad, M Roth, N Bredenkamp, N Illing and N Papalopulu, manuscript in preparation). These include phosphorylation by Casein kinase 1 and FGF signalling which result in nuclear localization and export, respectively. Additionally, following FGF-2 ectopic expression in the

Xenopus telencephalon, the export of FoxG1 from the nucleus is accompanied by the differentiation of the progenitor cells. It may be that FoxG1's disruption of the TGF-β signalling pathway is prevented once it is exported from the nucleus, allowing the pathway to inhibit cell proliferation and resulting in the differentiation of the progenitor cells. Furthermore, the effect of FGF-2 on inducing differentiation in the OP27 cell line has been characterized (Shoko, 2004; Shoko et al., manuscript under review). Thus, the OP27 cell line was used to track the changes in FoxG1 localization in response to FGF-2 induced differentiation in order to verify the observations of ectopic FGF-2 expression in *Xenopus* (T Regad and N Papalopulu, personal communication).

In agreement with the nuclear expression of FoxG1 in progenitor cells in *Xenopus* telencephalon, FoxG1 was shown to be expressed in the nuclei of undifferentiated, proliferating OP27 cells, with a low level of expression observed in the cytoplasm (Fig. 3.2A-K). The punctuate expression pattern in the nucleus may be regions where FoxG1 has bound to the regulatory components of its target genes (for example in the co-repressor complex with Groucho) or where FoxG1 has bound to the nuclear Smad complexes. Upon FGF-2 induced differentiation, there is a change in the sub-cellular localization of FoxG1: nuclear expression is reduced and cytoplasmic expression is increased (Fig. 3.2L-P). These changes become more evident as the cells are treated with FGF-2 for longer periods, such as 8 and 12 days. It can therefore be suggested that nuclear FoxG1 plays a role in maintaining the OP27 cells in an undifferentiated state and, when differentiation is induced with FGF-2, FoxG1 is excluded from the nucleus preventing its regulation of growth inhibition or neuronal differentiation genes, which results in the subsequent differentiation of the OP27 cells.

Following FGF-2 treatment, morphological changes were used to identify OP27 cells that were differentiated. This study also investigated if these morphological changes were associated with

differentiation-specific molecular changes. The OP27 cells have been characterized as immature ORNs following FGF-2 induced differentiation and hence OMP expression (the classical mature ORN marker) cannot be used as a marker of differentiation (Shoko et al., manuscript under review). Furthermore, other markers of differentiation, NeuroD and GAP-43, are only transiently expressed. Thus, components of the lateral inhibition pathway, Delta1 and Notch1 were used to characterize the differentiation state of the cells. It was expected that Delta1 should be up-regulated in differentiating OP27 ORNs, while actNotch1 should be down-regulated and/or excluded from the nucleus.

Delta1 was clearly up-regulated in the bipolar cells following FGF-2 treatment, compared to the cells in maintenance medium (Fig. 3.4). This is in accordance with mRNA levels that are also shown to increase as the cells differentiate (Shoko, 2004; Shoko et al., manuscript under review). It should be noted here that while the up-regulation of Delta1 seems to be relatively convincing using immunocytochemistry, western blot analysis, as the more conventional measure of protein levels, should be performed to confirm the Delta1 up-regulation. In addition, actNotch1 expression seems to become reduced in the nucleus and increased in the cytoplasm as the OP27 cells differentiate in response to FGF-2. This is in accordance with mRNA levels which were shown not to change significantly following FGF-2 treatment (Shoko, 2004). The reduction in active nuclear expression in differentiated cells is expected as actNotch1 normally maintains cells in an undifferentiated state. Thus, comparative changes in expression of Delta1 and actNotch1, after FGF-2 treatment, establish a molecular distinction between differentiated bipolar cells and undifferentiated radial cells in the OP27 cell line.

In summary, this study provides preliminary data supporting the hypothesis that FGF-2 signalling may be playing a role in down-regulating the transcriptional activity of FoxG1 by excluding it from the nucleus. This change in sub-cellular localization may contribute to the

differentiation of the OP27 cells along the ORN lineage. Furthermore, the differentiation state of the OP27 cells was confirmed by the change in morphology with the increase in Delta1 expression, and reduction in actNotch1 nuclear expression confirming the hypothesis that FoxG1 is excluded from the nuclei of OP27 cells when they differentiate in response to FGF-2. Lastly, additional experiments that would be useful to validate aspects of these preliminary findings include: western blots to confirm the up-regulation of Delta1 in response to FGF-2 signalling and tests to check if blocking FGF-2 signalling prevents the export of FoxG1 from the nucleus and the corresponding neuronal differentiation.

CHAPTER 4

Testing the transient transfection efficiency of *Xenopus* and mouse FoxG1 reporter constructs in the OP27 cell line

4.1. Introduction

In Chapter 2 it was shown that FoxG1 orthologs from a range of vertebrates exhibited highly conserved DNA-binding and C-terminal domains and a variable N-terminal domain. For example, the mouse ortholog shows a remarkable insertion of a stretch of histidines, prolines and glutamines in the N-terminal domain (common to all mammals), which is almost absent in the *Xenopus* ortholog. Furthermore, the mouse and *Xenopus* orthologs show an amino acid identity of 38% in the N-terminal domain, compared to 96% in the rest of the protein. This raises the question of whether these differences in the N-terminal domain translate into a functional difference between *Xenopus* FoxG1 and mouse (mammalian) FoxG1 orthologs. However, because the N-terminal is so different between mammals and non-mammals, codon based selection analysis cannot be used to examine the changes in the rate of adaptive evolution of FoxG1 between these two groups. Thus, in this chapter, a functional test into the difference between *Xenopus* and mouse FoxG1 is investigated by testing the effect of these orthologs on OP27 cell survival.

Preliminary observations and data suggest that there might be a functional difference between *Xenopus* FoxG1 and mammalian FoxG1. Bourguignon et al. (1998) had previously shown that there was a difference in the phenotype of *Xenopus* embryos injected with a high dose (500pg) and a low dose (90pg) of in vitro synthesized *Xenopus* FoxG1 mRNA. As an initial analysis to investigate whether mouse FoxG1 showed a similar phenotype, *Xenopus* embryos were injected with high and low doses of in vitro synthesized mouse FoxG1. When a high dose of mouse FoxG1 mRNA was injected into *Xenopus* embryos it resulted in a more severe effect compared

to the equivalent *Xenopus* FoxG1 mRNA injection. Embryos injected with a high dose of mouse FoxG1 mRNA showed a greater number of ruptured cells on the injected side, resulting in ruptured embryos, compared to embryos injected with an equivalent high dose of *Xenopus* FoxG1 mRNA (N Illing and N Papalopulu, unpublished data). In a separate experiment, the transfection of a plasmid encoding mouse FoxG1 fused to green fluorescent protein (pGFP:mFoxG1) into an OP cell line, OP6, yielded a transfection efficiency of significantly below 10% (Linda, 2003). Furthermore, when cells transfected with pGFP:mFoxG1 were tracked for 3 days post transfection at the permissive temperature, a proportion of them were shown to detach and die. Thus, it appears that constitutive expression of FoxG1 may affect cell survival, and that the effect may be more severe for mouse FoxG1 compared to *Xenopus* FoxG1. In agreement with this idea, Martynoga et al. (2005) showed that in the absence of FoxG1, the number of apoptotic labelled cells was clearly reduced in the telencephalon of E10.5 embryos compared to wildtype embryos – indicating that FoxG1 may positively regulate apoptosis. Conversely, however, retroviral mediated over-expression of chicken FoxG1 in the telencephalon of stage 7-8 chicken embryos resulted in a decrease in cell death; shown to be as a result of a significant decrease in the level of apoptosis within the telencephalon (Ahlgren et al., 2003). Therefore, while the precise effect of FoxG1 on cell survival remains undefined, there is some evidence to suggest that it is important in this regard.

This study tested the hypothesis that constitutive expression of a mammalian FoxG1 ortholog has a more severe effect on cell survival compared to *Xenopus* FoxG1. This was achieved by comparing the transfection efficiencies of mouse and *Xenopus* FoxG1:ECFP (enhanced cyan fluorescent protein) constructs under the control of the same constitutive CMV promoter the OP27 cells. It was reasoned that cells expressing constitutive levels of mouse FoxG1 were more likely to die, than cells expressing constitutive levels of *Xenopus* FoxG1. Consequently, it was predicted that this difference would translate into a lower transfection efficiency for the mouse

FoxG1:ECFP construct compared to the *Xenopus* FoxG1:ECFP construct. Furthermore, in order to see whether the differences in the N-termini of mammalian and *Xenopus* FoxG1 accounted for these differences in transfection efficiency, a mouse HPQ-region deletion mutant was constructed and used as a control.

As the initial step in the transient transfection analysis, the optimal transfection conditions needed to be established for the OP27 cell line. Each cell line has its own transfection methods and conditions that are specific to it. These methods are influenced by a number of factors such as cell type (e.g. neuronal or epithelial), cell culture conditions (e.g. growth media) or cell growth characteristics (e.g. adherent monolayer or suspension). Two transfection methods, liposome-mediated (LM) and calcium phosphate (CP) precipitation, were tested using various conditions in the OP27 cell line. These methods were selected because of their suitability for the OP27 cell line: the CP precipitation method is optimal for cells grown as monolayers in Dulbecco's Modified Eagle's medium and 10% heat-inactivated fetal bovine serum (Ausubel et al., 2001) while the LM method was previously found to be optimal for transfection of a neuronal rat PC12 cell line (Promega Transfection Guide, 1998).

4.2. Materials and Methods

4.2.1. OP27 cell culture conditions

OP27 cells were routinely maintained at 33°C and 10% CO_2 concentration in Dulbecco's Modified Eagle's medium (DMEM, Gibco) supplemented with 10% heat-inactivated fetal bovine serum (FBS, Highveld Biological) (called DM-10) (Illing et al., 2002). Cells were sub-cultured by washing with 1× phosphate buffered saline (PBS) (140mM NaCl, 2.7mM KCl, 8mM Na_2HPO_4, pH 7.2) and then harvested using 0.25% (w/v) trypsin and 0.04% (w/v) EDTA. Trypsin/EDTA was inactivated by addition of DM-10, and removed by centrifugation (1000×g for 5 minutes), followed by cell re-suspension and plating at the required density. Viable cells

were counted in a haemocytometer after incubation in an equal volume of trypan blue, which stains dead cells blue.

4.2.2. Construction of enhanced cyan florescent protein (ECFP) reporter plasmids

4.2.2.1. pECFP:nls construction

An expression plasmid with a nuclear localization sequence (nls) inserted upstream of the ECFP coding region was constructed as a control for the transfection experiments. The pECFP-N1 plasmid (BD Biosciences) was used as a template in the following 100µl reaction mix: 50ng pECFP-N1, 1× Supertherm buffer, 1.5mM $MgCl_2$, 0.8mM dNTPs, 1µM of each nlsECFPf and nlsECFPr primers (Table 4.1) and 2.5U Supertherm Taq DNA polymerase (Southern Cross Biotechnology). The nlsECFPf and nlsECFPr primers were used to create a nuclear localization sequence (the SV40 large T antigen nls, MAPKKKRKV, referenced from the nuc-lacZ plasmid (obtained from Dr. Nancy Papalopulu, Department of Anatomy, University of Cambridge)) fused to the 5' end of ECFP (nlsECFP). The PCR cycling conditions were as follows: 94°C for 3 minutes (1 cycle), 94°C for 30 seconds, 65°C for 30 seconds, 72°C for 1 minute (30 cycles), 72°C for 5 minutes (1 cycle). The nlsECFP PCR product was resolved on a 1% agarose gel, excised, and purified using the GeneClean Kit and then ligated into the pGEM-T Easy vector (pGEMT:nlsECFP) (as described in Section 2.2.5). The nlsECFP insert was subsequently substituted into the pECFP:N1 expression vector. pGEMT:nlsECFP and pECFP-N1 were digested separately in the following sequential salt concentration reactions: 10µg DNA, 1× Tango buffer and 20U *Cfr42I (SacII)* (Fermentas), digested for 90 minutes, followed by addition of Tango buffer to 2× concentration and 40U *NotI* (Fermentas), and further digestion for 90 minutes. These digestions excised the nlsECFP fragment from pGEMT:nlsECFP and the ECFP coding region from pECFP. The nlsECFP fragment and pECFP-N1 vector (with the ECFP region removed) were resolved on a 1% agarose gel, excised, purified and ligated in the following reaction: 50ng pECFP-N1 vector, 20ng nlsECFP, 1× Ligation buffer and 2U T4 DNA

4.2.2.4. Plasmid screening, sequencing and preparation

Potential positive clones for pECFP:XFoxG1 and pECFP:mFoxG1$\Delta_{65\text{-}320}$ were screened by PCR using the universal BF15'start and BF15'R primers (Table 2.1) and the corresponding PCR cycling conditions (described in Section 2.2.3) with 1µl of overnight culture as template.

polymerase (Roche). The ligation mix (10µl) was transformed into *E. coli* XL1-Blue competent cells (Chung et al., 1989) and transformants were selected for on Luria agar plates containing 75µg/ml kanamycin (Sigma).

Table 4.1. List of primers used to construct FoxG1:ECFP reporter plasmids.

Primer name	Target gene	Primer sequence (5' - 3')	T_m (°C)
XBF1xhoF	*Xenopus* FoxG1	GCTCGAGACCATGTTGGACATGGGGGATAG	76
XBF1sacR	*Xenopus* FoxG1	GCCGCGGTCCATGTATCAAAGAGTTGGACG	78
nlsECFPf	ECFP	GACCATGGCTCCAAAGAAGAAGCGTAAGGTAGT-GAGCAAGGGCGAG	84
nlsECFPr	ECFP	GATTATGATCTAGAGTCGCGGCCGCTTTACTTGT	74

Table notes:
1. All primers designed during this study.
2. T_m (melting temperature) calculated using nearest-neighbour thermodynamic values methods (Breslauer et al., 1986).

4.2.2.2. pECFP:XFoxG1 construction

The *Xenopus* FoxG1 coding region was inserted in-frame into the pECFP-N1 vector. The pCS2:XBF1 (*Xenopus* BF1 or FoxG1) plasmid (obtained from Dr. Nancy Papalopulu, Department of Anatomy, University of Cambridge) was used as a template in the following 100µl PCR reaction: 50ng pCS2:XBF1, 1× Supertherm buffer, 1.5mM $MgCl_2$, 0.8mM dNTPs, 0.5µM of XBF1xhoF and XBF1sacR primers (Table 4.1) and 2.5U Supertherm Taq DNA polymerase (Southern Cross Biotechnology). The XBF1xhoF and XBF1sacR primers were used to amplify XFoxG1 and introduce *XhoI* and *SacII* restriction sites at the ends of the product. The

1.
pECFP:mFoxG1 (25µg) was digested in buffer 4, containing 0.1% BSA, with 30U *SnaBI* at 37°C overnight

Product: 6167 bp (linear plasmid)

Resolved on a 1% agarose gel, excised and purified

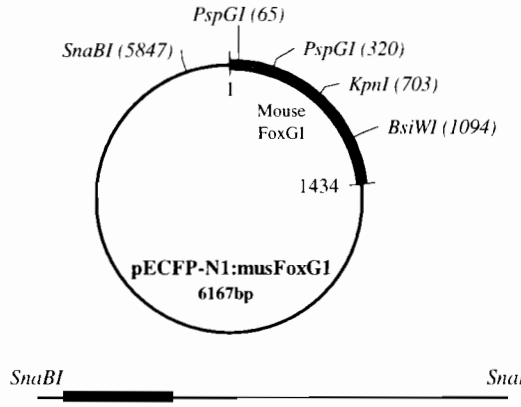

6167 bp

2.
Linear plasmid (15µg) was digested in buffer 3 with 20U *BsiWI* at 55°C for 90 minutes

Products: 1414 bp, 4753 bp (fragment A)

Resolved on a 1% agarose gel, excised and purified

1414 bp **A**: 4753 bp

3.
The 1414 bp product (7µg) was digested in buffer 2 with 10U *PspGI* at 75°C for 60 minutes

Products: 385 bp, 255 bp, 774 bp

Resolved on a 1.5% agarose gel, excised 385 bp (fragment B) and 774 bp (fragment C) fragments and purified

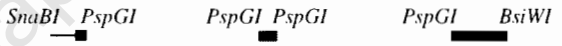

B: 385 bp *255 bp (discarded)* **C**: 774 bp

4.
Ligation of fragment A (100ng), B (200ng), C (200ng) in 1× ligation buffer and 2U T4 DNA ligase (Roche) in a 20µl reaction

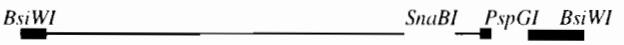

A **B** **C**

5.
10µl of ligation mix was transformed into *E. coli* (Chung et al., 1989), and transformants were selected for on LB plates containing 75µg/ml kanamycin (Sigma).

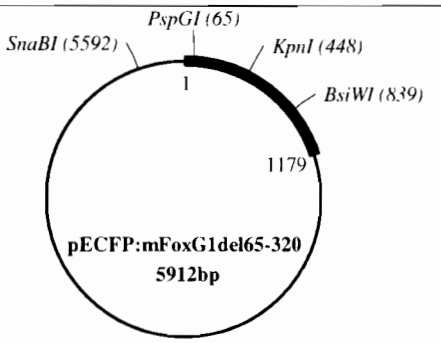

Figure 4.1. pECFP:mFoxG1Δ$_{65-320}$ plasmid construction strategy. The bold black line is the mouse FoxG1 sequence, with the HPQ region shown in grey and remainder of the plasmid (thin black line) is the pECFP vector sequence. All restriction enzymes and buffers were manufactured by New England Biolabs.

4.2.2.4. Plasmid screening, sequencing and preparation

Potential positive clones for pECFP:XFoxG1 and pECFP:mFoxG1$\Delta_{65\text{-}320}$ were screened by PCR using the universal BF15'start and BF15'R primers (Table 2.1) and the corresponding PCR cycling conditions (described in Section 2.2.3) with 1µl of overnight culture as template. Potential positive clones for pECFP:nls were screened by PCR using the nlsECFPf and nlsECFPr primers and corresponding PCR conditions (described in Section 4.2.2.1) with an annealing temperature of 70°C instead of 65°C and 1µl of overnight culture as template. Two PCR-confirmed positive clones for each construct were then sequenced using pECFP-N1 sequencing primers (ECFP-for and EGFP-N, BD Biosciences). One verified clone for each construct was then prepared using the PureYield Midiprep System according to the manufacturer's protocol (Promega). Additionally, all other previously constructed and commercial plasmids that were used in transfections experiments were prepared using the PureYield Midiprep Sysytem. The previously available plasmids used in the transfection experiments were pECFP-N1 (BD Biosciences), pECFP:mFoxG1 (mouse FoxG1 fused to ECFP) (Linda, 2003) and pcDNA4/TO/myc-His/*lacZ* (Invitrogen) (see section 4.2.3.1).

4.2.3. OP27 transient transfection

4.2.3.1. Transfection optimization using pcDNA4/TO/myc-His/lacZ

A β-galactosidase encoding reporter plasmid pcDNA4/TO/myc-His/*lacZ* (Invitrogen) was used to optimize the transfection conditions for the OP27 cell line. Cells were plated in 24-well plates at a density of 4250 cells/cm^2 the day prior to transfection in DM-10. Cells were transfected using either the liposome-mediated (LM) method (TransFast, Promega) or the calcium phosphate (CP) precipitation method (Ausubel et al., 2001). The TransFast reagent is composed of the cationic lipid, N,N [bis(2-hydroxyethyl)]-N-methyl-N-[2,3 di(tetradecanoyloxy) propyl] ammonium iodide and the neutral lipid, L-dioleoyl phosphatidylethanolamine (DOPE). Normally, optimal transfection efficiency is obtained when the DNA/lipid complex is neutral or

positive and therefore TransFast:DNA mass charge ratios of 1:1 and 2:1 were tested. Transfections using the TransFast reagent were performed according to the manufacturer's protocol: medium was removed from the cells, the DNA/lipid mixture was added and incubated for 1 hour at 33°C, following which, DM-10 was added to the cells (the DNA/lipid mixture is not removed) which were then incubated for 48 hours prior to being assayed. For CP transfections, 50µl 0.25M $CaCl_2$, 50µl 2× N,N-bis(2-hydroxethyl)-2-amino-ethanesulfonic (BES) buffered solution (pH 6.95) and plasmid DNA were mixed and added to each well. After the desired transfection time (11, 16 or 24 hours), the cells were washed twice with 1× PBS, then DM-10 was added, and the cells were incubated for a further 48 hours prior to being assayed. For both methods, plasmid amounts of 0.25, 0.5, 0.75 and 1µg per well were tested. Control transfection experiments were performed using no DNA (with the transfection reagent) and without any reagent or DNA. In both cases there was no β-gal positive staining, indicating that the *lacZ* expression observed resulted due to the transfected plasmid and not as an artefact of the OP27 cell line or either of the transfection reagents (Fig. 4.2G).

4.2.3.2. ECFP plasmid transfections

Cells were plated on circular glass coverslips in 24-well plates. Prior to use, the coverslips were acid cleaned in concentrated nitric acid for 1 hour, rinsed with water, and then coated with ECL (entactin, collagen IV, laminin) cell attachment matrix (Upstate Biotechnology). For coating, the coverslips were incubated at 37°C for 1 hour in DMEM serum-free media containing 6.5µg/ml ECL, and then washed twice with 1× PBS. OP27 cells were plated onto coated coverslips at a density of 2700 cells/cm^2 the day prior to transfection. Transfections with ECFP constructs (pECFP, pECFP:nls, pECFP:XFoxG1, pECFP:mFoxG1 and pECFP:mFoxG1$\Delta_{65\text{-}320}$) were performed using the CP precipitation method with a transfection time of 24 hours and 1µg of plasmid DNA per well. The cells were then either maintained at 33°C in DM-10 or shifted to 39°C in differentiation media (1:1 mixture of DMEM:Ham's F12 (Gibco) containing 5µg/ml

insulin, 100µg/ml transferrin, 100µM putrescein, 20nM progesterone and 30nM sodium selenite) containing 50µg/ml gentamycin sulphate (Highveld Biological), 5U/ml heparin (Sigma) and 5ng/ml basic FGF-2 (Promega). Cells, at 33°C and 39°C, were then incubated for 48 hours prior to being assayed for FoxG1:ECFP expression.

4.2.4. Expression assays

4.2.4.1. β-galactosiadse assay

After transfection, cells were fixed with 4% paraformaldehyde at 4°C for 30 min and washed 3 times for 5 minutes with 1× PBS. Cells were stained for 24 hours with 500µl X-gal staining solution per well (4mM $K_3Fe(CN)_6$, 4mM $K_4Fe(CN)_6 \cdot 3H_2O$, 2mM $MgCl_2 \cdot 6H_2O$, 1mg/ml X-gal) (Ausubel et al., 2001). Cells expressing β-galactosidase (blue) and unstained cells were counted, and the transfection efficiency was calculated as the percentage of β-galactosidase positive cells out of the total number of cells. Transfection efficiency experiments were repeated twice with 6 wells per condition in each experiment. Cells were viewed using an Olympus CK40 microscope and images were captured using a JVC TK-C721EG digital video camera.

4.2.4.2. ECFP assay

After transfection, the live cells on their coverslips were inverted and mounted in a drop of DM-10 medium on a glass slide for viewing. Fields of view were captured twice, as a fluorescent image using a green fluorescent protein filter (excitation 395-440nm (band pass), emission 470nm (long pass)) and as a phase contrast image. Total cells were counted using the phase contrast images and transfected cells were counted using the fluorescent images. Transfection efficiency was calculated as the percentage of ECFP positive cells out of the total number of cells. Transfection efficiency experiments were repeated twice with 4 wells per condition in each experiment. Cells were viewed using a Zeiss Axiovert 200M microscope and images were captured using a Zeiss AxioCam HRm camera.

4.3. Results

4.3.1. OP27 transient transfection optimization using a *lacZ* reporter plasmid

Different transfection methods and conditions are effective in different cell lines. Two transfection methods, LM and CP precipitation were tested and optimized in the OP27 cell line using the *lacZ* reporter plasmid, pcDNA4/TO/myc-His/*lacZ*. Transfected cells containing the *lacZ* plasmid stain positive for β-galactosidase activity (blue) (Fig. 4.2).

There are a number of CP transfection methods that make use of different phosphate buffer systems. The method used here involves mixing DNA with calcium chloride and a BES-buffered solution, resulting in a precipitate that is dispersed onto the cells and incorporated via endocytosis. The positive charge of the calcium ions gives the plasmid DNA a net positive/neutral charge, allowing a closer association with the negatively charged cell membrane, and thus facilitating the DNA incorporation into the cells. For this method, transfection times of 11, 16 and 24 hours were investigated using 0.25, 0.5, 0.75 and 1µg of DNA per well in a 24-well plate (as suggested in Ausubel et al., 2001).

For the CP precipitation method, a transfection exposure time of 24 hours gave the best transfection efficiencies of 45.4, 49.5 and 48.6% using 0.5, 0.75 and 1 µg plasmid amounts, respectively (Fig 4.2A, D). These transfection efficiencies were not significantly different from each other and were significantly better ($P < 0.0438$) (Fig. 4.2A, data point labelled *a*) than those obtained with transfections protocols that used less plasmid (0.25µg) and had shorter transfection exposure times (11 and 16 hours) (Fig. 4.2A (data point labelled *b* and all lower CP values), B, C).

following sequential salt concentration reactions: ~5µg DNA, 1× Tango buffer and 10U *Cfr42I (SacII)* (Fermentas), digested for 90 minutes, followed by addition of Tango buffer to 2× concentration and 10U *XhoI* (Fermentas), and further digestion for 90 minutes. The XFoxG1 fragment and pECFP-N1 vector were resolved on a 1% agarose gel, excised, purified and ligated in the following reaction: 50ng pECFP-N1, 35ng XFoxG1, 1× Ligation buffer and 2U T4 DNA polymerase (Roche). The ligation mix (10µl) was transformed into *E. coli* XL1-Blue competent cells (Chung et al., 1989), and transformants were selected for on Luria agar plates containing 75µg/ml kanamycin (Sigma).

4.2.2.3. pECFP:mFoxG1Δ/del$_{65\text{-}320}$ construction

The pECFP:mFoxG1 plasmid (Linda, 2003) was used to create a deletion construct – pECFP:mFoxG1$\Delta_{65\text{-}32}$ – where the HPQ region in the N-terminal domain of mouse FoxG1 was removed (corresponding to nucleotides 65 and 320, Δ/del$_{65\text{-}320}$). The cloning strategy is described in Fig. 4.1.

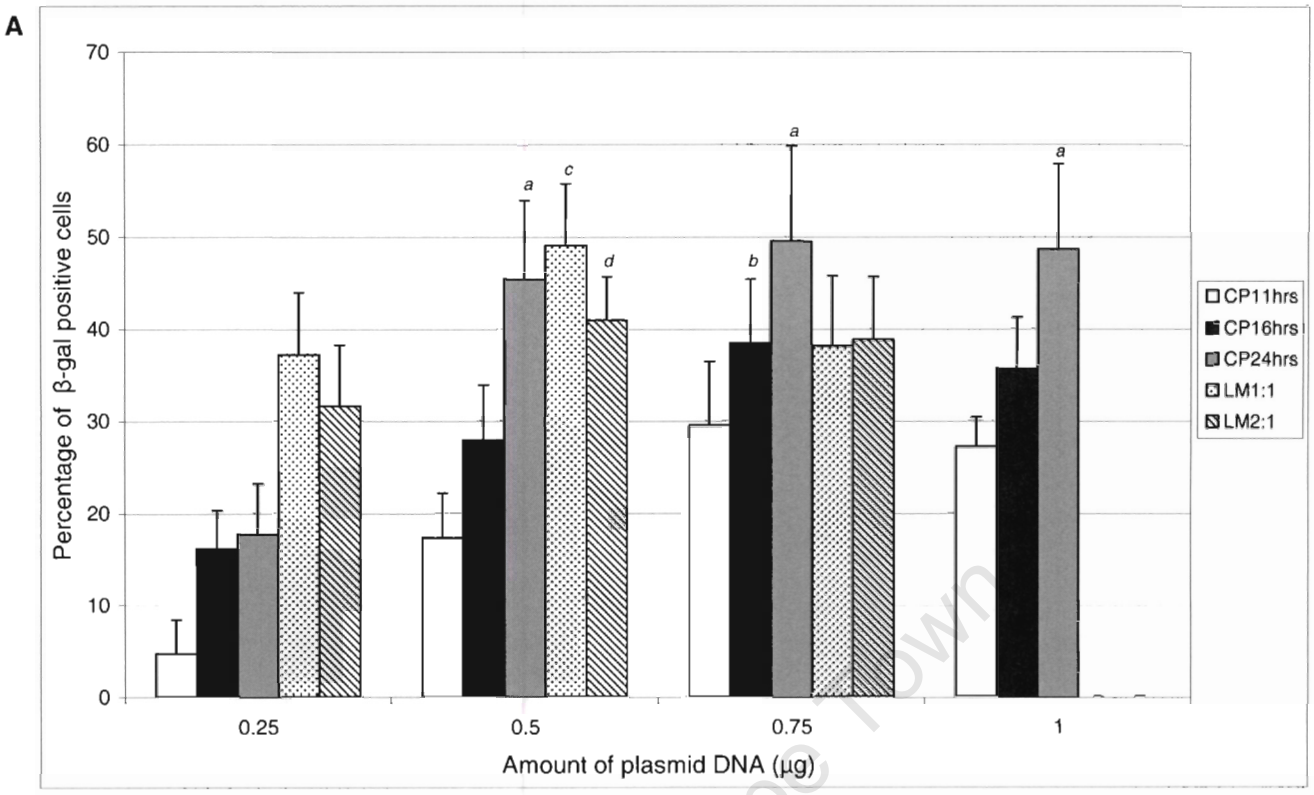

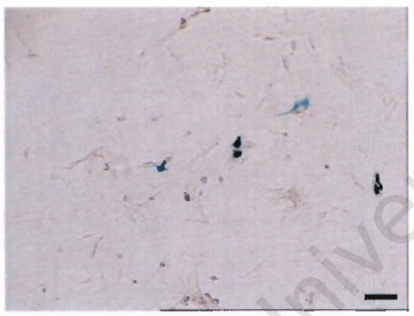

B. CP 11 hours, 0.25µg, 4.7%

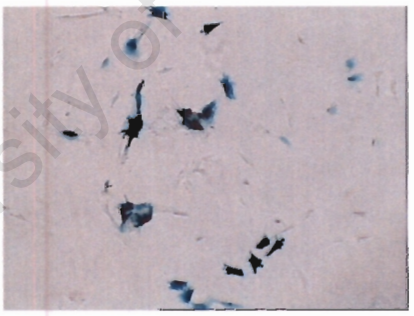

C. CP 16 hours, 0.5µg, 27.9%

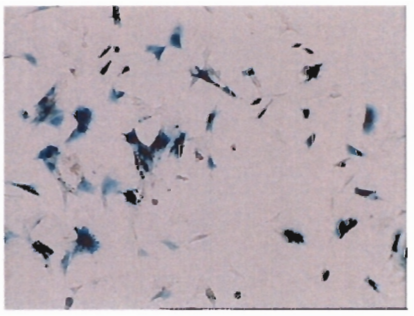

D. CP 24 hours, 0.75µg, 49.5%

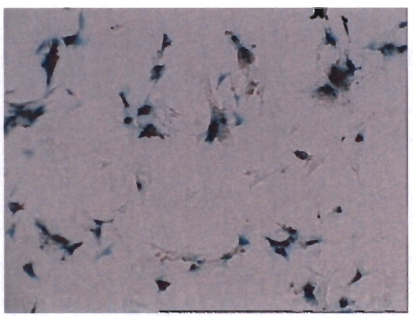

E. LM 1:1, 0.5µg, 49.0%

F. LM 1:1, 1µg, cell death

G. Negative control, 0%

Figure 4.2

Figure 4.2. Optimization of transfection conditions using the pcDNA4/TO/myc-His/*lacZ* reporter plasmid in the OP27 cell line. (A) Transfection efficiencies for calcium phosphate (CP) precipitation and liposome mediated (LM) methods. The amount of plasmid (0.25, 0.5, 0.75 and 1.0μg), time of transfection (CP: 11, 16, 24 hours) and reagent to DNA charge ratio (LM: 1:1, 2:1) were optimized. For CP precipitation the maximum efficiencies obtained, labelled *a*, are significantly different ($P < 0.0438$) from the next highest efficiency, labelled *b*, as well as the all the other efficiencies obtained. For LM method the maximum efficiency obtained, labelled *c*, is significantly different ($P < 0.0407$) from the next highest efficiency, labelled *d*, as well as all the other efficiencies obtained. Efficiency was calculated as the percentage of β-galactosidase positive cells of the total number of cells per field of view. Each data point represents the average of 24 fields of view (2 fields of view per well for 2 separate experiments of 6 well repeats per condition). Error bars represent standard deviation. For the LM method using 1μg plasmid there was complete cell death (F). **(B-G)** Representative images for some of the transfection conditions are shown (10×). The minimum (B) and maximum (D) efficiencies obtained for the CP transfection method and the maximum efficiency for the LM method (E) are shown. (C) shows an intermediate efficiency for the CP method. A negative control without transfection plasmid and reagents shows no β-galactosidase staining (G). Scale bar represents 100μm.

LM transfection methods utilize the overall net positive charge of synthetic liposomes in the transfer of nucleic acids into eukaryotic cells. A cationic portion of the lipid molecule associates with the negatively charged plasmid DNA resulting in the compaction of the DNA into a liposome/DNA complex. The overall net neutral/positive charge of this complex increases the transfection efficiency, presumably because the positive charge allows a closer association with the negatively charged cell membrane, after which the DNA is incorporated into the cells via endocytosis (Promega Transfection Guide). Thus, two important conditions that need to be optimized are the charge ratio of liposome reagent to DNA and the amount of plasmid DNA. For the cationic lipid reagent to function efficiently it should either neutralize or exceed the amount of negative charge contributed by the phosphates on the DNA backbone. Therefore, charge ratios of liposome reagent:plasmid DNA of 1:1 and 2:1 were investigated. Secondly, the optimization of the amount of DNA to be transfected was investigated by testing the transfection efficiency using 0.25, 0.5, 0.75 and 1μg of DNA per well in a 24-well plate. A transfection time of 1 hour was considered optimal and used for all experiments (according to the manufacturer's instruction).

For the LM method, a maximum transfection efficiency of 49% was obtained using 0.5μg plasmid DNA and a charge ratio 1:1 (Fig. 4.2A (data point *c*), E). This was significantly higher

($P < 0.0407$) than the same amount of plasmid used at a charge ratio of 2:1 (Fig. 4.2A, data point *d*) as well as all other efficiencies obtained using 0.25 or 0.75µg DNA at either 1:1 or 2:1 charge ratios. For transfections using 1µg DNA there was complete cell death at both charge ratios (Fig. 4.2F).

The maximum CP precipitation efficiencies of between 45 and 50% were obtained using a transfection exposure time of 24 hours with 0.5, 0.75 and 1µg plasmid. This is comparable to the maximum efficiency of 49%, obtained using the LM method with 0.5µg plasmid and a 1:1 charge ratio. Due to the availability and cost effectiveness of the CP precipitation transfection reagents, it was this method that was used for all subsequent transfection studies, utilizing a transfection time of 24 hours with 1µg plasmid DNA.

4.3.2. Transient transfection using various ECFP reporter plasmids to test the effect of FoxG1 on OP27 cell survival

4.3.2.1. Plasmid construction

Five ECFP reporter constructs were transfected into the OP27 cell line. Two of them, pECFP (the unaltered reporter plasmid) and pECFP:mFoxG1 (mouse FoxG1) were already available (BD Biosciences; Linda, 2003). The other three plasmids, pECFP:nls (nuclear localization sequence fused to the 5' end of ECFP), pECFP:XFoxG1 (*Xenopus* FoxG1) and pECFP:mFoxG1$\Delta_{65\text{-}320}$ (mouse FoxG1 with the HPQ region (nucleotides 65-320) deleted), were constructed in this study.

For the pECFP:nls plasmid, PCR using pECFP as template and a nls containing sense primer, produced a ECFP fragment with the nls fused to its 5' end (Fig. 4.3A, lane 1), which was

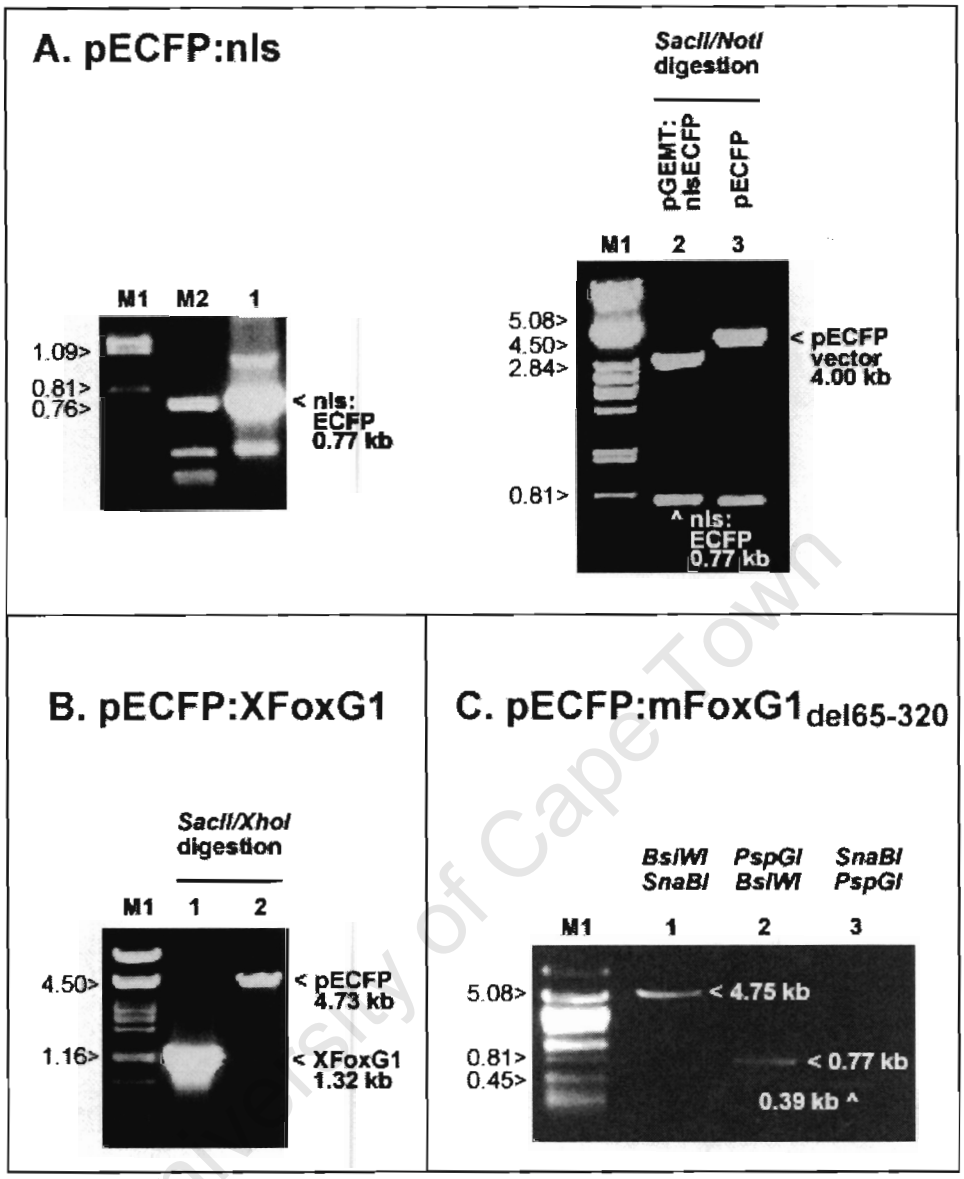

Figure 4.3. Enhanced cyan fluorescent protein (ECFP) reporter plasmid construction for transfection efficiency studies. M1 is a λDNA/*PstI* marker and M2 is a pGEM/*HpaII* marker, with the relevant fragment sizes shown on the left of each gel. (**A**) PCR was used create a nuclear localization sequence (nls) fused to the 5' end of ECFP (nls:ECFP, lane 1) which was then cloned into pGEM-T Easy (pGEMT:nlsECFP). pGEMT:nlsECFP and pECFP were digested with *SacII* and *NotI* (lanes 2 and 3), to yield nls:ECFP (arrowhead, lane 2) and pECFP vector (arrowhead in 3, the lower band is the released ECFP fragment), which were then ligated to form the final pECFP:nls plasmid. (**B**) Construction of *Xenopus* FoxG1 (XFoxG1) fused to ECFP. A previously constructed XFoxG1 plasmid was used as template in a PCR reaction with primers that introduced *SacII* and *XhoI* restriction at the ends of the XFoxG1 fragment. XFoxG1 and pECFP were then digested with *SacII* and *XhoI* (arrowheads in lanes 1 and 2) and ligated together to form the final pECFP:XFoxG1 plasmid. (**C**) Construction of the mouse FoxG1 (mFoxG1) HPQ region (nucleotides 65-320) deletion mutant fused to ECFP. The previously constructed pECFP:mFoxG1 plasmid (Linda, 2003) was digested with *SnaBI, BsiWI* and *PspGI* and yielded four fragments. The 255 bp HPQ region fragment was discarded and the remaining fragments (lanes 1, 2 and 3) were ligated together to form the final plasmid. The restriction enzymes names above the lanes show the restriction site at the end of the fragment, with the 5' end shown at the top and the 3' end shown at the bottom. For (A), (B) and (C) the detailed cloning is described in sections 4.2.2.1, 4.2.2.2 and 4.2.2.3, respectively.

subsequently cloned into pGEM-T Easy (pGEMT:nlsECFP). A *SacII/NotI* restriction digestion of pGEMT:nlsECFP and pECFP released the nlsECFP and ECFP fragments, respectively (Fig. 4.3A, lanes 2 and 3). The nlsECFP fragment and the ECFP vector (with the ECFP coding region excised) were ligated together to form the pECFP:nls plasmid. This plasmid was initially verified by sequencing and then by examining ECFP localization after transfection in the OP27 cells. In cells transfected with pECFP:nls, ECFP was localized to the nucleus, indicating that the construction of a functional nls:ECFP plasmid was successful (Fig. 4.4D, E). In some cases however, pECFP:nls did show some residual cytoplasmic expression although the expression was mainly concentrated in the nucleus (Fig. 4.4D). The detailed cloning strategy for pECFP:nls is described in section 4.2.2.1.

For the pECFP:XFoxG1 plasmid, XFoxG1 was amplified from an existing XFoxG1 plasmid by PCR with primers that introduced *SacII* and *XhoI* restriction sites at the ends of the fragment. The XFoxG1 PCR fragment and pECFP were digested with *SacII* and *XhoI* (Fig. 4.3B, lanes 1 and 2) and then ligated together to form the pECFP:XFoxG1 plasmid. The pECFP:mFoxG1$\Delta_{65\text{-}320}$ plasmid was constructed from the pECFP:mFoxG1 plasmid (Linda, 2003). Sequential restriction digestions with *SnaBI, BsiWI* and *PspGI* yielded four fragments, one of them corresponding to the HPQ region (nucleotide 65-320 of mFoxG1) was discarded, while the remaining three were ligated together to form the pECFP:mFoxG1$\Delta_{65\text{-}320}$ plasmid (Fig. 4.3C). These two plasmids were verified by sequencing and showed the expected FoxG1-mediated nuclear expression when transfected into the OP27 cells (Fig. 4.4F, G, J, K). The detailed cloning strategies for pECFP:XFoxG1 and pECFP:mFoxG1$\Delta_{65\text{-}320}$ are described in sections 4.2.2.2 and 4.2.2.3, respectively.

4.3.2.2. Effect at 33°C

Five ECFP reporter constructs were transfected into the OP27 cells, maintained at 33°C in an undifferentiated, proliferative state, in order to test the effect of constitutive FoxG1 expression on the survival of the cells. Two control plasmids pECFP (the unaltered reporter plasmid) and pECFP:nls (encoding a nuclear localization signal fused to ECFP) were used to establish the reference ECFP transfection efficiency levels. Transfection with pECFP establishes the transfection efficiencies that are specific to this reporter plasmid with regard to the factors that influence the expression of the ECFP protein, such as successful incorporation into the cells or transcription and translation rates. Additionally, because FoxG1:ECFP fusion proteins are targeted to the nucleus by FoxG1, it was also important to use a control where ECFP was targeted to the nucleus. This is because there may be a difference between the effect that nuclear ECFP and cytoplasmic ECFP have on OP27 cell survival.

The percentage of OP27 cells that expressed ECFP after transfection with pECFP was 12.3% (Fig. 4.4A) with the positive cells exhibiting a cytoplasmic expression pattern (Fig. 4.4B). The importance of establishing these plasmid-specific levels is immediately evident by comparing the maximum transfection efficiency of 49.5% obtained for the *lacZ* reporter construct (Section 4.3.1.) to the 12.3% obtained for pECFP. Similarly, the pECFP:nls plasmid was used to establish the efficiency of ECFP expression after targeting it to the nucleus. The pECFP:nls transfection efficiency (12.1%) (Fig. 4.4D) was not significantly different to the cytoplasmic pECFP efficiency (12.3%) (Fig. 4.4A), indicating that the nuclear localization of ECFP has no significant effect on transfection efficiency levels.

A

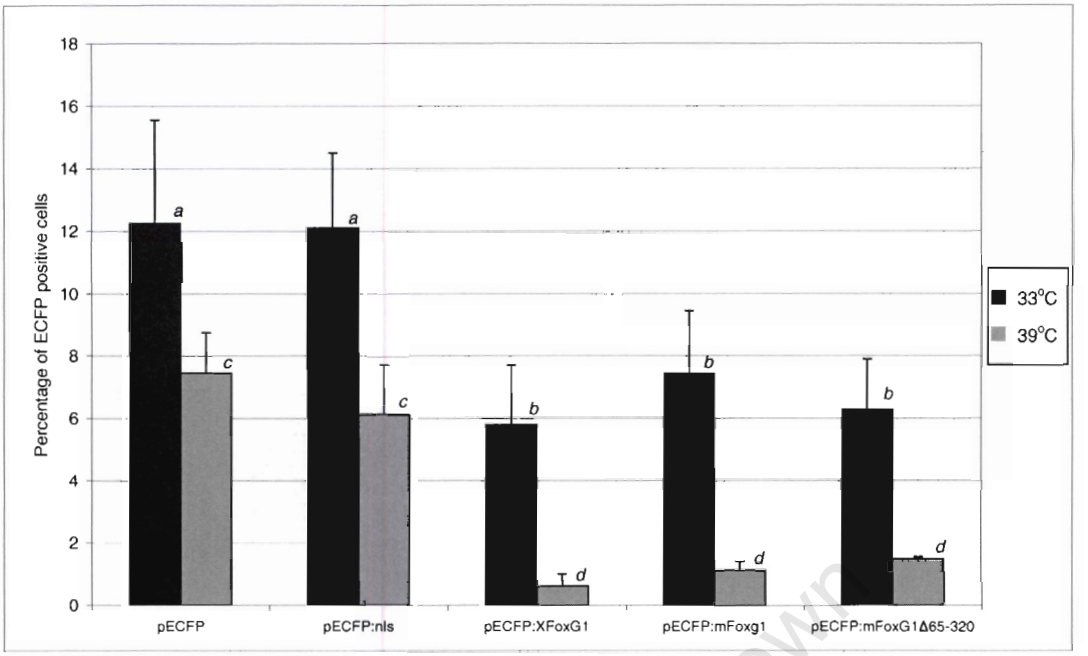

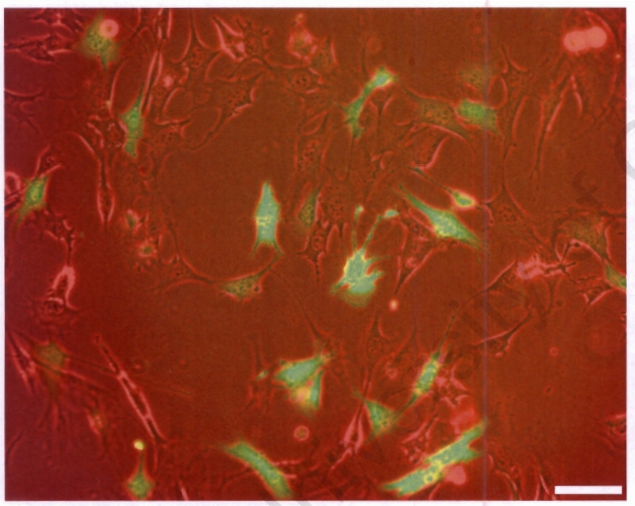

B. 33°C, pECFP

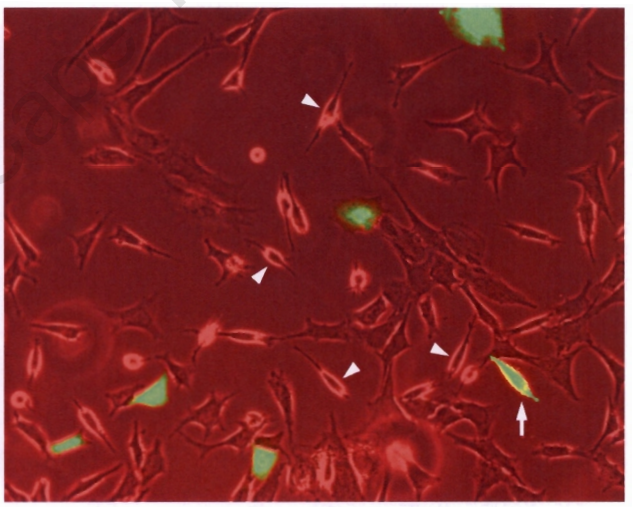

C. 39°C, pECFP

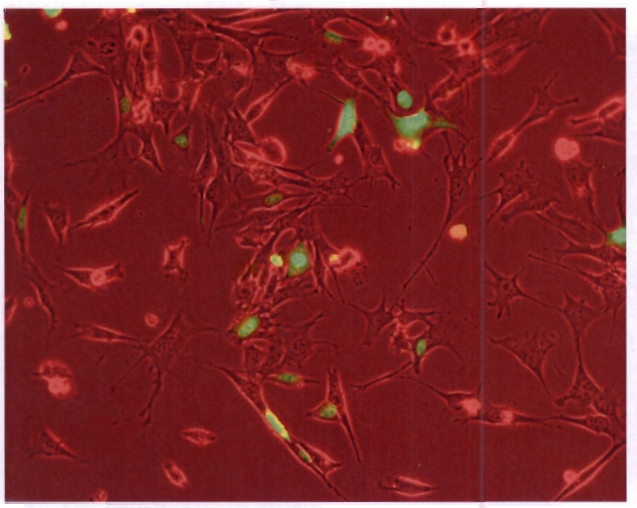

D. 33°C, pECFP:nls

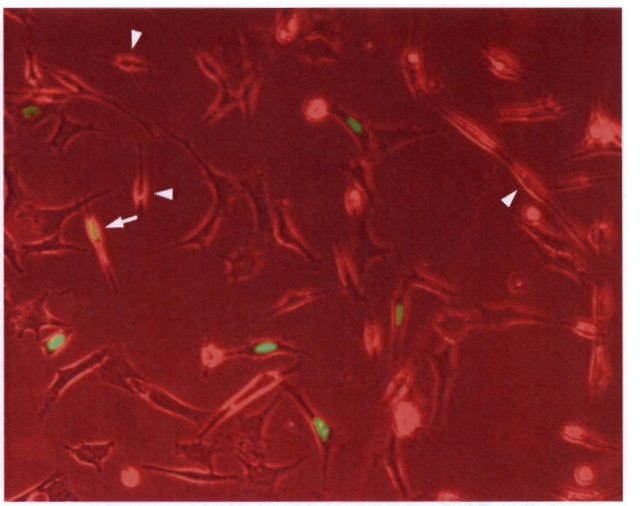

E. 39°C, pECFP:nls

Figure 4.4

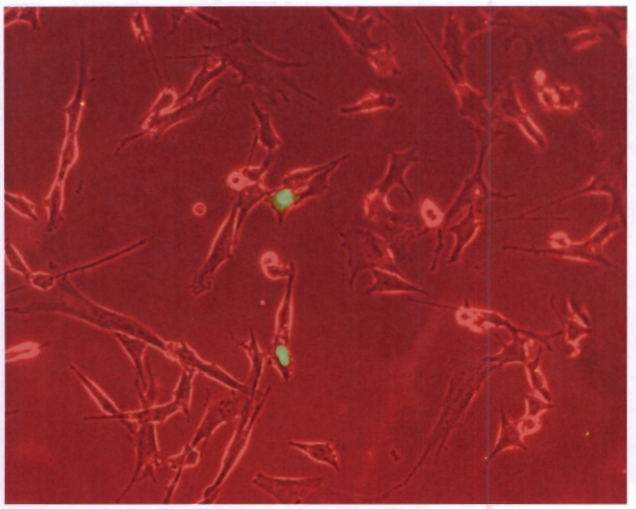

F. 33°C, pECFP:XFoxG1

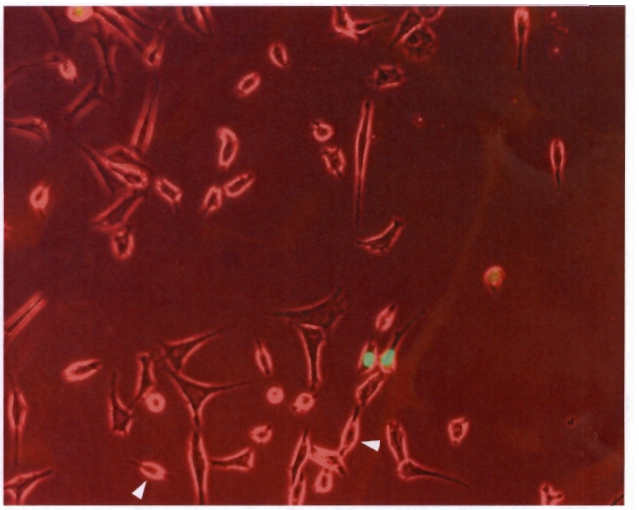

G. 39°C, pECFP:XFoxG1

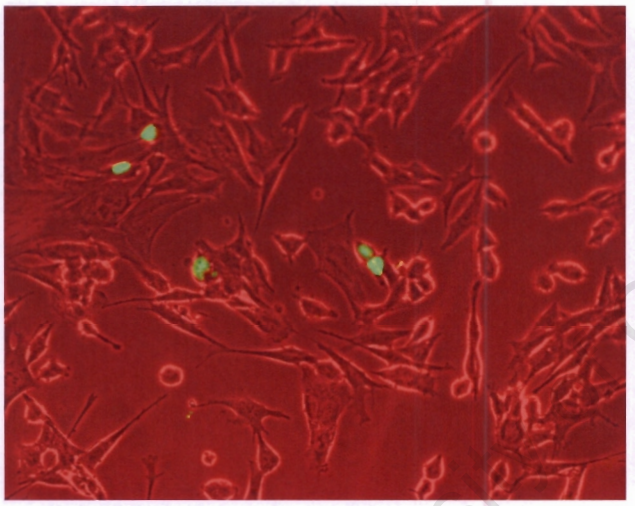

H. 33°C, pECFP:mFoxG1

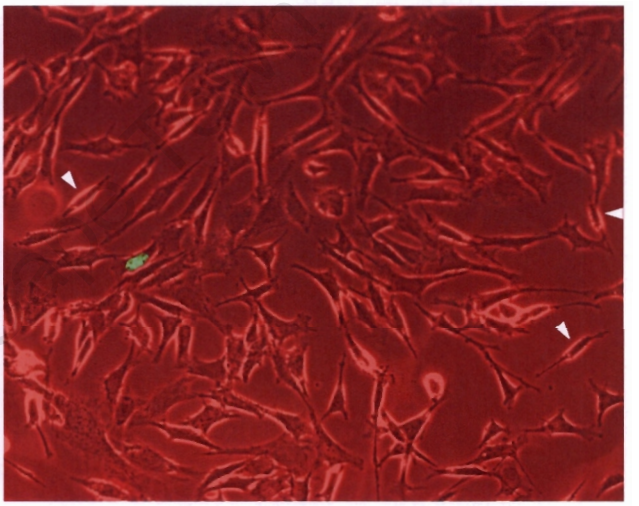

I. 39°C, pECFP:mFoxG1

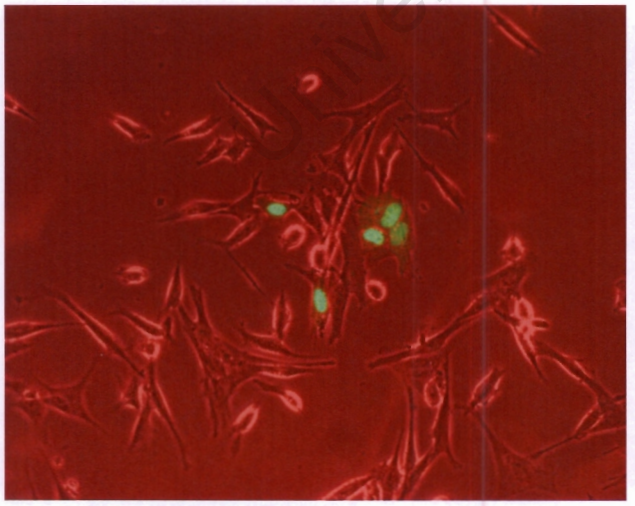

J. 33°C, pECFP:mFoxG1$\Delta_{65\text{-}320}$

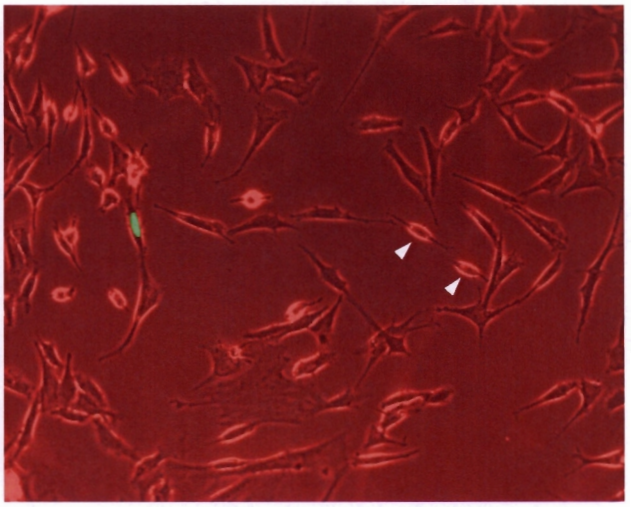

K. 39°C, pECFP:mFoxG1$\Delta_{65\text{-}320}$

Figure 4.4 continued

Figure 4.4. Transient transfections in the OP27 cell line using various ECFP reporter constructs to determine the potency effect of FoxG1. **(A)** Percentage of OP27 cells expressing ECFP after transient transfection with various plasmids at 33°C (undifferentiated in DM-10 medium) and 39°C (FGF-2 induced differentiation). Efficiency was calculated as the percentage of ECFP positive cells of the total number of cells per field of view. Each data point represents the average of 24 fields of view (3 fields of view per well for 2 separate experiments of 4 well repeats per plasmid). Error bars show standard deviation. Data points labelled *a* are significantly different from points labelled *b* ($P < 0.001$); data points labelled *c* are significantly different from points labelled *d* ($P < 0.02$). **(B-K)** Pseudocoloured representative images (20×) merged from a fluorescent image showing ECFP localization (green) and a phase contrast image showing the OP27 cell bodies (red). The growth conditions (33°C or 39°C) are shown for each of the transfected constructs, as indicated. At 39°C a portion of the OP27 cells differentiate into bipolar neurons with phase bright cell bodies and neurite extensions (arrow and arrowheads). Scale bar (B) represents 250µm for all images.

With the reference ECFP and nuclear ECFP efficiency levels established at approximately 12%, it was sought to determine whether FoxG1 had any effect on the survival of the OP27 cells, and whether different FoxG1 orthologs exerted different effects. Transfection of OP27 cells with mouse FoxG1:ECFP showed an expression level of 7.5% ECFP positive cells (Fig. 4.4A, H). This is significantly different to the efficiencies of pECFP and pECFP:nls plasmids ($P < 0.001$), indicting that mouse FoxG1 may have a negative effect on OP27 cell survival. It was hypothesized that mouse FoxG1 may have a greater effect on cell survival compared to *Xenopus* FoxG1, resulting in lower transfection efficiencies; this however, was not the case as *Xenopus* FoxG1 exhibited a transfection efficiency of 5.8% which was not significantly different ($P = 0.3398$) to transfection efficiencies for mouse FoxG1. Finally, the construct used to test if the HPQ-rich region in the terminal domain was responsible for the cell survival effect of mouse FoxG1, pECFP:mFoxG1$\Delta_{65\text{-}320}$, showed a transfection efficiency of 6.3% (significantly different from the pECFP/pECFP:nls ($P < 0.0001$) but not significantly different from mouse FoxG1 ($P = 0.6764$) or *Xenopus* FoxG1 ($P = 0.5555$); Fig. 4.2A, J). This transfection efficiency was similar to the wildtype mouse FoxG1 expression level of 7.5%, indicating that the HPQ region does not affect cell survival and transfection efficiency of constitutively expressed exogenous mouse FoxG1 in OP27 cells. Thus, although the expression of constitutive exogenous FoxG1:ECFP showed reduced transfection efficiency compared to the pECFP and pECFP:nls control plasmids,

no significant difference in transfection efficiency was observed between mouse, *Xenopus* and the mouse HPQ-deletion plasmids.

4.3.2.3. Effect at 39°C after FGF-2 induced differentiation

After two days of FGF-2 treatment, endogenous FoxG1 was excluded from the nucleus (although not completely) in OP27 cells that adopted the characteristic differentiating olfactory receptor neuron (ORN) morphology and the corresponding Notch signalling molecular changes (Chapter 3). This suggests that FoxG1 transcriptional activity may be down-regulated by exclusion from the nucleus, in order for OP27 cells differentiate. With this in mind, the effect of constitutive FoxG1:ECFP expression in the OP27 cells following FGF-2 induced differentiation was examined for the following reasons: (1) to test whether expression of different FoxG1:ECFP orthologs affected cell survival under differentiation conditions, (2) to test whether the constitutively expressed FoxG1:ECFP was exported from the nucleus in response to FGF-2 treatment and, (3) to test whether constitutive over-expression of FoxG1:ECFP inhibited differentiation of OP27, measured by the number of cells with neurite extensions.

When shifted to 39°C and induced to differentiate with FGF-2, a sub-population of the cells adopted the characteristic bipolar morphology after the 48 hours (phase bright cell bodies with neurite-like extensions) (arrow and arrowheads in Fig. 4.4C, E, G, I, K). Transfection efficiencies of the pECFP and pECFP:nls control plasmids in OP27 cells at 39°C, were significantly reduced to 7.5% and 6.1% respectively, which is an approximately two fold reduction compared to transfection efficiency at 33°C (Fig. 4.4A, C, E). Thus, although the transfection efficiency of the OP27 cells was reduced when the cells were cultured at 39°C in the presence of FGF-2, the transfection efficiency was not significantly affected by the expression of nuclear ECFP compared to cytoplasmic ECFP expression. The transfection levels of pECFP:XFoxG1, pECFP:mFoxG1 and pECFP:mFoxG1$\Delta_{65\text{-}320}$ were 0.6%, 1.1% and 1.5%

respectively (Fig. 4.4A, G, I, K). These FoxG1 levels are all significantly different from the pECFP and pECFP:nls levels ($P < 0.02$) but not from each other, as was the case at 33°C. Interestingly, while the differences in transfection efficiency between the control and FoxG1:ECFP plasmids is 1.6-2.7 fold at 33°C, it is 4.1-12.5 fold at 39°C. Thus, although there was no significant difference between Xenopus, mouse and the mouse HPQ-deletion mutant plasmids, it is possible that constitutive expression of all FoxG1:ECFP orthologs has a greater effect on cell survival under conditions of differentiation compared to growth at 33°C.

Next, the sub-cellular localization of FoxG1:ECFP was examined to check if it was exported from the nucleus following FGF-2 treatment. At the corresponding time point (2 days) following FGF-2 treatment, endogenous FoxG1 was shown to be partially excluded from the nucleus (Chapter 3). However, although the transfection efficiencies were low, all FoxG1:ECFP transfected cells showed a nuclear expression pattern, indicating that FoxG1:ECFP is not excluded/exported from the nucleus during the time frame used for these experiments.

In Chapter 3 the hypothesis was formulated that FGF-2 signalling induced down-regulation of FoxG1 by exporting it from the nucleus, leading to neuronal differentiation. Thus, if constitutive FoxG1:ECFP was not being exported from the nucleus, then presumably it would maintain the cells expressing it in a undifferentiated state, thus affecting the proportion of cells that adopt the bipolar morphology. pECFP showed expression in only 14 bipolar cells (approximately 1% of total cells assayed) while pECFP:nls expression could only be detected in 6 bipolar cells (approximately 0.4% of total cells assayed) (for example, arrows in Fig. 4.4C, E). Conversely, no bipolar cells expressing nuclear FoxG1:ECFP could be detected. This suggests that if FoxG1:ECFP is expressed in a cell, then it maintains the cell in an undifferentiated, proliferating state. However, because the number of cells expressing pECFP and pECFP:nls is so small, no significant comparisons can be made.

4.4. Discussion

The focus of this chapter was to check whether there was a functional difference between mammalian (mouse) and non-mammalian (*Xenopus*) FoxG1 orthologs. This was investigated by examining if constitutive expression of these orthologs had different effects on cell survival, as determined by transient transfection efficiencies of various plasmids in the OP27 cell line. The first step was to optimize a transient transfection protocol for the OP27 cell line using the calcium phosphate precipitation and liposome-mediated methods. A transfection time of 24 hours with 0.5, 0.75 or 1µg of plasmid DNA for the CP precipitation method, and a reagent to DNA ratio of 1:1 and 0.5µg of plasmid DNA for the LM method, yielded the maximum transfection efficiencies obtained of between 45 and 50%. The establishment of the optimal transfection conditions for the OP27 cell line provides an important and necessary foundation for any subsequent transfection studies using this cell line. Because the reagents for the CP precipitation method are cheaper and are readily available from laboratory stocks, this method was used for subsequent transfection experiments in this study.

It was sought to determine whether constitutive expression of FoxG1 affected transfection efficiency of OP27 cells at 33°C and following FGF-2 induced differentiation at 39°C. Although the optimal transfection conditions were determined for the OP27 cell line using a *lacZ* reporter plasmid, it was still necessary to determine the reference expression levels that were specific to the pECFP plasmid. This pECFP expression level was established at 12.3%, markedly lower the *lacZ* reporter plasmid levels of 49.5%. This 4-fold difference is surprising as both reporter plasmids are specifically constructed for mammalian cell line transfection and are under the control of the CMV promoter. Factors that could explain this disparity include the difference in the ability of the plasmids to form a favourable incorporation complex with the transfection reagents. While this difference should be noted, it is not as important as the establishment of the pECFP-specific expression levels for subsequent FoxG1:ECFP comparisons.

Next, the effect on expression levels of targeting ECFP to the nucleus was established. This is an important control because FoxG1:ECFP fusion proteins are targeted to the nucleus by FoxG1 and thus a reference nuclear ECFP expression level is required to be established, independently of FoxG1. Transfection efficiency with the pECFP:nls plasmid (12.1%) was not significantly different to transfection efficiency with the pECFP plasmid (12.3%). With the pECFP and pECFP:nls expression levels established, it was sought to determine whether constitutive expression of different FoxG1:ECFP orthologs affected the survival of the OP27 cells as measured by transfection efficiency. While overall transfection efficiencies were significantly reduced compared to the control plasmids there was no significant difference in the transfection efficiencies between mouse FoxG1 (7.5%), *Xenopus* FoxG1 (4.6%) and the mouse HPQ-deletion mutant (6.3%). Similarly, when induced to differentiate at the non-permissive temperature (39°C), the constructs show comparable relative transfection efficiencies to those at 33°C: the FoxG1:ECFP constructs are not significantly different from each other (mouse FoxG1 1.1%, *Xenopus* FoxG1 0.6% and mouse HPQ-deletion mutant 1.5%), but are significantly lower than the control pECFP and pECFP:nls plasmids (7.5% and 6.1%, respectively). Thus, although there is no functional difference between the FoxG1 constructs these results show that constitutive FoxG1 expression may have an effect on cell survival in the OP27 cell line, as determined by transfection efficiency rates. A possible explanation is that constitutive expression of FoxG1 causes cell death. Martynoga et al. (2005) reported that the telencephalon of E10.5 FoxG1 null mutant mice embryos showed a clear reduction in the number of apoptotic labelled cells compared to the wildtype embryos – indicating that FoxG1 may promote apoptosis in the telencephalon. The observations that constitutive FoxG1 expression may have a negative effect on cell survival are surprising because FoxG1 has been shown to play a role in promoting the proliferation of the cortical progenitor cells during telencephalon development.

Interestingly, while the difference in transfection efficiencies between the control and FoxG1:ECFP plasmids is 1.6-2.7 fold at 33°C, it is significantly higher at 4.1-12.5 fold at 39°C. This suggests that cells constitutively expressing FoxG1:ECFP constructs (irrespective of whether they are mouse or *Xenopus* orthologs) are less likely to survive when they are induced to differentiate.

Endogenous FoxG1 begins to be exported from the nucleus in OP27 cells that adopt the characteristic differentiated bipolar morphology following FGF-2 treatment (Chapter 3). Thus it was tested whether FoxG1:ECFP was exported from the nucleus after the cells were induced to differentiate with FGF-2. However, after 2 days of ECFP expression (the suggested expression time for transient transfections (Ausubel et al., 2001)), no cells expressed cytoplasmic FoxG1:ECFP. This could be explained by the following reasons: (1) 2 days of FGF-2 treatment is not a long enough period to observe FoxG1:ECFP export from the nucleus – endogenous FoxG1 becomes convincingly localized in the cytoplasm after 8 and 12 days of FGF-2 treatment (Chapter 3) or, (2) if FoxG1:ECFP is exported from the nucleus then it has a detrimental effect on cell survival, and hence no cells exhibit cytoplasmic FoxG1:ECFP. Furthermore, because FoxG1:ECFP was not exported from the nucleus – presumably maintaining the progenitor cells in a proliferative state – it was tested to see if there was a reduction in the number of cells that differentiated. No cells that expressed FoxG1:ECFP showed the bipolar morphology, compared to approximately 1% and 0.4% for pECFP and pECFP:nls, respectively, indicating that nuclear FoxG1 may maintain the cells that express it in an undifferentiated state. However, because the number of expressing FoxG1:ECFP was so low (≤ 1.5% of total cell population) no significant conclusions can be made.

From above, there are three interesting features of the cells expressing FoxG1:ECFP at 39°C: (1) there is a bigger difference in transfection efficiencies between the control and FoxG1:ECFP

plasmids, compared to 33°C, (2) there is no export of FoxG1:ECFP from the nucleus and, (3) no cells that express FoxG1:ECFP exhibit a bipolar morphology. A suggestion that could be offered to correlate these observations is that at 39°C, if a cell expresses FoxG1:ECFP in the nucleus and responds to FGF-2 signalling cues, then this has a detrimental effect on cell survival. This would explain all the observations listed above: there is a decrease in survival of cells expressing FoxG1:ECFP, no evidence of FoxG1:ECFP export from the nucleus and no bipolar FoxG1:ECFP-expressing cells because these cells die when response to FGF-2 signalling cues. Thus it may be that if the opposing actions of FoxG1 (proliferation) and FGF-2 (differentiation) are active in the same cells, then this results in a detrimental effect on cell survival. However, this conflicts with the findings of Chapter 3, where differentiating bipolar cells showed both nuclear and cytoplasmic endogenous FoxG1 expression. Thus, it is more likely that other factors may be responsible for the continual constitutive expression of FoxG1:ECFP in the nuclei of the OP27 cells in differentiation medium. These include the following factors: the ECFP protein may be folded in such a way that it is masking the FGF-2 responsive phosphorylation site, or the actual size of the ECFP protein may be inhibiting the export of FoxG1 from the nucleus (although numerous other ECFP fused constructs show sub-cellular change in localization). Furthermore, it may be that because there is constitutive expression of FoxG1 and therefore higher levels of the protein compared to endogenous FoxG1, more time (i.e. longer than two days) is required for the FoxG1:ECFP protein to be excluded from the nucleus, however, if this is the case then some level of residual cytoplasmic expression would be expected. Also, the very low number of cells expressing FoxG1:ECFP under differentiation conditions prevents any significant conclusions from being made. To validate these results, stable transfections with FoxG1:ECFP under the control of an inducible promoter should be performed.

In summary, effects of different FoxG1 orthologs on OP27 cell survival were tested by examining transfection efficiency. As an initial step in this analysis the optimal transfection conditions were determined for the OP27 cell line. Comparison of mouse, *Xenopus* and a mouse HPQ deletion mutant FoxG1:ECFP constructs showed no significant difference in their effects on the survival of the OP27 cell line, as determined by transfection efficiency. However, these constructs did show a more detrimental effect than the control plasmids, suggesting that FoxG1 may mediate a negative effect on OP27 cell survival, which may be achieved through the regulation of apoptosis.

CHAPTER 5
Conclusions

This study investigated two main themes related to the brain-specific transcription factor FoxG1: (1) the variation in FoxG1 sequence across the vertebrate evolutionary spectrum and the functional significance thereof and, (2) the sub-cellular regulation of FoxG1 by FGF-2.

Because FoxG1 promotes cortical progenitor cell proliferation and has a similar mutant human phenotype to genes that show signatures of adaptive evolution, it was investigated whether FoxG1 may play a role in determining the expansion and complexity of the cortex across vertebrates. This was investigated by examining the changes in sequence in the variable N-terminal domain of FoxG1 across vertebrates and testing if these changes translated into functional differences and, by examining the primate lineage for signatures of adaptive evolution acting on FoxG1.

New orthologs were cloned from nine organisms, including three reptiles, a vertebrate class with no previous FoxG1 members, and six mammals. The mammalian orthologs showed a high degree of conservation, with the insertion of an HPQ-rich region in the N-terminal. In contrast, the non-mammal orthologs lacked this extended HPQ region and showed a lower degree of conservation.

The role of FoxG1 in the expansion of the cortex across vertebrates was hypothesized to be mediated through two possible mechanisms: (1) adaptive evolution as determined by changes in the coding sequence and, (2) the effect of the FOXG1 duplication in humans. Analysis of the primate FoxG1 orthologs showed that there was no evidence for adaptive evolution in the

lineage leading to humans. Additionally, PCR and human genome analysis showed that the presence of the duplicated form of FOXG1, FOXG1A could not be substantiated.

Because no positive selection characteristics were observed in primates and because the nature of K_a/K_s analysis did not allow for mammal/non-mammal comparisons, functional studies were carried out to test the difference in effect of a mammalian ortholog (mouse) compared to a non-mammalian ortholog (*Xenopus*) on the survival of the OP27 cell line (as measured by transfection efficiency). However, while the FoxG1:ECFP constructs showed lower transfection efficiencies compared to the control plasmids, there was no difference between the mouse and *Xenopus* orthologs, indicting that this test for effect on cell survival showed no functional differences between these two orthologs.

Analysis of the 3' UTR of available FoxG1 reference sequences together with Vervet monkey and crocodile sequences (cloned during this study) showed high levels of conservation. Two possible regulatory mechanisms which could explain the selection of a conserved 3' UTR, secondary structure and microRNAs, were investigated. No conserved or highly stable secondary structures were predicted in the 3' UTR, however, there was evidence for possible miRNA regulation. Four miRNA target sites, corresponding to miRNA 9, 33, 34 and 299 were identified using the PicTar algorithm (Krek, et al., 2005). MiR-9 was the most interesting as it was the only miRNA site that showed conservation in the most distantly related ortholog, zebrafish, and also showed expression in proliferating cells in the brain (Farh et al., 2005). Thus, this conservation across all orthologs and the correlation between the cells expressing FoxG1 and miR-9, suggests that miR-9 might play a role in FoxG1 regulation by suppressing translation or by regulating mRNA stability.

Lastly, the changes in FoxG1 localization in response to FGF-2 signalling were monitored. There is a conserved FGF-2 responsive Protein kinase B site in the DNA-binding domain of FoxG1 that is important for the export of the protein from the nucleus of differentiating neurons (T Regad and N Papalopulu, personal communication). It was therefore tested in this study if there were changes in endogenous sub-cellular localization of FoxG1 in response to FGF-2 induced differentiation in the OP27 cell line. The differentiation state of the OP27 cells was monitored by examining neuron morphology and changes in the neural signalling components Notch1 and Delta1. When undifferentiated, the OP27 cells expressed FoxG1 in their nuclei where it drives cell proliferation and inhibits neuronal differentiation. However, when the OP27 cells were induced to differentiate with FGF-2, FoxG1 was shown to be exported from the nucleus, indicating a possible FGF-2-mediated down-regulation of FoxG1's transcriptional activity.

Thus, this study provides insight into the evolutionary characteristics of FoxG1 by presenting the sequences of new orthologs, by testing for adaptive evolution acting on FoxG1 and, by showing that the conserved 3' UTR of FoxG1 may be the target for miRNA regulation. Additionally, FGF-2 is shown to regulate the localization and possibly the activity of FoxG1, indicating that FGF-2 may play a role in regulating FoxG1 during the development of the telencephalon.

CHAPTER 6
References

Ahlgren S, Vogt P, Bronner-Fraser M (2003). Excess FoxG1 Causes Overgrowth of the Neural Tube. *Journal of Neurobiology* 57, 337-349.

Allman J, Hakeem A and Watson K (2002). Two phylogenetic specializations in the human brain. *Neuroscientist* 8, 335-346.

Altuvia Y, Landgraf P, Lithwick G, Elefant N, Pfeffer S, Aravin A, Brownstein MJ, Tuschl T and Margalit H (2005). Clustering and conservation patterns of human microRNAs. *Nucleic Acids Research* 33, 2697-2706.

Ambros V (2004). The functions of animal microRNAs. *Nature* 431, 350-355.

Arnason U, Adegoke JA, Bodin K, Born EW, Esa YB, Gullberg A, Nilsson M, Short RV, Xu X and Janke A (2002). Mammalian mitogenomic relationships and the root of the eutherian tree. *Proc. Natl. Acad. Sci. USA* 99, 8151-8156.

Ausubel FM, Brent R, Kingston RE, Moore DD, Siedman JG, Smith JA and Struhl K (2001). *Current Protocols in Molecular Biology, Volumes 1-4*. John Wiley & Sons, Inc.

Bond J, Roberts E, Mochida GH, Hampshire DJ, Scott S, Askham JM, Springell K, Mahadevan M, Crow YJ, Markham AF, Walsh CA, Woods CG (2002). ASPM is a major determinant of cerebral cortical size. *Nature Genetics* 32, 316-320.

Bond J, Scott S, Hampshire DJ, Springell K, Corry P, Abramowicz MJ, Mochida GH, Hennekam RCM, Maher ER, Fryns JP, Alswaid A, Jafri H, Rashid Y, Mubaidin A, Walsh CA, Roberts E, and Woods CG (2003). Protein-truncating mutations in ASPM cause variable reduction in brain size. *American Journal of Human Genetics* 73, 1170-1177.

Bourguignon C, Li J and Papalopulu N. (1998). XBF-1, a winged helix transcription factor with dual activity, has a role in positioning neurogenesis in *Xenopus* competent ectoderm. *Development* 125, 4889-4900.

Breslauer KJ, Frank R, Blocker H and Marky LA (1986). Predicting DNA duplex stability from the base sequence. *Proc. Natl. Acad. Sci. USA* 83, 3746-50.

Carroll SB (2005). Evolution at two levels: on genes and form. *PLoS Biology* 3, e245.

Caviness Jr VS, Takahashi T and Nowakowski RS (1995). Numbers, time and neocortical neurogenesis: a general developmental and evolutionary model. *Trends in Neuroscience* 18, 379-383.

Chung CT, Niemela SL and Miller RH (1989). One-step preparation of competent *Escherichia coli*: transformation and storage of bacterial cells in the same solution. *Proc. Natl. Acad. Sci. USA* 86, 2172-75.

Conboy IM, Conboy MJ, Wagers AJ, Girma ER, Weissman IL and Rando TA (2005). Rejuvenation o aged progenitor cells by exposure to a young systemic environment. *Nature* 433, 760-764.

Decker CI and Parker R (1995). Diversity of cytoplasmic functions for the 3' untranslated region of eukaryotic transcripts. *Current Opinion in Cell Biology* 7 386-392.

Derynck R, Zhang Y and Feng X-H (1998). Smads: Transcriptional activators of TGF-β responses. *Cell* 95, 737-740.

Dey A, Ellenberg J, Farina A, Coleman AE, Maruyama T, Sciortino S, Lippincott-Schwartz J, Ozato K (2000). A bromodomain protein, MCAP, associates with mitotic chromosomes and affects G(2)-to-M transition. *Molecular and Cellular Biology* 20, 6537-6549.

Dobyns WB (2002). Primary microcephaly: new approaches for an old disorder. *American Journal of Human Genetics* 112, 315–317.

Dorus S, Vallender EJ, Evans P, Anderson JR, Gilbert SL, Mahowald M, Wyckoff GJ, Malcom CM and Lahn BT (2004). Accelerated Evolution of Nervous System Genes in the Origin of *Homo sapiens. Cell* 119, 1026-1040.

Dou C, Lee J, Liu B, Liu F, Massague J, Xuan S and Lai, E (2000). BF-1 Interferes with Transforming Growth Factor β Signalling by Associating with Smad Partners. *Molecular and Cellular Biology* 20, 6201-6211.

Dou C, Li S and Lai E (1999). Dual role of Brain Factor-1 in Regulating Growth and Patterning of the Cerebral Hemispheres. *Cerebral Cortex* 9, 543-550.

Evans PD, Anderson JR, Vallender EJ, Choi SS and Lahn BT (2004a). Reconstructing the evolutionary history of microcephalin, a gene controlling human brain size. *Human Molecular Genetics* 13, 1139-1145.

Evans PD, Anderson JR, Vallender EJ, Gilbert SL, Malcom CM, Dorus S and Lahn BT (2004b). Adaptive evolution of ASPM, a major determinant of cerebral cortical size in humans. *Human Molecular Genetics* 13, 489-494.

Evans PD, Gilbert SL, Mekel-Bobrov N, Vallender EJ, Anderson JR, Vaez-Azizi LM, Tishkoff SA, Hudson RR and Lahn BT (2005). Microcepalin, a gene regulating brain size continues to evolve adaptively in humans. *Science* 309, 1717-1720.

Farh K K-H, Grimson A, Jan C, Lewis BP, Johnston WK, Lim LP, Burge CB and Bartel DP (2005). The widespread impact of the mammalian microRNAs on mRNA repression and evolution. *Science* 310, 1817-1821.

Felsenstein J (2004). *Inferring Phylogenies.* Sinauer Associates, Sunderland, Massachusetts.

Frank J, Pignata C, Panteleyev AA, Prowse DM, Baden H, Weiner L, Gaetaniello L, Ahmad W, Pozzi N, Cserhalmi-Friedman PB, Aita WM, Uyttendaele H, Gordon D, Ott J, Brissette JL and Christiano AM (1999). Exposing the human nude phenotype. *Nature* 398, 473-474.

Fukuchi-Shimogori T and Grove EA (2001). Neocortex patterning by the secreted signalling molecule FGF8. *Science* 294, 1071-1074.

Gilbert SF (2000). *Developmental Biology, Sixth Edition.* Sinauer Associates, Inc., Sunderland, Massachusetts.

Grindley JC Davidson DR and Hill RE (1995). The role of Pax6 in eye and nasal development. *Development* 121, 1433-1442.

Hall TA (1999). BioEdit: a user friendly biological sequence alignment editor and analysis program for Windows 95/98/NT. *Nucleic Acids Symposium Ser.* 41, 95-98.

Hanashima C, Li SC, Shen L, Lai E, and Fishell G (2004). FoxG1 suppresses early cortical cell fate. *Science* 303: 56-59.

Hanashima C, Shen L, Li SC and Lai E (2002). Brain Factor-1 Controls the Proliferation and Differentiation of Neocortical Progenitor Cells through Independent Mechanisms. *The Journal of Neuroscience* 22, 6526-6536.

Harada A, Katoh H and Negishi M (2005). Direct interaction of Rnd1 with FRS2β regulates Rnd1-induced down-regulation of RhoA activity and is involved in fibroblast growth factor-induced neurite outgrowth in PC12 cells. *The Journal Biological Chemistry* 280, 18418-18424.

Hardcastle Z and Papalopulu N (2000). Distinct effects of XBF-1in regulating the cell cycle inhibitor $p27^{XIC1}$ and imparting a neural fate. *Development* 127, 1303-1314.

Hedges SB and Poling LL (1999). A Molecular Phylogeny of Reptiles. *Science* 283, 998-1001.

Henke W, Herdel K, Jung K, Schnorr D and Loening SA (1997). Betaine improves the PCR amplification of GC-rich DNA sequences. *Nucleic Acids Research* 25, 3957-3958.

Hew Y, Grzelczak Z, Lau C and Keeley FW (1999). Identification of a large region of secondary structure in the 3'-untranslated region of chicken elastin mRNA with implications for the regulation of mRNA stability. *The Journal of Biological Chemistry* 274, 14415-14421.

Hill RS and Walsh CA (2005). Molecular insights into human brain evolution. *Nature* 437, 64-67.

Houbaviy HB, Murray MF and Sharp PA (2003). Embryonic Stem Cell-Specific MicroRNAs the regulation of development. *Developmental Cell* 5, 351–358.

Hüttemann M (2002). Partial heat denaturation step during reverse transcription and PCR-screening yields full-length 5' cDNAs. *BioTechniques* 32, 730-736.

Illing N, Boolay S, Siwoski JS, Casper D, Lucero MT and Roskams JA (2002). Conditionally immortalized clonal cell lines from the mouse olfactory placode differentiate into olfactory receptor neurons. *Molecular and Cellular Neuroscience* 20, 225-243.

Jackson AP, Eastwood H, Bell SM, Adu J, Toomes C, Carr IM, Roberts E, Hampshire DJ, Crow YJ, Mighell AJ, Karbani G, Jafri H, Rashid Y, Mueller RF, Markham AF, and Woods CG (2002). Identification of microcephalin, a protein implicated in determining the size of the human brain. *American Journal of Human Genetics* 71, 136–142.

Kaestner KH, Knochel W and Martinez DE (2000). Unified nomenclature of the winged helix/forkhead transcription factors. *Genes and Development* 14, 142-146.

Kandel ER, Schwartz JH and Jessel TM (1991). *Principles of Neural Science, Third Edition.* Elsevier Science Publishing Company Inc., USA.

Katoh M and Katoh M (2004). Human FOX gene family (Review). *International Journal of Oncology* 25, 1495-1500.

Kimura (1983). *The neutral theory of molecular evolution.* Cambridge University Press, UK.

Kornack DR and Rakic P (1998). Changes in cell-cycle kinetics during the development and evolution of primate neocortex. . *Proc. Natl. Acad. Sci. USA* 95, 1242-1246.

Krek A, Grun D, Poy MN, Wolf R, Rosenberg L, Epstein EJ, MacMenamin P, da Piedade I, Gunsalus KC, Stoffel M and Rajewsky N (2005). Combinatorial microRNA target predictions. *Nature Genetics* 37, 495-500.

Kumar A, Markandaya M and Girimaji SC (2002). Primary microcephaly: microcephalin and ASPM determine the size of the human brain. *Journal of Biosciences* 27, 629–632.

Kumar S, Tamura K & Nei M (2004). MEGA3: Integrated Software for Molecular Evolutionary Genetics Analysis and Sequence Alignment. *Briefings in Bioinformatics* 5, 150-163.

Lagos-Quintana M, Rauhut R, Lendeckel W, Tuschl T (2001). Identification of novel genes coding for small expressed RNAs, *Science* 294, 853-858.

Lagos-Quintana M, Rauhut R, Yalcin A, Meyer J, Lendeckel W and Tuschl T (2002). Identification of Tissue-Specific MicroRNAs from Mouse. *Current Biology* 12, 735-739.

Lai CS, Fisher SE, Hurst JA, Vargha-Khadem F and Monaco AP (2001). A forkhead-domain gene is mutated in a severe speech and language disorder. *Nature* 413, 519-523.

Lai E, Clark KL, Burley SK and Darnell JE (1993). Hepatocyte nuclear factor 3/fork head or "winged helix" proteins: A family of transcription factors of diverse biological function. *Proc. Natl. Acad. Sci. USA* 90, 10421-10423.

Lai E, Prezioso VR, Tao W, Chen WS and Darnell Jr E (1990). Hepatocyte nuclear factor 3α belongs to a gene in mammals that is homologous to the Drosophila homeotic gene fork head. *Genes and Development* 5, 416-427.

Lee SM, Danielian PS, Fritsch B and McMahon AP (1997). Evidence that FGF8 signalling from the midbrain-hindbrain junction regulates growth and polarity in the developing brain. *Development* 124, 959-969.

Lewis BJ, Burge CB and Bartel DP (2005). Conserved seed pairing, often flanked by adenosines, indicates that thousands of human genes are microRNA targets. *Cell* 120, 15-20.

Li H, Tao W and Lai E (1996). Characterization of the structure and function of the gene for transcription factor BF-1, an essential regulator o forebrain development. *Molecular Brain Research* 37, 96-104.

Li J and Vogt PK (1993). The retroviral oncogene qin belongs to the transcription factor family that includes the homeotic gene fork head. *Proc. Natl. Acad. Sci. USA* 90, 4490-4494.

Li J, Chang HW, Lai E, Parker EJ and Vogt PK (1995). The oncogene *qin* codes for a transcriptional repressor. *Cancer Research* 55, 5540-5544.

Li J, Thurm H, Chang HW, Ianocovi JS and Vogt PK (1997). Oncogenic transformation induced by the Qin protein is correlated with transcriptional repression. *Proc. Natl. Acad. Sci. USA* 94, 10885-10888.

Li W, Cogswell C and LoTurco J (1998).Neuronal differentiation of precursors in the neocortical ventricular zone is trigged by BMP. *The Journal of Neuroscience* 18, 8853-8862.

Li W-H (1993). Unbiased estimation of the rates of synonymous and nonsynonymous substitution. *Journal of Molecular Evolution* 36, 96-99.

Linda P (2003). *Characterization of the role of Brain Factor 1 in the olfactory neuroepithelium during neuronal development.* M.Sc. thesis, Department of Molecular and Cell Biology, University of Cape Town.

Marçal N, Patel H, Dong Z, Belanger-Jasmin S, Hoffman B, Helgason CD, Dang J and Stifani S (2005). Antagonistic effects of Grg6 and Groucho/TLE on the transcription repression activity of Brain Factor1/FoxG1 and cortical neuron differentiation. *Molecular and Cellular Biology* 25, 10916-10929.

Marin-Padilla M (1992). Ontogenesis of the pyramidal cell of the mammalian neocortex and developmental cytoarchitectonics: a unifying theory. *Journal of Comparative Neurology* 321, 223-240.

Martynoga B, Morrison H, Price DJ and Mason JO (2005). Foxg1 is required for specification of ventral telencephalon and region specific regulation of dorsal telencephalic precursor proliferation and apoptosis. *Developmental Biology* 283, 113-127.

Mathews DH, Disney MD, Childs JL, Schroeder SJ, Zuker M and Turner DH. (2004) Incorporating Chemical Modification Constraints into a Dynamic Programming Algorithm for Prediction of RNA Secondary Structure. *Proc. Natl. Acad. Sci. USA* 101, 7287-7292.

Mekel-Bobrov N, Gilbert SL, Evans PD, Vallender EJ, Anderson JR, Hudson RR, Tishkoff SA and Lahn BT (2005). Ongoing adaptive evolution of ASPM, a brain size determinant in *Homo sapiens. Science* 309, 1720-1722.

Miyata T, Yasunaga T and Nishida T (1980). Nucleotide sequence divergence and functional constraint in mRNA evolution. *Proc. Natl. Acad. Sci. USA* 77, 7328-7332.

Mochida GH and Walsh CA (2001) Molecular genetics of human microcephaly. *Current Opinion in Neurology* 14, 151–156.

Murphy DB, Wiese S, Burfeind P, Schmundt D, Mattei M-G, Schulz-Schaeffer W and Theis U (1994). Human Brain Factor 1, a New Member of the Fork Head Gene Family. *Genomics* 21, 551-557.

Muzio L and Mallamaci A (2005). Foxg1 confines Cajal-Retzius neurogenesis and hippocampal morphogenesis to the dorsomedial pallium. *The Journal of Neuroscience* 25, 4435-4441.

Ornitz D, Xu J, Colvin J, McEwen D, MacArthur C, Coulier F, Gao G, and Goldfarb M (1996). Receptor specificity of the fibroblast growth factor family. *Journal of Biological Chemistry* 271, 15292-15297.

Pamilo P and Bianchi NO (1993). Evolution of the Zfx and Zfy, genes: Rates and interdependence between the genes. *Molecular Biology and Evolution* 10, 271-281.

Pelting R, Saxena B, Jones M, Moses H and Gold L (1991). Immunohistochemical localization of TGFβ1, TGFβ2 and TGFβ3 in the mouse embryo: expression patterns suggest multiple role during embryonic development. *Journal of Cell Biology* 115, 1091-1105.

Ponting C and Jackson P (2005). Evolution of primary microcephaly genes and the enlargement of primate brains. *Current Opinions in Genetics and Development* 15, 241-248.

Pratt T, Natasha M. M.-L. Tian NMM-L, Simpson TI, Mason JO and Price DJ (2004). The winged helix transcription factor Foxg1 facilitates retinal ganglion cell axon crossing of the ventral midline in the mouse. *Development* 131, 3773-3784.

Promega corporation (1998) *Transfection guide.* USA.

Ridley M (2004). *Evolution, Third edition.* Blackwell Publishing, Oxford, UK.

Rodriguez C, Huang L J-S, Son JK, McKee A, Xiao Z and Lodish HF (2001). Functional Cloning of the Proto-oncogene Brain Factor-1 (BF-1) As a Smad-binding antagonist of Transforming Growth Factor- β signalling. *The Journal of Biological Chemistry* 276, 30224-30230.

Romer AS (1966). *Vertebrate Palaeontology.* University of Chicago Press, Chicago, Illinois.

Seoane J, Le H-V, Shen L, Anderson SA and Massague J (2004). Integration of Smad and Forkhead pathways in the control of the neuroepithelial and glioblastoma cell proliferation. *Cell* 117, 211-223.

Shoichet S, Kunde S-A, Viertel P, Schell-Apacik C, von Voss H, Tommerup N, Ropers H-H and Kalscheuer VM (2005). Haplionsufficiency of novel FOXG1B variants in a patient with severe mental retardation, brain malformations and microcephaly. *Human Genetics*, 117 (6), 536-544.

Shoko A (2004). *The OP27 cell line as a model system to study the effects of FGF-2 in olfactory neuronal development*. Ph.D. thesis, Department of Molecular and Cell Biology, University of Cape Town.

Shoko A, Roskams J, and Illing N. FGF-2 Stimulates the Differentiation and Survival of the OP27 Olfactory Precursor Cell Line. Manuscript under review.

Smith Fernandez A, Pieau C, Reperant J, Boncinelli E and Wassef M (1998). Expression of the Emx-1 and Dlx-1 homeobox genes define three molecularly distinct domains in the telencephalon of mouse, chick, turtle and frog embryos: implications for the evolution of telencephalic subdivisions in amniotes. *Development* 125, 2099-2111.

Sultan F (2002). Analysis of mammalian brain architecture. *Nature* 415, 133-134.

Sur M and Rubenstein JLR (2005) Patterning and Plasticity of the Cerebral Cortex. *Science* 310, 805-810.

Takahashi T, Nowakowski RS and Caviness Jr. VS (1995). The cell cycle of the pseudostratified ventricular epithelium of the embryonic murine cerebral wall. *The Journal of Neuroscience* 15, 6046-6057.

Tao W and Lai E (1992). Telecephalon-Restricted Expression of BF-1 a New Member of the HNF/fork head Gene Family, in the Developing Rat Brain. *Neuron* 8, 957-966.

Thompson JD, Gibson TJ, Plewniak F, Jeanmougin F and Higgins DG (1997). The ClustalX windows interface: flexible strategies for multiple sequence alignment aided by quality analysis tools. *Nucleic Acids Research* 25, 4876-4882.

Tokunaga A, Kohyama J, Yoshida T, Nakao K, Sawamoto K and Okana H (2004). Mapping and spatio-temporal activation of Notch signalling during neurogenesis and gliogenesis in the developing mouse brain. *Journal of Neurochemistry* 90, 142-154.

Toresson H, Martinez-Barbera JP, Bardsley A, Caubit X and Krauss S (1998). Conservation of BF-1 expression in amphioxus and zebrafish suggests evolutionary ancestry of anterior cell types that contribute to the vertebrate telencephalon. *Development, Genes and Evolution* 208, 431-439.

Wedemeyera N, Schmitt-Johna J, Eversb D, Thiela C, Eberharda D and Jockuscha H (2000). Conservation of the 3P-untranslated region of the Rab1a gene in amniote vertebrates: exceptional structure in marsupials and possible role for posttranscriptional regulation. *FEBS Letters* 477, 49-54.

Weigel D, Jurgens G, Kuttner F, Seifert E and Jackle H (1989). The homeotic gene *fork head* encodes a nuclear protein and is expressed in the terminal regions of the Drosophila embryo. *Cell* 57, 645-658.

Wiese S, Murphy DB, Schlung A, Burfeind P, Schmundt D, Schnülle V, Mattei M-G and Theis U (1995). The genes for human brain factor 1 and 2, members of the fork head gene family, are clustered on chromosome 14q. *Biochimica et Biophysica Acta* 1262, 105-112.

Williams MF (2002). Primate encephalization and intelligence. *Medical Hypotheses* 58, 284-290.

Xuan S, Baptista CA, Balas G, Tao W, Soares VC and Lai E. (1995). Winged Helix Transcription Factor BF-1 is Essential for the Development of the Cerebral Hemispheres. *Neuron* 14, 1141-1152.

Yao J, Lai E and Stifani S (2001). The Winged-Helix Protein Brain Factor 1 Interacts with Groucho and Hes Proteins To Repress Transcription. *Molecular and Cellular Biology* 21 (6), 1962-1972.

Yao J, Liu Y, Lo R, Tretjakoff I, Peterson A and Stifani S (2000). Disrupted development of the cerebral hemispheres in transgenic mice expressing the mammalian Groucho homologue Transducin-like Enhancer of split in postmitotic neurons. *Mechanisms of Development* 93, 105-115.

Plagiarism Declaration

1. I know that plagiarism is wrong. Plagiarism is to use another's work and pretend that it is one's own.
2. Each contribution to, and quotation in, this research report from the works of other people has been attributed, and has been cited and referenced.
3. This report is my own work and has not previously in its entirety or in part been submitted at any other university for another degree.
4. I have not allowed, and will not allow, anyone to copy my work with the intention of passing it off as his or her own work.

Signature signature removal

Date 22-05-2006